universität wien

DISSERTATION / DOCTORAL THESIS

Titel der Dissertation /Title of the Doctoral Thesis

„A multidimensional approach on the ecology and biology of recent and fossil heterostegenid taxa and its application on biostratigraphy and palaeoecology“

verfasst von / submitted by

Wolfgang Eder, BSc, MSc

angestrebter akademischer Grad / in partial fulfilment of the requirements for the degree of

Doktor der Naturwissenschaften (Dr.rer.nat.)

Wien, 2016 / Vienna 2016

Studienkennzahl lt. Studienblatt / degree programme code as it appears on the student record sheet:	A 796 605 426
Dissertationsgebiet lt. Studienblatt / field of study as it appears on the student record sheet:	Erdwissenschaften
Betreut von / Supervisor:	Ao. Prof. Dr. Johann Hohenegger
Mitbetreut von / Co-Supervisor:	

Content

Abstract

The cosmopolitan larger symbiont-bearing foraminifera*, Heterostegina depressa* prefers oligotrophic tropic to warm-temperate seas. Within the nummulitid family, it shows the broadest water depth distribution and high ecological adaptability by test modification. This allows it to settle in a variety of niches influenced by light intensity, hydrodynamic energy and substrate. As the only living representative of the heterostegenid subfamily it is a perfect model species to infer information gathered by extensive actuopalaeontological studies onto its fossil relatives. *Heterostegina depressa* tests grown under natural and laboratory conditions have been studied by microCT analysis and 3D visualization to extract the chamber volume sequence of each specimen. Similar as in previous studies on volumetric growth of larger foraminifera, it is shown in this work that the chamber volume sequence of *H. depressa* oscillates around a theoretical growth function. In all investigated specimens these oscillations exhibit similar periodic lengths, hinting towards a common intrinsic or extrinsic factor. Short-term oscillations around 15 and 30 day periods point towards lunar and tidal forcing, while long-term cycles around 70 and 180 days are more enigmatic and probably induced by seasonal-climatic events. Surprisingly, similar cyclicities were observed in natural and laboratory-cultured specimens. However, a solely genetic origin of these cycles couldn't be verified either. Serendipitous results revealed intraspecific patterns concerning proloculus size, hinting towards an ecological and biogeographic dependence of this commonly used biometric parameter. In order to test the hypothesis that some of the observed morphological differences may reflect environmental conditions, morphometric analysis to equatorial sections of megalospehric *H. depressa*, sampled along a water depth transect from 5 to 90 meters, were applied. These analyses clearly differentiated two morphogroups corresponding to two megalospheric generations: gamonts with significantly larger prolоculi and schizonts with smaller prolоculi. In high energy environments, asexual reproduction (schizogony) dominates, while sexual reproduction (gametogony) is the dominant mode under low energy conditions. Thus, there is a shift in proportions between schizonts with smaller prolоculi and gamonts with larger proluculi along the hydrodynamic gradient. Both generations retain the characters of their initial tests regardless of depth. Where both megalospheric generations co-occur, the change in proportion of generations with depth results in an environmental morphological trend that matches apparent fossil evolutionary trends. In addition, this study revealed that many of the generally used biometric parameters correlate with proloculus size and are therefore of minor informational value. To resolve the complex ecological and biogeographical dependence of *H. depressa'*s test morphology, multiple morphometric approaches have been combined. Equatorial section of *Heterostegina* have been investigated regarding certain biometric characters. Among others, both proloculus size and number of operculinid chambers have been used as metric characters not only in the evolution of *Heterostegina* lineages, but also in many other nummulitds (e.g., *Nummulites*, *Spiroclypeus*, *Cycloclypeus*), neglecting the environmental dependence. Additionally, proloculus size can differ between biogeographically different populations (e.g., Okinawa and Hawaii) taken under similar hydrodynamic conditions. By using growth-independent and growth-invariant characters to describe internal test morphology, interpretation regarding evolutionary tendencies can be enhanced emphasizing the distinction between environmental, biogeographic and stratigraphic diversification. In addition, due to its endosymbionts, *Heterostegina* exhibits a strong light dependence correlated with water depth, which is managed by increasing surface/volume ratios realized by test flattening. Hence, the tests are modified to maximize light exposure, while maintaining mechanical resistance against hydrodynamic energy. As already mentioned, *H. depressa* is a perfect model species to study test modification of nummulitid larger foraminifera according to different environmental settings. To calibrate test flattening as a bathymetric signal for fossil

assemblages, four growth-invariant characters have been used to describe the change of test thickness throughout ontogeny. The presented analysis clearly quantifies this transition of individuals with thicker to thinner central parts along the water depth gradient. Thus, shallower specimens grow thicker to reduce light penetration, while specimens living deeper than the light optimum increase their surface to reach a better light exposure for the symbiotic microalgae.

Publication Overview

Published:

Eder, W., Briguglio, A., Hohenegger, J., 2016. Growth of *Heterostegina depressa* under natural and laboratory conditions. Marine Micropaleontology 122, 27-43. 10.1016/j.marmicro.2015.11.005

Accepted:

Eder, W., Hohenegger, J., Briguglio, A., (29.04.2016). Depth-related morphoclines of megalospheric test of Heterostegina depressa d'Orbigny: biostratigraphic and palaeobiological implications. PALAIOS.

Eder, W., Hohenegger, J., Torres-Silva, A.I., Briguglio, A., (25.03.2016). Morphometry of the larger foraminifera Heterostegina explaining environmental dependence, evolution and palaeogeographic diversification. Proceedings of the 13th International Corel Reefs Symposium.

Unpublished:

Eder, W., Hohenegger, J., Briguglio, A., Test flattening in the larger foraminifera *Heterostegina depressa*: predicting bathymetry from axial sections.

General Introduction

These studies concentrate on the morphology, ecology and growth of the nummulitid larger foraminifer *Heterostegina depressa* d'Orbigny and the comparison to its fossil relatives. Further, this thesis discusses the way actuopalaeontological investigations on the ecology and biology of recent taxa can improve the knowledge about the fossil realm and augment larger foraminifera's value as a reconstructing tool for shallow marine environments in the past. Yet, for the time being, one major question arises, what is a larger benthic foraminifera? In modern tropic to warm-temperate shallow seas larger benthic foraminifer (LBF) are one of the major faunal components. They are a non-taxonomic polyphyletic group of benthic foraminifera with various test shapes and growth patterns and, within the last 300 million years, they arose multiple times out of smaller benthic foraminifera. LBF are unified by one most significant character, namely the acquisition of endosymbiontic microalgae. These microalgae enable them to reach larger test sizes, generally larger than 3 mm^3 (Ross, 1974; Hallock, 1985; Hohenegger, 2011a). From recent species (e.g., *Cycloclypeus carpenter*i) maximal test sizes up to 13 cm are known, while from the fossil record even larger specimens can be found (e.g., *Nummulites millecaput*) (Beavington-Penney and Racey, 2004).

Tests of larger benthic foraminifera fulfil two major key functions; first, to protect against and diminish the influence of external factors (e.g., hydrodynamic energy and light intensity) and, second, to facilitate physiological processes (e.g., intracellular mass transport and symbiont movement). Hence, tests of LBF take on many functional and regulatory processes known from greenhouses, so they are essentially microscopic gardeners of the ocean (Hallock, 1985; Hottinger, 2000; Hohenegger, 2011a).

Like their smaller relatives, larger benthic foraminifera have rather complex reproduction cycle (see Fig.1.), consisting of three generations differentiated by the number of homologues chromosomes. Two haploid generations (one set of chromosomes) and one diploid generation (double set of chromosomes) (Röttger, 1974; Hohenegger, 2011a). The reproductive cycle can be subdivided into three phases; the gamogeny, the agamogeny and the schizogeny. During the agamogeny the gamonts (one of the haploid generations) release thousands of gametes. These gametes merge to form a zygote, from which the diploid generations, the agamonts, emerge. During the gamogeny, the haploid generations are formed by agamonts via a meiotic cell fission. This reproduction phase results either in the production of gamonts, closing the first reproductive cycle, or in the second haploid generation, the schizonts. Schizonts can reproduce by mitotic multiple fission, introducing a second reproductive cycle. Alternatively, they are also able to produce gamonts, therefore feeding into the gamogeny (Röttger et al., 1990).

Yet, the terminology based on reproductive phases is seldomly used in palaeontology. Generations are rather differentiated by morphological characters, like the size of the first embryonic chamber (= proloculus). In accordance to this, gamonts and schizonts are referred to as megalospheres or megalospheric generation (A) and agamonts as microspheres or microspheric generation (B) (Hottinger, 2006a). Further, in most genera A and B generations show a strong dimorphism, where B forms reach much larger test sizes than A forms do. However, morphological differences within the two megalospheric generations are generally not acknowledged and are rarely subdivided into A_1 (schizonts) and A_2 (gamonts) (Leutenegger, 1977).

The common habitat of larger foraminifera are the photic zones of oligotrophic tropic to warm-temperate coastal seas, where water is generally depleted in inorganic nutrients. Therefore, as a survival strategy, unicellular plants

develop symbiosis with “animal” hosts. These can be either multicellular (e.g., corals or bivalves) or unicellular (e.g., foraminifera). In this way, the host organism, in our case the LBF, gains certain independence from external

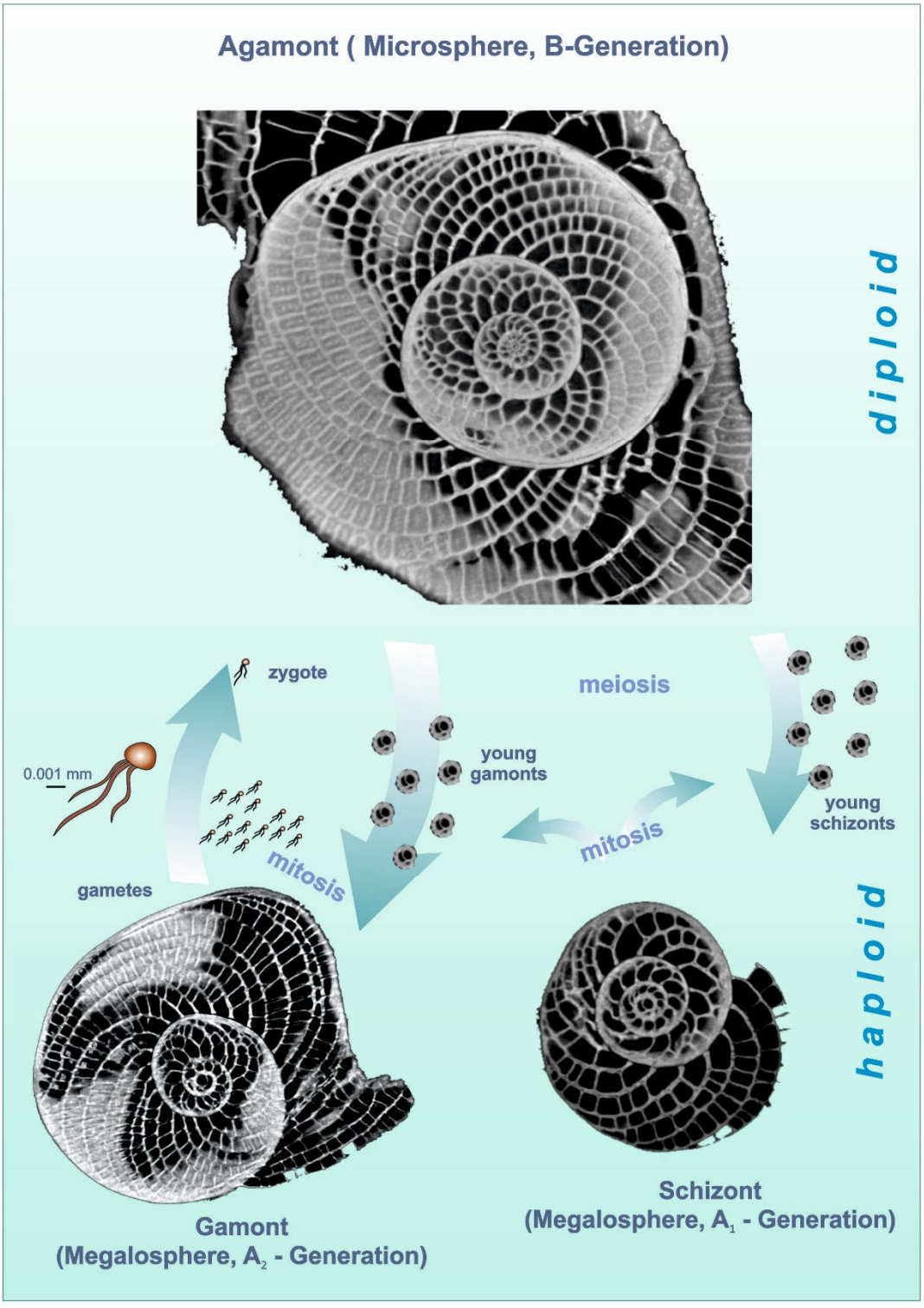

Figure 1 – Illustration of the complex trimorphic life cycle of larger benthic foraminifera here: *Heterostegina depressa* altered from (Hohenegger, 2011).

food sources by feeding on organic products of their endosymbionts. In some cases, symbiosis can reach a degree where the host may become “quasi-autotroph”. Microalgae gain in return inorganic nutrients, mainly nitrogen and

phosphor compounds derived from the host's metabolic products. Further, inorganic carbon dioxide becomes readily available during the calcification of the host, feeding into the photosynthetic processes of the symbionts (Lee and Hallock, 1987; Lee, 2006).

Microalgal symbionts occurring in larger benthic foraminifera belong to four different phyla, Rhodophyta (red algae), Chlorophyta (green algae), Pyrrhophyta (dinoflagellates) and Bacillariophyta (diatomes). Rhodophyta are known from recent oceans as encrusting or branching multicellular plants; especially the family Corallinacea is known as the binding key element in modern reef structures. Only the unicellular species *Porphyridium purreum* has been identified as symbiont in larger benthic foraminifera. The intensive reddish to purple color, which is observed in LBF hosting *P. purreum,* results from the photopigment Phytoerythrin. It reflects light with longer wavelength (red) and absorb shorter wavelengths (green to blue). Since shorter wavelengths reach down to maximum 200 meters, photosynthesis can be maintained in deeper settings. Red algae have the lowest production of organic nutrients of the four symbionts groups; LBF hosting them must additionally uptake nutrients from external sources.

Foraminiferal symbionts of the phylum Chlorophyta all belong to the genus *Chlamydomonas*. The biflagellate unicellular plants possess the photopigments chlorophyll a and chlorophyll b. Hence, they are adapted to absorbing longer wavelengths (red) and reflecting shorter wavelengths (greenish-blue). This, however, restricts hosts to shallower regions, since red light reaches a maximum depth around 40 m. The yield of available organic nutrient is similar to red algae.

The next group, Pyrrhophyta, are very common planktonic unicellular organisms and make up a high percentage of the phytoplankton. In open water, the single cells are covered by cellulose plates and have two flagella, one for movement and one for stabilization. As endosymbionts those characteristics become lost. The genus *Symbiodinium* is widespread as endosymbionts in multi-cellular hosts (e.g., stony corals, giant clams). The group possesses chlorophyll a and c, which allows them to absorb wavelengths at the lower and upper limit of the visible light. Therefore, they can maintain photosynthesis in deeper and shallower environments. Since they miss Chlorophyll b, dinoflagellates never show the same verdant green as green algae, but rather range from ochre to olive green. The energy yield of dinoflagellates symbionts is up to 25 % greater than of red or green algae.

The fourth group of microalgae are the Bacillariophyta, which presents the major part of marine phytoplankton and, therefore, are responsible for the main primary production on earth. Diatoms live as single-celled organisms either benthic or planktonic protected by a frustulum, a test consisting of silicic acid. Like dinoflagellates, they possess chlorophyll a and b, positioning their absorption maximum at the upper and lower end of the visible light (greenish-blueish and red). However, diatoms are the only phytoplankton group that maintains a positive photosynthetic rate at very low light levels, even as deep as 250 meters in tropical seas. Therefore, diatoms provide the highest number of organic nutrients for their host, granting them near independence from external food sources. All recent nummulitids, including *Heterostegina*, have a group of monophyletic diatoms akin to *Thalassionema* as endosymbionts (Lee and Anderson, 1991; Hottinger, 2000; Holzmann et al., 2006; Hohenegger, 2011a).

The complex biotic interaction with their endosymbionts has been the centre of many studies on larger foraminifera. In addition, the constraints of their distribution, depth occurrence and morphology have been thoroughly discussed. Research on their reaction to external factors, such as hydrodynamic energy and light attenuation, provided essential information to refine the knowledge on palaeoecology and palaeoenvironments of fossil larger benthic foraminifera (Hottinger, 1977a; Reiss and Hottinger, 1984; Hallock et al., 1991; Racey, 1992; Briguglio and Hohenegger, 2009; Hohenegger, 2009). Several studies on the functional morphology and external

ornamentation of the shells yielded important information on their ecological niches in terms of water depth (Hohenegger, 2006), trophic resources (Hallock, 1988) and light intensity (Hohenegger, 2009). According to Hohenegger (2004), primary ecological factors correlate in a non-linear or discontinuous way to water depth. Temperature is an important factor controlling the distribution of most LBF; the critical temperature of their habitat should never fall below 14°C. In tropical and subtropical regions, the water depth characterizing this temperature limit is much deeper than the depth limit based on light. Light intensity plays a very important role influencing the water depth distribution of larger benthic foraminifera. Accordingly, the different species occupy various niches along the light gradient (Hohenegger, 2000). Since light intensity changes not only with depth (different penetration of wavelengths) but is also influenced by different factors of water quality (e.g., content of inorganic and organic particles, heightened turbidity, submarine topography), a general correlation between water depth and species distribution is difficult to approach (Hallock et al., 2003; Hohenegger, 2004). Uthicke and Nobes (2008) showed that not all symbiont-bearing larger foraminifera are equally influenced by a change in water quality. Additionally, they emphasize the connection between attenuation of light and lower depth limit of foraminifera. Wind-induced hydrodynamic motion is one major factor which can be correlated directly to water depth because it decreases with depth. This dependency, however, varies due to changing wind intensities and the presence of sublittoral and/or tidal currents. For unidirectional hydrodynamics (e.g., tidal and ocean currents) this depth correlation can be further altered by local topography and sea bottom roughness (Hohenegger, 2004). Apart from that, internal waves can periodically alter temperature and nutrient conditions of meso- and oligophotic biotas (Hallock and Pomar, 2008). Generally, internal waves can be observed along discontinuities within the water columns (e.g., thermoclines and pycnoclines). For shallow water environments, surface tides and storms might start internal waves at bathymetric breaks. However, while surface currents influence shallow water environments on a larger scale, the influence of internal waves can be restricted to smaller areas (Pomar et al., 2011). Thus, LBF communities can regionally differ at the same water depth due to different energetic conditions and regionally altered water composition. In recent time, but also in the fossil realm, LBF are significant carbonate producers in shallow marine environments (Langer and Lipps, 2003; Hohenegger, 2006) and are further important index fossils (Serra-Kiel et al., 1998)

To improve how endosymbionts are hosted within the test and the need for adapting to requirements of their immediate surroundings has led to an optimization trend in LBF evolution. Balancing these intrinsic and extrinsic factor goes so far that function often dictates the form of larger benthic foraminifera's tests. Therefore, many different growth strategies are known, which can differ either based on overall test shape and chamber arrangement or on microstructures and crystal arrangement of the test (Hallock, 1985; Hohenegger, 2009). The most common wall material in larger benthic foraminifera is calcium carbonate, since all the educts for the crystallization process are readily available in tropic and warm-temperate coastal seas. While in recent larger benthic foraminifera either low-magnesium (4%) or high-magnesium (24%) crystallites are used as building material, in some fossil groups agglutinated calcium carbonate cemented walls or microgranular (consisting of small spherical calcite crystallites) can be observed. The one of the two modern wall structure is the hyaline type. It consists of small plate like crystallites, which are densely packed. Thus, the test walls become highly light transparent since the optical axis of crystals are aligned. Yet it becomes impenetrable for molecules. Therefore, pores must be constructed to allow molecule transport. Since hyaline tests are highly transparent independent of thickness they are better adapted to deeper photic environments (Hohenegger, 2011a).

The second wall structure is the so-called porcelaineous test, which consist of three layers. The inner layer is build-up of randomly oriented needle-shape crystals, which results in a porous structure filled with organic material to allow molecule transport. The randomly orientated crystals scatters light and diminishes light penetration of the test. The upper and lower layer of the wall, consisting of plate like crystals oriented perpendicular to their optical axis, additionally reflect light. Due to this strong light reflection, the test has a white and polished appearance similar to porcelain. Therefore, foraminifera with porcelaineous tests are adapted to very shallow and highly illuminated environments. Larger foraminifera with this wall type construct window-like structures by test thinning to provide endosymbionts with sufficient light (Hottinger, 2000; Hohenegger, 2009).

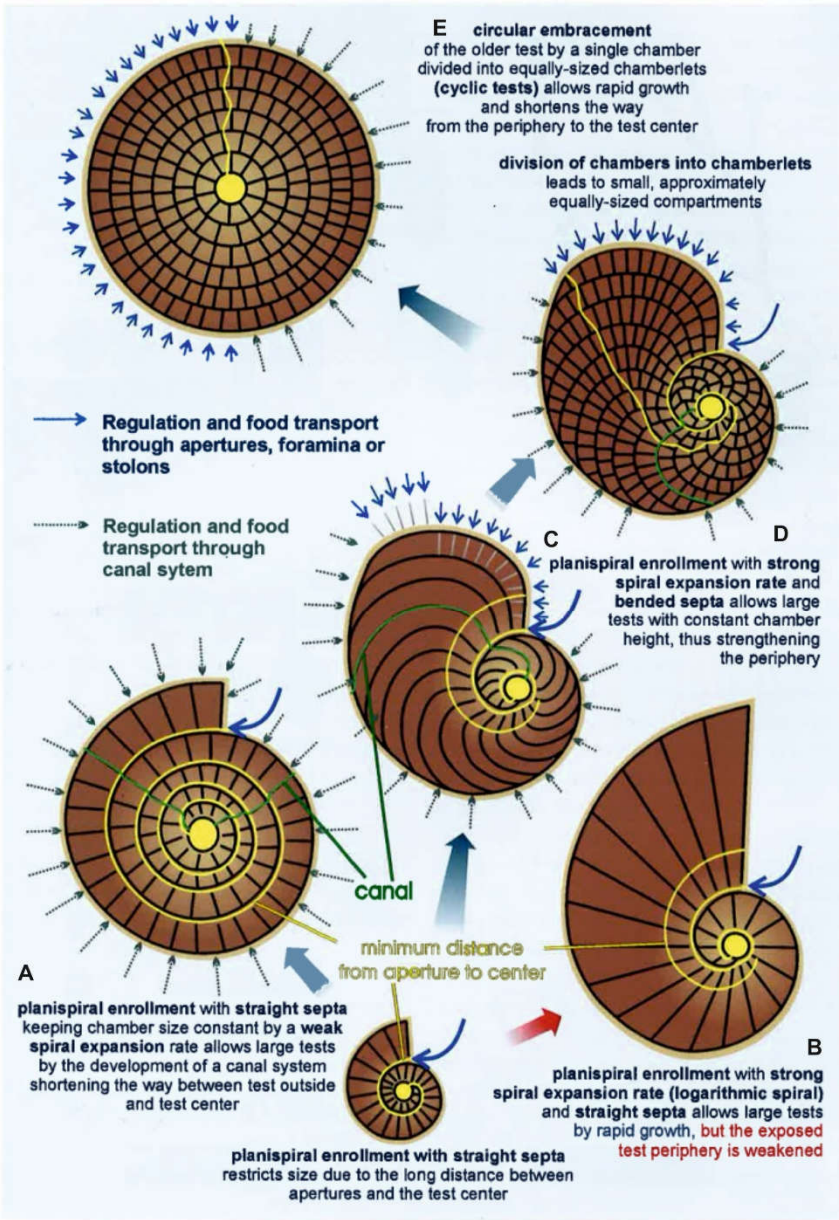

Figure 2 – Different ways of test construction based on planispiral enrolment in larger foraminifera (after Hohenegger, 2011)

Apart from the wall material, foraminifera utilize an extreme variety of test geometry and chamber arrangement – from straight, branching or randomly coiling tubes towards a set of trochospiral to planispiral globular chambers.

Modern foraminifera systematics use the shape of chambers to divide foraminifera in three classes; Monothalamea, Tubothalamea and Globothalamea.

In larger benthic foraminifera, especially within the nummulitid family, planspiral tests are most common. Hence, it is the best approach to maximize surface/volume ratio and to construct rather flat tests. The simplest construction of such tests is a sequence of constantly sized chambers coiling in one plane around the embryonic chambers, similar to an archimedean spiral. This allows a constant increase in size over a longer period (e.g., Fig.2.A - common in the genera *Nummulites* and *Assilina*). An optimization of this construction plan is the continuous increase in chamber height with consecutive chamber. In this case, the test correlates to a logarithmic spiral, which allows faster test growth. However, the construction of logarithmic spiral with straight septa introduces structural deficiencies with increasing test size (e.g., Fig.2.B), which is counteracted by a backward bending of chambers (e.g., Fig.2.C *Operculina* and *Operculinella*). An additional approach to gain further stability is the construction of incomplete or complete subdivision of chambers by secondary septa or septula (Hottinger, 2006a). This type of test outlay, with strong septal backbending and additional septula, allows the construction of extremely thin test (e.g., Fig.2.D *Planoperculina, Planostegina,* and *Heterostegina*). LBF utilizing this bauplan can settle in the deepest habitats of the photic zone. This septal backbending can take such extreme forms, that tests transcend from spiral to a cyclic growth, achieving the highest possible stability (e.g., Fig.2.E *Cycloclypeus* and *Heterocyclina*) (Hottinger, 2005; Hohenegger, 2009, 2011a).

As mentioned at the beginning of this chapter, *Heterostegina* belongs to the Nummulitidae, which is one of the most dominant families within larger foraminifera during the Cenozoic up to the Recent. Nummulitids belong to the suborder Rotaliina and originate from the base of the Paleogene. Over the Paleocene to Eocene, especially the taxa *Nummulites* and *Assilina* reach extremely high evolutionary rates and achieve a great biodiversity in the Tethyan realm. Their extreme abundance declines during the Oligocene and are replaced by other nummulitid groups over the Oligocene-Miocene transition (e.g.; *Operculina*, *Heterostegina, Planostegina, Spiroclypeus* and *Cycloclypeus*) (Hottinger, 1977b; BouDagher-Fadel, 2008).

<table>
<tr><td>Planostegina</td><td>Heterostegina</td><td>Hetero.
(Vlerkina)</td><td>Grzybowskia</td><td>Tansinhokella</td><td>Spiroclypeus</td></tr>
<tr><td>evolute</td><td>maturoevolute</td><td colspan="4">involute</td></tr>
<tr><td colspan="3">chamberlets
subrectangular</td><td>chamberlets
polygonal</td><td colspan="2">chamberlets
subrectangular</td></tr>
<tr><td>no lateral
chamberlets</td><td colspan="4">lateral
chamberlets</td><td>cubicula</td></tr>
<tr><td>no alar
prolongations</td><td colspan="3">umbilically unembracing
alar prolongations</td><td>umbilically
embracing
alar
prolongations</td><td>lateral
cubicula</td></tr>
</table>

Figure 3 – Overview of the morphological differentiation between genera and groups of Heterosteginae based on qualitative morphological characters (after Banner and Hodgkinson, 1911). According to (Holzmann et al., 2003) Planosteginids shouldn't be considered part of the Heterosteginae anymore.

Nummulitidae are generally differentiated into two subfamilies based on their internal morphology: Nummulitinae and Heterosteginae, according to presence and absence of septula. Apart from this subdivision of chambers, heterostegenid genera commonly have a planispiral enrolment with varying degrees of involution. This morphology, present since the late Eocene, is the diagnostic character of the heterosteginid subfamily (Banner and Hodgkinson, 1991). Heterosteginae are again split into a *Heterostegina sensu stricto* lineage and a *Heterostegina sensu lato* group mainly by their degree of involution and stratigraphic position. The first group *Heterostegina sensu stricto* supposedly originated around the Oligocene/Miocene transitions and leads up to the recent, with the monotypic taxon *H. depressa*. The second group includes the fossil genera and subgenera *Heterostegina* (*Vlerkina*) Eames et al. 1968, *Spiroclypeus* Douvillé 1905, *Grzybowskia* Bieda 1950, and *Tansinhokella* Banner and Hodgkinson 1991. However, phylogenetic connections between these groups are yet highly sepculative.

Major parts of this work concentrate on the recent taxon *Heterostegina depressa* d'Orbigny 1826, a cosmopolitan species of tropical to warm temperate shallow-water environments. Formerly absent from the Mediterranean since the Messinian Salinity crisis, it belongs to the so-called Lessepsian immigrants invading through the Suez Canal. This species hosts *Thalassionema*-type diatom symbionts, which clearly differ from diatoms of all other recent nummulitids (Holzmann et al., 2006); this allows the broadest depth distribution within the family. Hence, due to its long evolutionary history, ecological adaptability and characteristic internal morphology, the genus *Heterostegina* is of great interest for biostratigraphic as well as palaeoenvironmental application. Using its sole recent representative in an actuopalaeontological approach might yield great information on morphometry and growth of the whole subfamily. Hence, the following chapters add up to the broad knowledge of environmental dependence of test morphology of nummulitids.

The sequence of chamber volumes in some LBF has been reported to oscillate around theoretical growth functions in larger foraminifera (Briguglio and Hohenegger, 2014). In chapter one, a study following the instructions of (Hohenegger and Briguglio, 2014) has been conducted on *H. depressa* specimens of naturally grown and laboratory conditions to test whether such oscillations reflect environmental oscillations. Since stable culture conditions should inhibit any environmentally induced oscillatory growth. In chapter two, the current biometric system is reevaluated by applying it on megalospheric tests of *H. depressa* sampled along a water depth transect (5-90 meters) to test, if the range of different living morphotypes along environmental or geographic gradients within this single species might span the differences among fossil evolutionary lineages.

Chapter three of this thesis explores how environmental and biogeographic dependences of equatorial and axial test morphologies in *Heterostegina* can be quantified by utilizing growth-independent function and growth-invariant characters, improving reconstruction of bathymetric and palaeobiogeographic distribution.

In chapter four this approach is used to investigate heterosteginid test geometry in axial sections by quantifying the continuous test flattening of *H. depressa* along the water depth range and elaborating the underlying factors for ecologically driven morphological changes.

References

Banner, F.T., Hodgkinson, R.L., 1991. A Revision of the Foraminiferal Subfamiliy *Heterosteginae*. Revista Espanola de Micropaleontologia 23, 101-140.

Beavington-Penney, S.J., Racey, A., 2004. Ecology of extant nummulitids and other larger benthic foraminifera: applications in palaeoenvironmental analysis. Earth-Science Reviews 67, 219-265.

BouDagher-Fadel, M.K., 2008. Evolution and geological significance of larger benthic foraminifera. Elsevier.

Briguglio, A., Hohenegger, J., 2009. Nummulitids hydrodynamics: an example using Nummulites globulus Leymerie. Bollettino della societa paleontologica italiana 48, 105-111.

Briguglio, A., Hohenegger, J., 2014. Growth oscillation in larger foraminifera. Paleobiology 40, 494-509.

Hallock, P., 1985. Why are larger foraminifera large? Paleobiology 11, 195-208.

Hallock, P., 1988. The role of nutrient availability in bioerosion: consequences to carbonate buildups. Palaeogeography, Palaeoclimatology, Palaeoecology 63, 275-291.

Hallock, P., Pomar, L., 2008. Cenozoic evolution of larger benthic foraminifers: paleoceanographic evidence for changing habitats, Proceedings of the 11th International Coral Reef Symposium, Ft. Lauderdale, Florida, pp. 16-20.

Hallock, P., Röttger, R., Wetmore, K., 1991. Hypotheses on form and function in foraminifera. Biology of Foraminifera. Academic, 41-72.

Hallock, P., Lidz, B.H., Cockey-Burkhard, E.M., Donnelly, K.B., 2003. Foraminifera as bioindicators in coral reef assessment and monitoring: the FORAM index, Coastal Monitoring through Partnerships. Springer, pp. 221-238.

Hohenegger, J., 2000. Coenoclines of larger foraminifera. Micropaleontology, 127-151.

Hohenegger, J., 2004. Depth coenoclines and environmental considerations of western Pacific larger foraminifera. The Journal of Foraminiferal Research 34, 9-33.

Hohenegger, J., 2006. The importance of symbiont-bearing benthic foraminifera for West Pacific carbonate beach environments. Marine Micropaleontology 61, 4-39.

Hohenegger, J., 2009. Functional shell geometry of symbiont-bearing benthic Foraminifera. Galaxea, Journal of Coral Reef Studies 11, 81-89.

Hohenegger, J., 2011a. Larger foraminifera: Greenhouse Constructions and Gardeners in the Oceanic Microcosm. The Kagoshima University Museum, Japan, Kagoshima.

Hohenegger, J., Briguglio, A., 2014. Methods for estimating growth pattern and lifetime of foraminifera on chamber volumes, in: Kitazato, H., Bernhard, J. (Eds.), Experimental Approaches in Foraminifera: Collection, Maintenance and Experiments. Springer book, Environmental Science Series, Tokyo, pp. 29-54.

Holzmann, M., Hohenegger, J., Pawlowski, J., 2003. Molecular data reveal parallel evolution in nummulitid foraminifera. J Foramin Res 33, 277-284.

Holzmann, M., Berney, C., Hohenegger, J., 2006. Molecular identification of diatom endosymbionts in nummulitid Foraminifera, Symbiosis. Balaban Publishers, pp. 93-101.

Hottinger, L., 1977a. Distribution of larger Peneroplidae, *Borelis* and Nummulitidae in the Gulf of Elat, Red Sea. Utrecht Micropaleontological Bulletins 15, 35-109.

Hottinger, L., 1977b. Foraminifères operculiniformes. Éditions du Muséum.

Hottinger, L., 2005. Geometrical constraints in foraminiferal architecture: Consequences of change from

planispiral to annular growth. Stud Geol Polon 124, 99-115.

Hottinger, L., 2006a. Illustrated glossary of terms used in foraminiferal research (on-line): Museum of Natural History. CH.

Hottinger, L.C., 2000. Functional Morphology of Benthic Foraminiferal Shells, Envelopes of Cells beyond Measure. Micropaleontology 46, 57-86.

Langer, M.R., Lipps, J.H., 2003. Foraminiferal distribution and diversity, Madang reef and lagoon, Papua New Guinea. Coral reefs 22, 143-154.

Lee, J., 2006. Algal symbiosis in larger foraminifera. Symbiosis 42, 63-75.

Lee, J.J., Hallock, P., 1987. Algal Symbiosis as the Driving Force in the Evolution of Larger Foraminiferaa. Annals of the New York Academy of Sciences 503, 330-347.

Lee, J.J., Anderson, O.R., 1991. Symbiosis in foraminifera. Biology of Foraminifera. Academic Press, London 1, 157-220.

Leutenegger, S., 1977. Reproduction cycles of larger foraminifera and depth distribution of generations. Utrecht Micropaleontological Bulletins 15, 27-34.

Pomar, L., Morsilli, M., Hallock, P., Bádenas, B., 2011. Internal waves, an under-explored source of turbulence events in the sedimentary record. Earth-Science Reviews 111, 56-81.

Racey, A., 1992. The relative taxonomic value of morphological characters in the genus *Nummulites* (Foraminiferida). Journal of Micropalaeontology 11, 197-209.

Reiss, Z., Hottinger, L., 1984. The Gulf of Aqaba: ecological micropaleontology. Springer Science & Business Media.

Ross, C.A., 1974. Evolutionary and ecological significance of large calcareous Foraminiferida (Protozoa), Great Barrier Reef, Proceedings of the Second International Coral Reef Symposium, pp. 327-333.

Röttger, R., 1974. Larger foraminifera: Reproduction and early stages of development in *Heterostegina depressa*. Marine Biology 26, 5-12.

Röttger, R., Krüger, R., de Rijk, S., 1990. Trimorphism in foraminifera (Protozoa)—verification of an old hypothesis. European journal of protistology 25, 226-228.

Serra-Kiel, J., Hottinger, L., Caus, E., Drobne, K., Ferrandez, C., Jauhri, A.K., Less, G., Pavlovec, R., Pignatti, J., Samso, J.M., 1998. Larger foraminiferal biostratigraphy of the Tethyan Paleocene and Eocene. Bulletin de la Societé géologique de France 169, 281-299.

Uthicke, S., Nobes, K., 2008. Benthic Foraminifera as ecological indicators for water quality on the Great Barrier Reef. Estuarine, Coastal and Shelf Science 78, 763-773.

Chapter 1 (published in *Marine Micropalaeontology*)

GROWTH OF *HETEROSTEGINA DEPRESSA* UNDER NATURAL AND LABORATORY CONDITIONS

***Wolfgang Eder[1]** , Antonino Briguglio[2], Johann Hohenegger[1]

[1] University of Vienna, Department of Palaeontology, Althanstrasse 14, 1090, Vienna, Austria

[2] Universiti Brunei Darussalam, Faculty of Science, Jalan Tungku, BE1410, Brunei Darussalam

***corresponding author:** wolfgang.eder@univie.ac.at, +0043 1/427753563

Keywords – larger benthic foraminifera, tomography, cyclicity, biometry, biological oscillators

Highlights: three-dimensional internal visualisation – testing the lunar and environmental influence on foraminiferal ontogeny – growth of larger benthic foraminifera can be used as deep time palaeoenvironmental proxies

Abstract

The use of micro-computed tomography (µCT) provides a unique opportunity to look inside the shells of larger benthic foraminifera to investigate their structure by measuring linear and volumetric parameters. For this study, gamonts/schizonts and agamonts of the species *Heterostegina depressa* d'Orbigny were examined by µCT; each single chamber's volume was digitally measured. This approach enables cell growth to be recognised in terms of chamber volume sequence, which progressively increases until reproduction occurs. This sequence represents the ontogeny of the foraminiferal cell and has been used here to investigate controlling factors potentially affecting the process of chamber formation. This is manifested as instantaneous or periodic deviations of the realised chamber volumes derived from modelled growth functions. The results obtained on naturally grown specimens show oscillations in chamber volumes which can be modelled by sums of sinusoidal functions. A set of functions with similar periods in all investigated specimens points to lunar and tidal cycles.

To determine whether such cyclic signals are genuine and not the effects of a theoretical model, the same analysis was conducted on specimens held in a closed laboratory facility, as they should not be affected by natural environmental effects. Surprisingly, similar cyclicities were observed in such samples. However, a solely genetic origin of these cycles couldn't be verified either. Therefore, detailed analysis on the phase equality of these growth oscillations have been done. This approach is pivotal for proving that the oscillatory patterns discovered in LBF are indeed genuine signals, and on how chamber growth might be influenced by tidal currents or lunar months.

1. Introduction

Larger benthic foraminifera (LBF) are an informal group of benthic, symbiont-bearing, marine shallow-water foraminifera that commonly possess a volume larger than 3 mm³ (Ross, 1974). They host phototrophic algal symbionts within their shells, thus functioning as greenhouses (Lee and Hallock, 1987; Lee, 2006; Hohenegger,

2011a). The need to provide their symbionts with sufficient light, restricts LBF to the photic zone, forcing LBF to build shells in equilibrium with the physical constraints of their environment such as hydrodynamic energy, light penetrations or nutrient influx (Hohenegger, 2004; Briguglio and Hohenegger, 2009, 2011b). The complexity, beauty and giant size of these tests has long attracted scientific interest and revealed interesting data on the biology and ontogeny of these protists (Lee et al., 1979; Hottinger, 1982; Hallock, 1985; Beavington-Penney and Racey, 2004; Ferrandez-Canadell et al., 2014). Several studies on the functional morphology and external ornamentation of the shells yielded important information on their ecological niches and distribution (Renema and Troelstra, 2001) in terms of water depth (Hottinger, 2006b), trophic resources (Hallock, 1988) and light intensity (Hohenegger, 2009). According to Hohenegger (2004), primary ecological factors correlate in a non-linear or discontinuous way to water depth. Temperature is an important factor controlling the distribution of most LBF; the critical temperature of their habitat should never fall below 14°C. In tropical and subtropical regions, the water depth characterising this temperature limit is much deeper than the depth limit based on light.

Light intensity plays a very important role in influencing the water depth distribution of larger benthic foraminifera. Accordingly, the different species occupy various niches along the light gradient (Hohenegger, 2000). In *Heterostegina depressa,* light is noted to be an inverse restriction, since it copes better with low light conditions than with high light conditions (Nobes et al., 2008). Since light intensity changes not only with depth (different penetration of wavelengths) but is also influenced by different factors of water quality (e.g., content of inorganic and organic particles, heightened turbidity, submarine topography), a general correlation between water depth and species distribution is difficult to approach (Hallock et al., 2003; Hohenegger, 2004). Uthicke and Nobes (2008) showed that not all symbiontic larger foraminifera are equally influenced by a change in water quality. For *H. depressa* no distributional changes in accordance with water quality could be found by the authors. Additional, they emphasize the connection between attenuation of light and lower depth limit of foraminifera.

Wind-induced hydrodynamic motion is one major factor, which can be correlated directly to water depth because it decreases with depth. This dependency, however, varies due to changing wind intensities and the presence of sublittoral and/or tidal currents. For unidirectional hydrodynamics (e.g., tidal and ocean currents) this depth correlation can be further altered by local topography and sea bottom roughness (Hohenegger, 2004).

Apart from that, internal waves can periodically alter temperature and nutrient conditions of meso- and oligophotic biotas (Hallock and Pomar, 2008). Generally, internal waves can be observed along discontinuities within the water columns (e.g., thermoclines and pycnoclines). For shallow water environments surface tides and storms might start internal waves at bathymetric breaks. However while surface currents influence shallow water environments on a larger scale, the influence of internal waves can be restricted to smaller areas (Pomar et al., 2011). Thus, LBF communities can regionally differ at the same water depth due to different energetic conditions and regionally altered water composition. This can be closely observed when looking at different localities of the indo-pacific and indo-malayan communities (Ekman, 1953). By looking at west pacific carbonatic and oligotrophic environments, like Okinawa and Belau, quite similar distributional patterns can be observed. However, for Hawaii, which is a more marginal indo-pacific site, a lack of the shallowest subtidal community has been documented (Hallock, 1984). In Okinawa and Belau those are normally dominated by calcarinid taxa. Yet, Hawaii can be seen as a subset of the Indo-Pacific larger benthic foraminiferal community (Hallock, 1984; Hohenegger, 2000).

In comparison communities of the indo-malayan regions, like on the Spermonde Archipelago, show also similar distribution, albeit with lower diversity and shallower water depth limits. This is due to higher runoff and higher

light attenuation in the mesotrophic mixed siliciclatsic environments of the archipelago (Renema and Troelstra, 2001).

Apart from the earlier mentionted factors influencing distribution of larger benthic foraminifera, also seasonal ecological stability (e.g., salinity, influx, nutrients) should be considered as an important factor (Hallock, 1984; Hohenegger, 2000; Renema and Troelstra, 2001).

As the substrate inhabited by LBF is affected by water energy, differences in sediment conditions – firm and soft substrates in combination with the complex interaction of all the factors above – require these organisms to diversify their life strategies. This is reflected in their test morphologies: During the construction of their shell, LBF are strongly influenced by their surroundings, and are forced to reach an equilibrium between their internal physiological need (e.g., growth) and abiotic and biotic external factors. This is reflected within each growth step (i.e., each chamber) of their life (Hohenegger, 2004). Researchers have therefore focused on the chamber-building process and recorded calcification time and symbionts' movement (Spindler and Röttger, 1973), observed calcification potential under different geochemical conditions in relation to climatic variation (Fujita et al., 2011; Hosono et al., 2012) and even confirmed strong pH variation during the chamber-building process (De Nooijer et al., 2009). All this information reveals that the calcification of a new chamber is a complex event that occurs only if many parameters are simultaneously conducive for calcification. This should include also a positive net rate of symbiotic photosynthesis and carbonate availability. However, the exact timing of the chamber-building process is still currently under research and the correlation between chamber formation and environmental conditions is still unknown. Most of the current research deals on how the foraminiferal growth differs along with environmental changes (Prazeres et al., 2015, among others) instead of looking how they normally grow. It is known from cultivation experiments on *H. depressa* that megalospheric specimens apparently follow a quite strict pattern of chamber-building events (Röttger, 1972), therefore suggesting weak correlation with environmental variations.

Chamber growth is intrinsically controlled by genetic factors, but constantly or abruptly changing environmental conditions might influence this process. However the exact trigger of foraminiferal biomineralisation events is unknown so far. Hence, the degree of morphogenetic variability can be higher than caused by the genetic programme and could vary among taxa. Some taxa may have very strict "morphogenetic algorithms", while others are more susceptible to environmental factors (Tyszka, 2004). Accordingly, changes in chamber size and shape during the chamber-building process might serve as information sources to investigate environmental conditions in the past, using living LBF as control fauna.

The present study concentrates on chamber size, represented by volume measurements, using micro-computed tomography (µCT). This technique enables estimating the volume of each chamber within single tests, revealing the ontogeny of the cell.

Recently, the sequence of chamber volumes has been reported to oscillate around theoretical growth functions. These oscillations have been shown to correlate with tidal, lunar and environmental signals (Briguglio and Hohenegger, 2014; Hohenegger and Briguglio, 2014); to test whether such oscillations reflect environmental oscillations, the same study has been conducted on specimens naturally grown and cultivated under laboratory conditions. The stable culture conditions should inhibit any environmentally induced oscillatory growth. In addition, the comparison between two indo-pacific locailites (Okinawa and Hawaii) will test how strong geographical and seasonal differences are reflected in the growth oscillations of *H. depressa*.

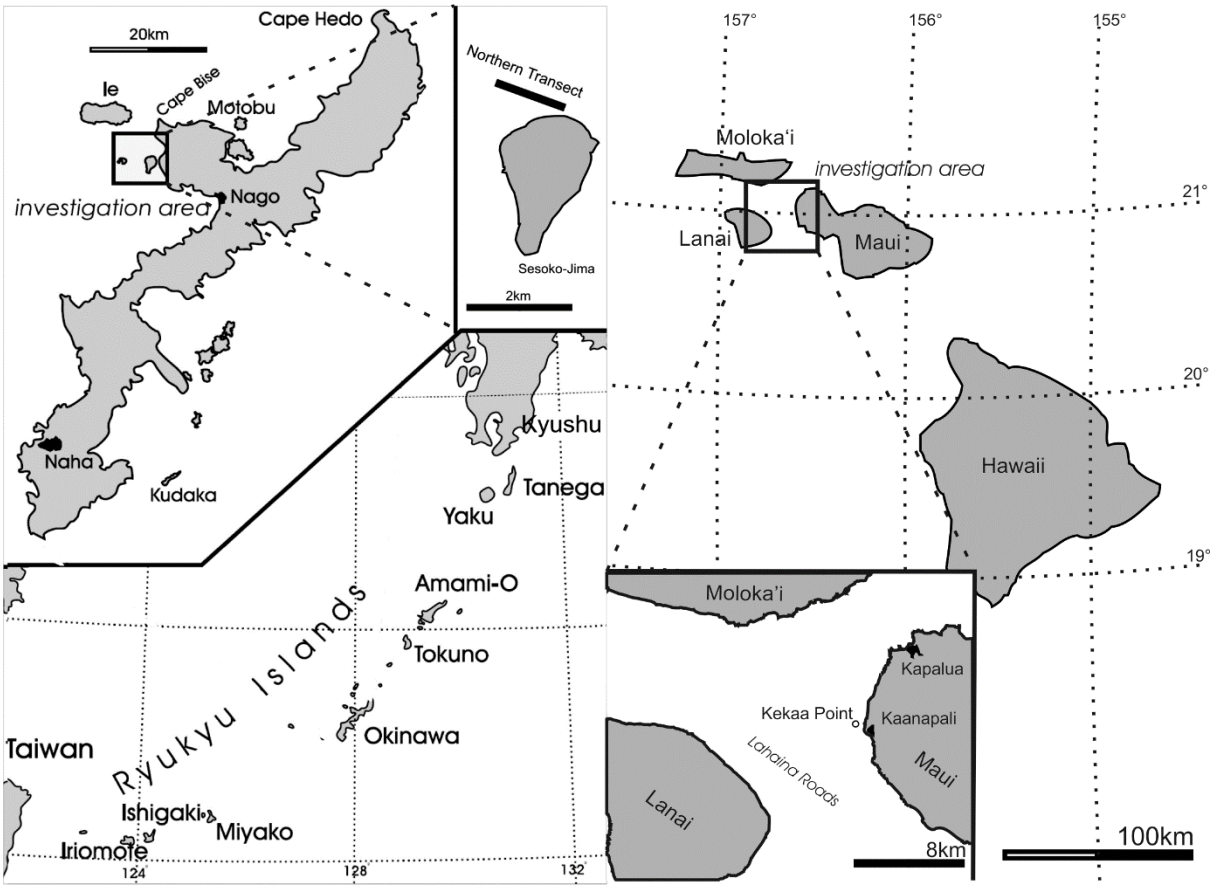

Figure 1 - Maps of the sample localities: a. Sample locality Sesoko-Jima: Okinawa, showing transect A and B; after Hohenegger et al. (1999) B. Sketch of western Maui coastline: sampling area accented.

2. Materials and Methods

The species selected for these analyses is *Heterostegina depressa* d'Orbigny: it constructs chambers divided into chamberlets, which are arranged in a coil that can be approximated by a modified logarithmic spiral (Hohenegger 2011, Fig. 3). This shell structure and its biological implications are broadly discussed in the literature (Spindler and Röttger, 1973; Hottinger, 2000; Briguglio et al., 2011a; Hohenegger, 2011b). Additionally, Röttger (1972) published growth data reporting the chamber-building rate for a time span of one year (see figs 1 and 4 in Röttger, 1972). This data set has been used to estimate the lifetime and growth pattern of this species using growth functions (i.e., the Michaelis - Menten function) (Hohenegger and Briguglio, 2014), which have been used to estimate the environmental cycles in the analyses presented here. In fully grown individuals, the average chamber number of 60 for gamonts/schizonts (all investigations have been done on empty tests, therefore the megalospheric tests are called gamonts/schizonts) and 100 chambers for agamonts is sufficient to detect cycles.

Fifteen specimens were used in this work (see Table 1, in Supplementary Data). The samples consist of six naturally grown gamonts/schizonts collected from Maui, Hawaii (D1-68, D2-68, D3-68), and Sesoko-Jima, Japan (A1, A2, A3), one naturally grown agamont from Sesoko-Jima (B1) and four naturally grown agamonts from Hawaii (B13, B30, B44, B69) as well as four gamonts/schizonts cultivated by Röttger in 1991 at the University of Kiel, Germany (R1, R2, R3, R6).

The Hawaiian specimens used here, belong to the private collection of Röttger and Krüger. The samples originating from Maui, Kekaa Point (20° 55' 38.38" N, 156° 41' 55.91" E, 20.7. - 25.7.1991; Fig. 1) were dredged between 15

to 60 meters water depth and split into 0.8, 2.8 and 5.0 mm fractions.

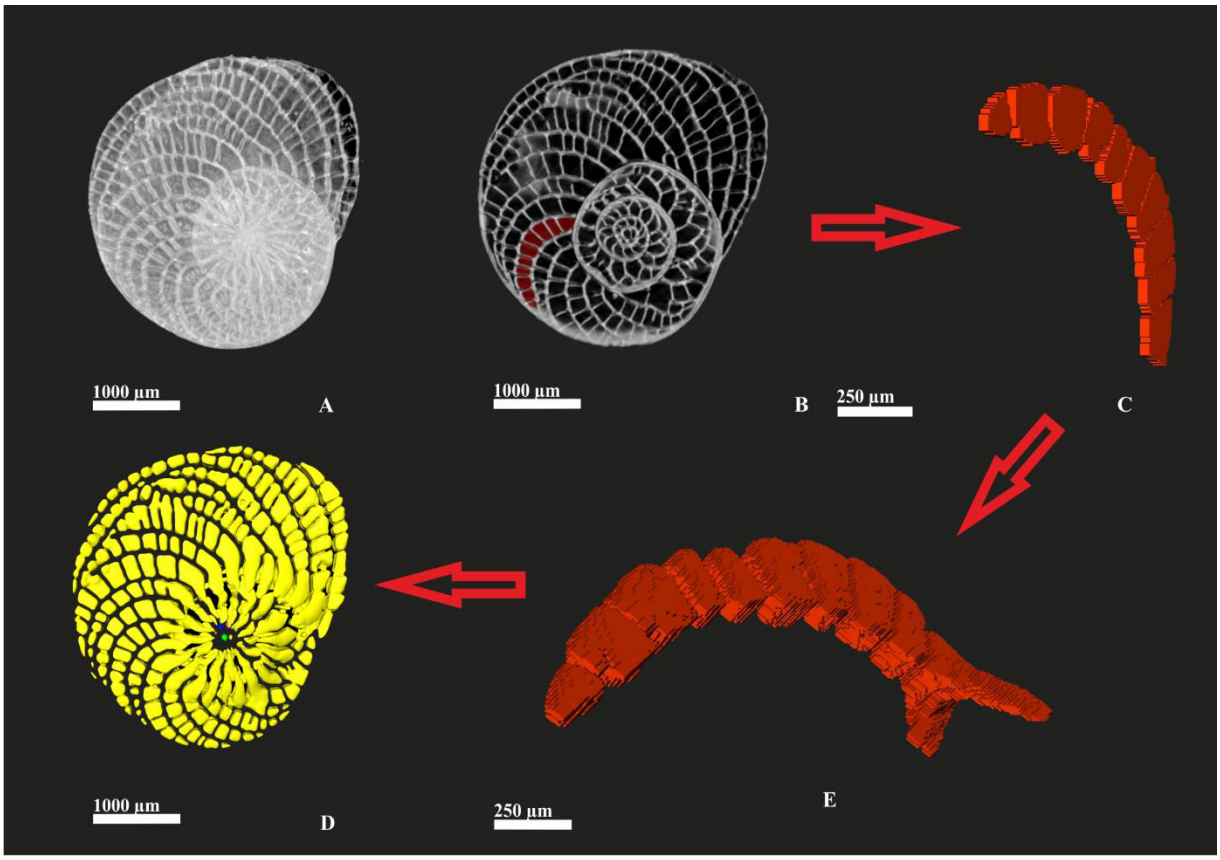

Figure 2 - Closer examination of the segmentation process: A: test of specimen D1-68, B: equatorial tomographic slice C: unrendered model of a chamber, E: single layer of voxels, D: reconstruction of the chamber volume sequence.

The gamonts/schizonts used in this study originate from the 2.8 mm fraction, which were collected at 40 m water depth. They originate from a living and “fresh”-dead assemblage (Röttger, pers. comm.). The “fresh”-dead specimens might have originated from an earlier reproduction season or were transported from other locations. Only the fraction above 5 mm in size was searched for living agamonts, which is where the investigated gamonts come from. The exact water depth of those specimens is unknown (Krüger, 1994). According to Krüger (1994), 113 agamonts were sampled at Kekaa Point and maintained at 22°C in clear "open ocean water". Afterwards, they were shipped to the University of Kiel and maintained at 25°C, 450 Lux at a day-night interval of 12/12 h. Half synthetic seawater was used as a culture medium; the mixture was based on Helgolandian seawater (northern Germany) with 30 to 33 ‰ salinity and was enriched with concentrated "simple synthetic seawater"(sensu Hauenschild, 1962), enhancing the salinity to 35‰ (Krüger, 1994). The gamonts/schizonts R1, R2, R3 and R6 originated after 76 days of captivity (Krüger, 1994) from one of those agamonts kept in culture from 12.08.1991 until their reproduction on 27.10.1991.

The specimens A1, A2, A3 and B1 were collected at Sesoko-Jima (26° 39' 38.776" N, 127° 51' 56.28" E, 1.6. - 31.7.1996, Fig. 1) around 20 m water depth by SCUBA at transect A described in Hohenegger et al. (1999).

Micro-computed-tomography (µCT), recently applied to observe, quantify and study foraminiferal shells (Banner and Hodgkinson, 1991; Speijer et al., 2008; Briguglio et al., 2011a; Görög et al., 2012; Briguglio et al., 2013; Schmidt et al., 2013), was used to more closely examine the internal structure of *H. depressa* by measuring

volumes of the chamber sequences within each individual.

Images were taken with the high-energy scanner Skyscan 1173 at the Department of Palaeontology of the University of Vienna (see Briguglio et al. 2014, Fig. 4.1). The dedicated software Amira 5.4.3 VSG was used to work on the three-dimensional models obtained.

The most complete specimens of *H. depressa* were chosen as they yield the highest amount of chambers.

2.1 Statistical Analysis

Chamber lumina (sensu Hottinger, 2006) of each specimen were extracted from the three-dimensional model and their volume calculated; these were summed up to obtain a cumulative distribution representing the overall cell growth (Fig. 3).

This dataset can be fitted by different functions explaining limited growth (see Hohenegger et al., 2014, Fig. 3.3). The generalised logistic function (Eq. 1, Richards, 1959) allows the best modelling of growth in naturally grown specimens.

$$V_e = A + (K - A)/(1 + Qe^{-B(j-M)})^{1/v} \qquad (1)$$

The six parameters *A*(lower asymptote), *K* (upper asymptote), *Q* (relation to *Ve(0)*), *B* (growth rate), *M* (represents the starting time t_0) and *v* (position of maximal growth) were estimated using SPSS statistics v. 18.0 (see Table 2 in the Supplementary Data). Additionally, an exponential fit for the initial chambers of the gamonts/schizonts (e.g., up to the first 25 chambers) allows a better comparison of the individual cell growth, because of strong growth deviations in later chambers. This aberrance is shown as an increasing fluctuation in later chamber volumes. Therefore, the datasets include for most specimens the chambers of the first to second spiral and represent the growth before the full onset of the "maturo-evolute" growth stage (sensu Banner and Hodgkinson, 1991). This is done using the equation

$$V_e = a\, e^{bj} \qquad (2)$$

The parameters *a* and *b* of the exponential function were estimated using SPSS 18 (see Table 2). Additionally, a one way ANOVA combined with a post-hoc test was done on the above parameters also using SPSS 18.0.

Afterwards the first derivatives of the V_e values, gained by the generalised logistic function, for each chamber were computed to compare these to the observed chamber volumes, as seen in Figure 3.

To quantify differences between the observed volume and the theoretical (expected) ones, standardised residuals of the chamber volumes were obtained using Eq. 3

$$d_j = \frac{v_{oj} - v_{ej}}{v_{ej}} \qquad (3)$$

where v_{oj} represents the measured (observed) chamber volumes and v_{ej} the first derivative of the generalised logistic function for the j^{th} chamber. Residuals depict how intensively the predicted data of the regression model deviate from the measured data and may represent periodic or instantaneous deviations from the estimated growth function.

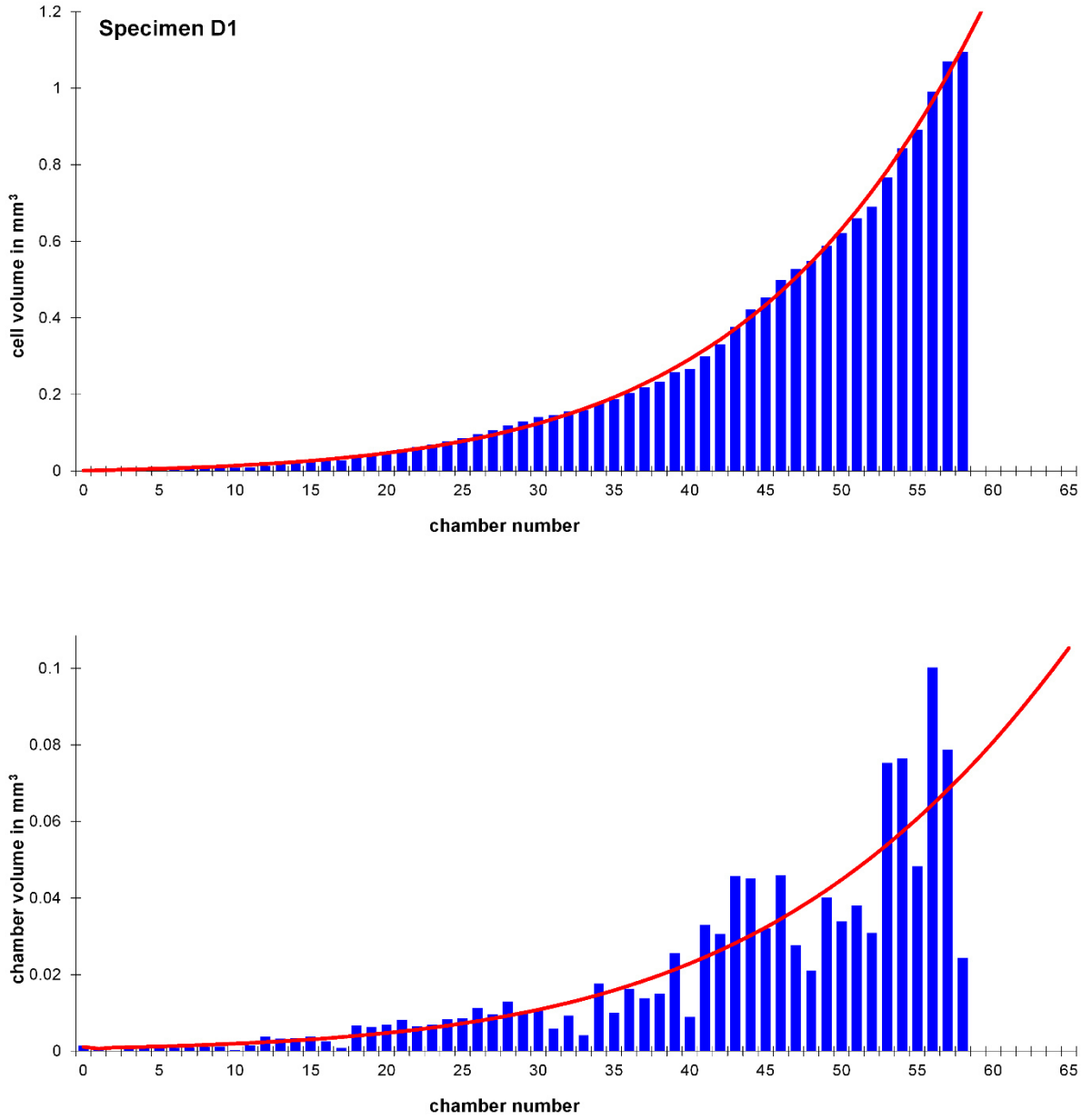

Figure 3 - Comparison of the measured cell volumes: The observed cell volume (blue) of specimen D1 (gamont/schizont – Kekaa Point) against the estimated cell volume (red), and of the measured chamber volume (blue) against the estimated chamber volume (red). The oscillations of the measured values around the theoretical growth is visible.

To obtain time-dependent periodic functions, this dataset has to be related to the chamber-building rate in order to reveal oscillations and cyclic patterns related to time in days.

The chamber-building rate is based on laboratory observations of *H. depressa* (Röttger, 1972) and can be approximated by the power function that poses as a mean chamber building rate. Therefore individual chamber building rates might deviate from the given function (Fig. 4).

However, the used dataset is limited to one experimental setup with specimens originating from a single locality. Therefore, the difference in population or environmental factors that change the timing of chamber-building events cannot be taken into consideration. Based on this assumption, the following equation can be used to express the chamber-building rate.

$$j = 1.4t^{0.64} \quad (4)$$

where t is the time when chamber j has been built. Equation (4) must be inverted to obtain the timing of chamber formation, resulting in

$$t_j = (j/1.4)^{1/0.64} \quad (5)$$

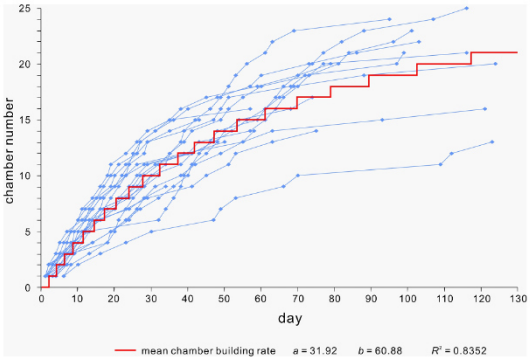

Figure 4 - Chamber building rate of 20 *H. depressa* specimens from laboratory cultivation and fit by Michaelis-Menten function (from Hohenegger & Briguglio 2014).

Since no data are available on chamber-building rates for agamonts, a theoretical growth function was estimated based on gamont/schizont data, considering that the chamber-building rate in agamonts should differ from gamonts/schizonts. During the earliest life phases the agamont growth rate should be accelerated, while later life stages show adaptations to a *K*-strategy (Hottinger, 1982, 2000; BouDagher-Fadel, 2008). Power regression was used to approximate to limited functions, like the Michaelis-Menten or Bertalanffy functions, to gain a function for chamber-building rates of *H. depressa* agamonts for a life span of three years. Although the actual agamont lifespan is unknown, it seems to be very close to this value (Hohenegger & Briguglio, 2014):

$$j = 4.39t^{0.5} \quad (6)$$

leading to the inverse function for the chamber-building rate in agamonts.

$$t_j = (j/4.39)^{1/0.5} \quad (7)$$

For further analyses, residuals were calculated using chamber volumes (Eq. 3) that are linearised by cubic roots. Then, cyclic patterns were sought by power spectra using Lomb periodograms combined with a sinusoidal regression model (Press et al., 1992) as well as by REDFIT spectral analysis (Schulz and Mudelsee, 2002) to check for significant cycles. An oversampling rate of 4 (by Monte Carlo integration) was used to increase the number of points in REDFIT analysis. Cycles exhibiting power > 80% χ^2 false alarm level lines were considered as significant and included in the model.

The computed sinusoidal functions contain all significant cycles with their amplitudes α, phases ϕ and periods τ. Additionally, probability p and the coefficient of determination (R^2) for these summed functions are given in the

Supplementary Data.

Importantly, the basic target of the used method is to find cycles within a given data set; this implies that cycles can be found within every data set whether they are significant or not (Banner and Hodgkinson, 1991; Press et al., 1992; Hammer et al., 2001; Schulz and Mudelsee, 2002). Therefore significant periods were also proven based on their frequency distribution. Because of different life-times expressed in chamber number n of specimen j and differing amplitude height α_{ij} of the i^{th} period, the periods τ_{ij} must not be used as single measurements giving equal weight to all periods by

$$f(\tau_{ij}) = 1 \qquad (8)$$

but should be weighted based on amplitudes a_{ij} by

$$f(\tau_{ij}) = a_{ij} \qquad (9)$$

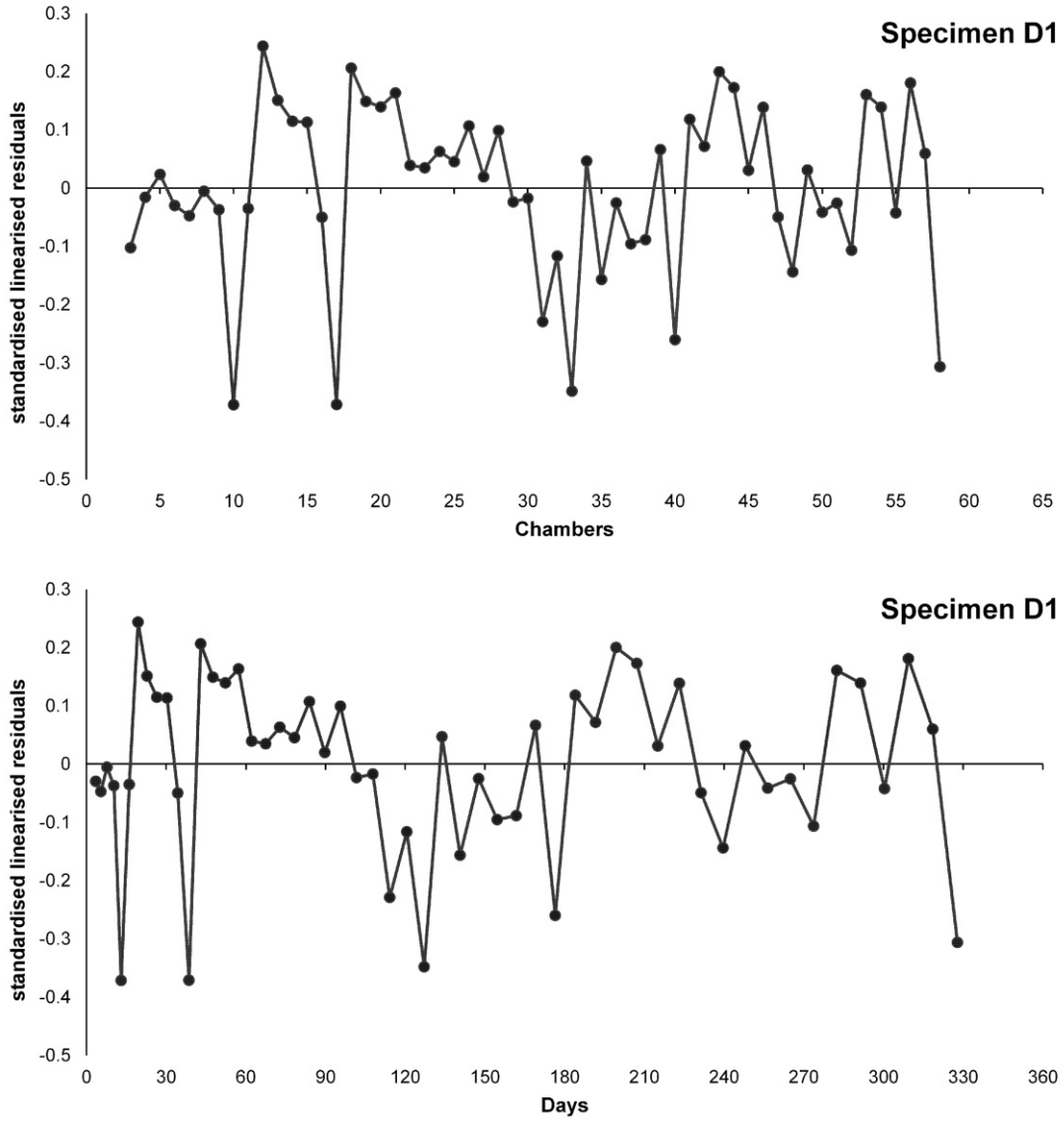

Figure 5 - Illustration of standardised and linearised residuals and their transformation from chamber number into days.

When the resulting frequency histogram of weighted periods is inhomogeneous, it confirms concentration centres around distinct and thus significant periods. Conversely, a more or less homogeneous distribution with wide ranges argues against significant periods.

Logistic functions, exponential functions and their parameters were calculated in SPSS statistics v. 18.0. REDFIT spectral analysis and sinusoidal functions were computed in PAST 3.04 (Hammer et al., 2001), and Microsoft Office EXCEL 2003 was used for other calculations.

3.Results

The most significant periodic functions of each specimen with amplitudes α, phases ϕ and periods τ, as well as R^2 for correlation and probabilities p and the parameters for the generalised logistic functions and the exponential functions for the initial spiral are given in the Supplementary Data (Tables 1 and 2). These functions describe the foraminiferal cell growth. Figures 6, 7 and 8 show the observed versus estimated cell and chamber volume of naturally grown gamonts/schizonts, laboratory-cultured gamonts/schizonts and naturally grown agamonts. Figure 9 shows a scatter plot of the parameters for the exponential fit to initial cell growth of all investigated gamonts/schizonts. These parameters have been used for a one-way ANOVA with a post-hoc test, where the results are given in the Supplementary Data.

For the observed cycles in foraminiferal growth, histograms on weighted frequencies are presented for the Hawaiian and Okinawan gamonts/schizonts and the cultivated Kiel specimens, as well as for the agamonts from Kekaa Point and Sesoko.

Periods with an average length of 14.75 (SD: 0.03), 28.6 (SD: 0.8), 75.9 (SD: 2.0), 129.8 (only present in one specimen) and 176.3 (SD: 3.2) days were the most significant in naturally grown gamonts/schizonts from Sesoko Jima (Fig. 7). For the Hawaiian gamonts/schizonts, the dominant values were 14.1 (SD: 0.5), 27.8 (SD: 0.9), 76.5 (SD: 3.3), 130.5 (SD: 3.9) and 173.8 (SD: 1.12) days (Fig. 10).

The significant periods in the cultivated gamonts do not differ from those of naturally grown ones on a large scale. These specimens showed cycles with broad ranges at an average period length of 14.8 (SD: 0.4), 27.8 (SD: 0.2) and 69.9 (SD: 4.6), but a single specimen exhibited one period at 165.6 days (Fig. 10).

The agamont of Sesoko-Jima showed short-term cycles at 12.7 (SD: 0.1) and 34.6 (SD: 1.7) days and longer significant cycles around 105.9 and 239.5 days. Similar cycles were found in the agamonts of Kekaa Point with the most significant periods around 16.4 (SD: 0.6), 28.5 (SD: 1.2), 47.2 (SD: 0.06), 74.7 (SD: 2.5) and 187.5 days (SD: 0.2) (Fig. 11).

In addition, the µCT investigation revealed that all investigated specimens cultured by Röttger in 1991 showed various internal test anomalies (Hohenegger et al., 2014) such as incomplete septula, undulated septa and the formation of large internal cavities connecting multiple consecutive chambers. Such malformations were not clearly visible from the external surface of these cultivated specimens (Krüger, 1994). Afflicted chambers have been excluded from the analysis.

4. Discussion

By measuring and computing chamber volumes and cell volume, the growth of *H. depressa* can be investigated more thoroughly than in two dimensional studies focusing on the foraminiferal growth. The chamber volume represents every growth step of the foraminiferal cell, therefore the chamber volume sequence allows detailed modelling of the cell ontogeny.

Generally speaking, the overall cell growth of *H. depressa* follows a restricted growth model, as predicted by the Gompertz (Gompertz, 1825), Michaelis-Menten (Michaelis and Menten, 1913) or Bertalanffy function (Bertalanffy, 1951). This major scheme is evident in all investigated specimens. The best fit of these observed chamber volumes is given by the generalised logistic function (Richards, 1959), which results in accurate estimation of both initial cell growth, and the successive life stages. Even though the Richards' curve allows the most precise alignment to natural growth, its complexity and high number of parameters hinders a direct comparison between different individuals. Therefore an exponential fit of the initial spiral (e.g., first 25 chambers, including pro- and deuteroloculus) was used to generate the two comparable and significant parameters *a* and *b*. growth rate. These two parameters were observed to reflect distinct information either on provenance or on ecology. In the investigated specimens the initial size showed a clear dependence on locality, as seen in Figure 9. Hawaiian gamonts/schizonts have a much larger initial size than the representatives of the Okinawan population, while the laboratory-cultured gamonts/schizonts, which originate from the Hawaiian population, show an intermediate initial size in-between the natural grown specimens of both localities. This allows two interpretations: either the different proloculus size is a genetic trait of the population and might show an evolutionary trend within the taxon; or the initial size is influenced by an inherent ecological parameter of those geographic localities. However, it is intriguing that laboratory-cultured specimens have a smaller proloculus size than their natural relatives. This might either imply that the initial size depends indeed on an ecological parameter, which couldn't be simulated in the petri-dish, or the reduced embryonic size is due to suboptimal culturing conditions.

The parameter *b* gives the increase of the growth function, meaning the growth rate. It is apparently much more similar in natural grown specimens of different localities than natural and cultured specimens originating from the same population. Therefore, it is most likely that parameter *b* has a higher ecological plasticity than parameter *a*. This might be an additional indicator for the discrepancy between simulated environments and actual natural conditions as assumed by Hohenegger et al. (2014). The complexity of ecological variables affecting the growth of LBF thus cannot be easily substituted by laboratory conditions and should always be combined with continuous field observations (Hohenegger et al., 2014).

Additional observations on the chamber volume reveals evident periodic patterns in all investigated specimens of naturally grown *H. depressa.* Periods around 14 and 29 days most frequently showed the highest significance, possibly documenting the influence of tides and lunar months on foraminiferal growth. Dependency on moonlight cycles has already been demonstrated within many marine and terrestrial metazoan groups (Winter and Sammarco, 2010; Mercier et al., 2011) and also within planktonic foraminifera based on population dynamic studies (Bijma et al., 1990; Erez et al., 1991; Bijma et al., 1994; Lončarić et al., 2005). One explanation for this correlation between foraminiferal growth and moon phases (every ~29 days) could be that the endosymbiotic microalgae hosted by the LBF have higher photosynthetic rates during full moon periods.

More complicated and speculative is the correlation between oscillations in new moon spring tides and foraminiferal growth. The semi-diurnal tidal regime of Sesoko and Hawaii have a periodicity in spring tides of half a lunar month (~14 days). Tides can produce strong and deep tidal currents, which run along the substrate layer, influencing semi-sessile benthic organisms like LBF (Hohenegger, 1999; Zuo et al., 2009). Abundant fine-grained deposits can be suspended, diminishing light intensity but increasing inorganic nutrient availability. This might affect foraminiferal endosymbiont activity.

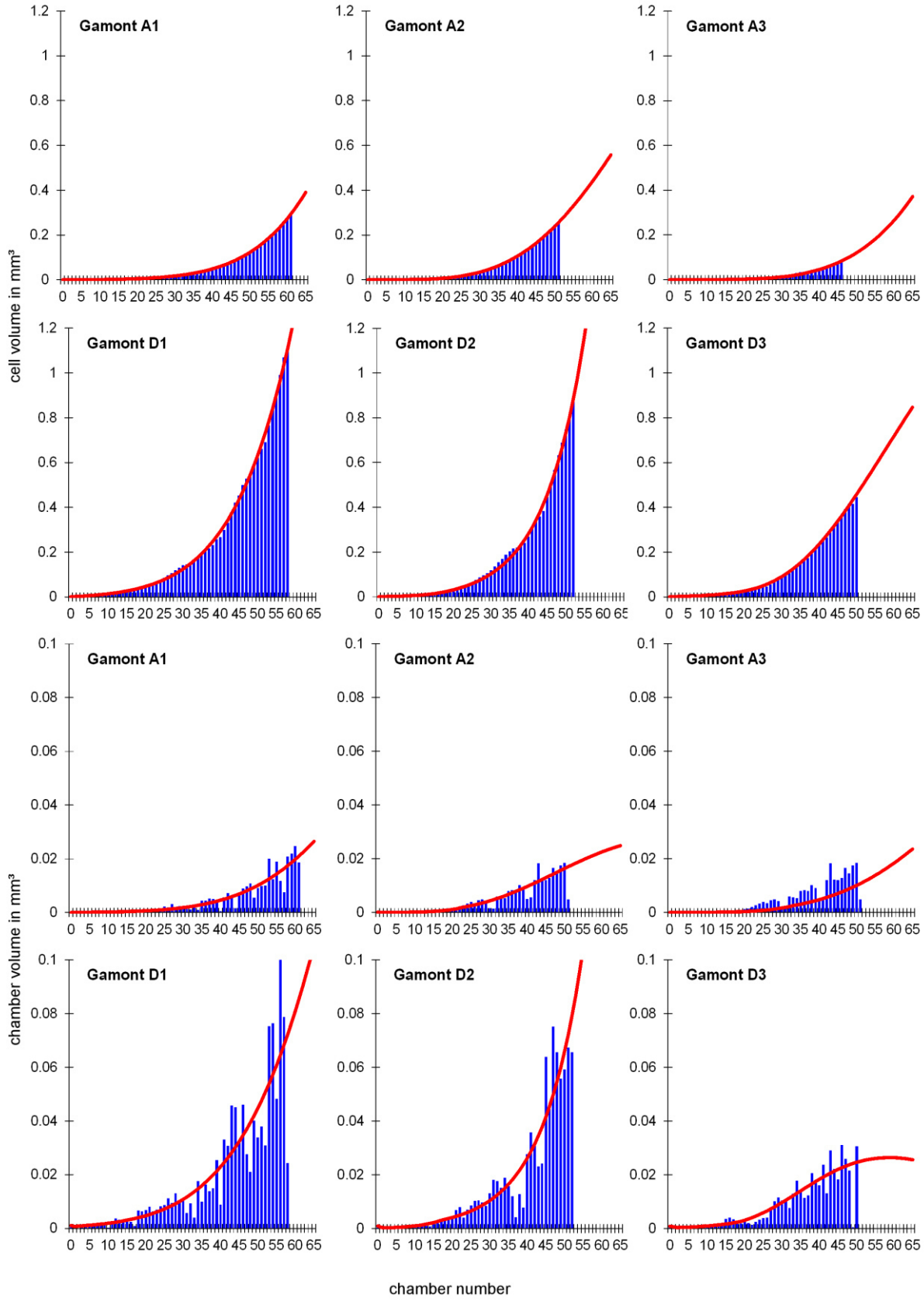

Figure 6 - Observed and estimated cell volumes and chamber volumes of all investigated naturally grown gamonts/schizonts (A1-A3: Sesoko-Jima, D1-D3: Kekaa Point)

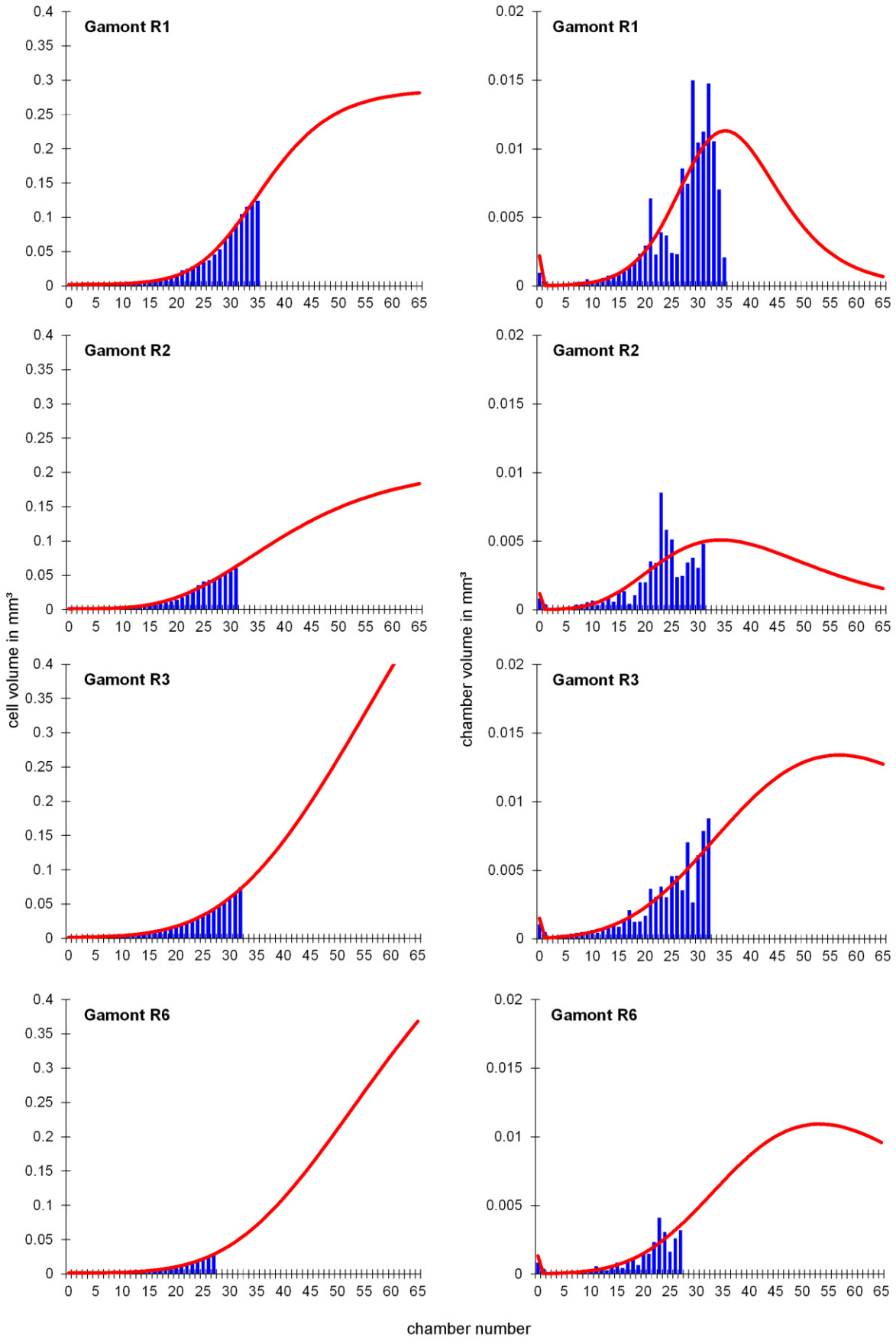

Figure 7 - Observed and estimated cell volumes and chamber volumes of all laboratory-cultured gamonts/ schizonts.

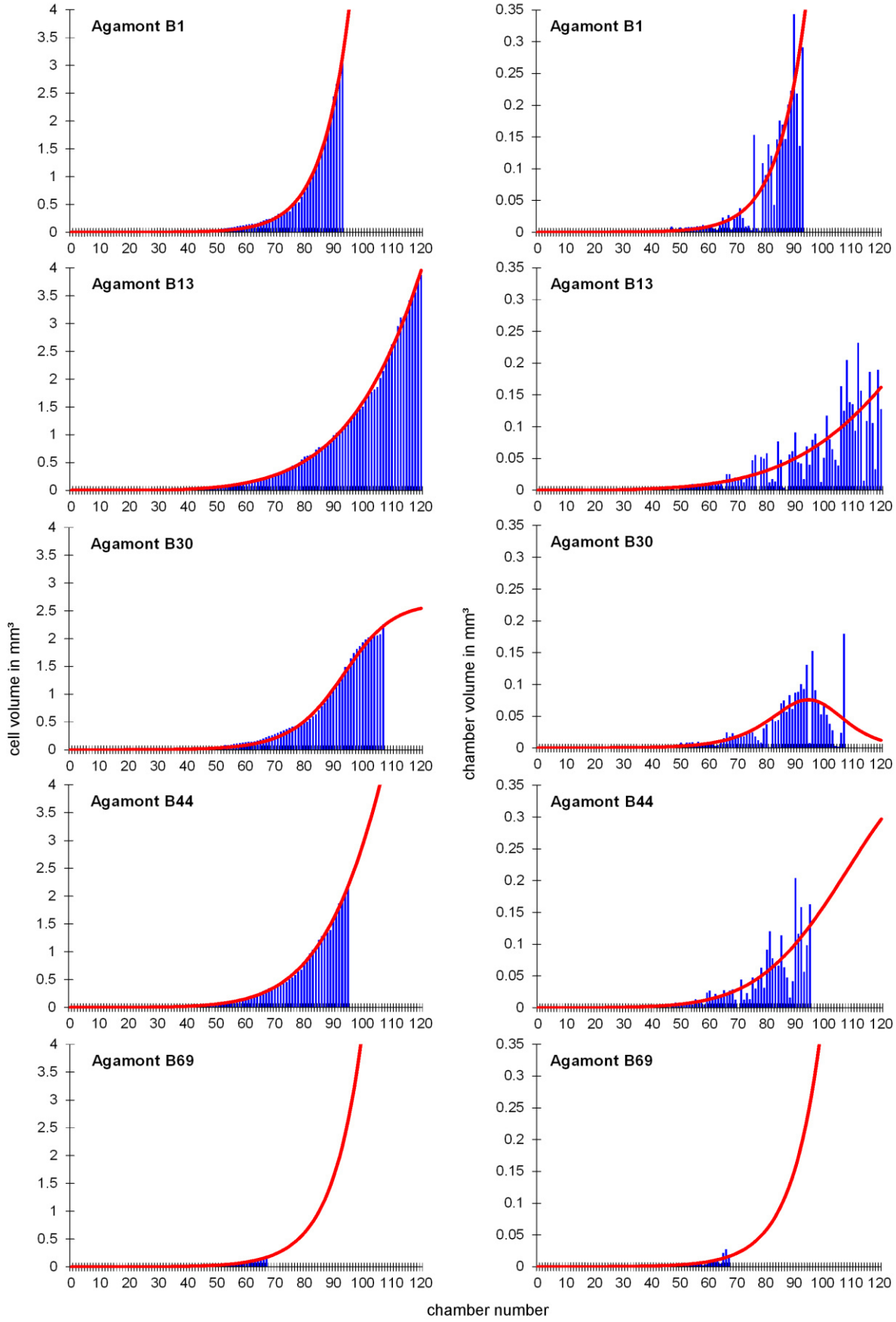

Figure 8 - Observed and estimated cell volumes and chamber volumes of all naturally grown agamonts (B1: Sesoko-Jima, B13, B30, B44, B69: Kekaa Point)

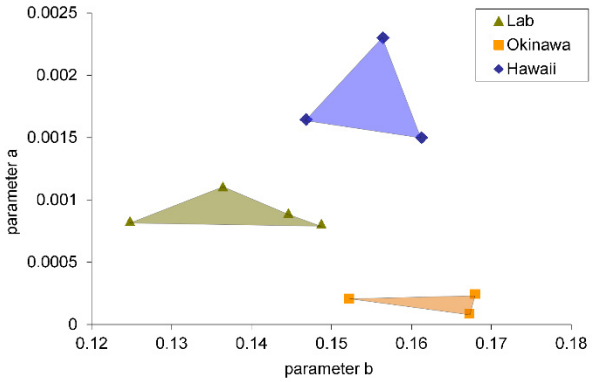

Figure 9 - Scatter plot of the parameters for the exponential fit of the first 25 chambers for all investigated gamonts/schizonts.

Apart from this quite regional tidal influence, new results of geophysical studies on the seismicity of rifting zones implicate an impact of gravitational forces on the oceans. A strong correlation between lows in ocean tides (fortnightly cycle: 14.5 days) and heightened volcanic activity at mid-ocean ridges, as well as low-magnitude earthquakes has been postulated (Tolstoy et al., 2002; Tolstoy, 2015). These events could influence sea life on a far larger and global scale.

The cycles observed in LBF growth should be the result of two corresponding effects: light intensity increase due to the moon light and light attenuation due to turbid tidal currents. Therefore, their phases should always be in a correlative context to each other, resulting in a partially constructive or destructive interference (Hohenegger & Briguglio 2014, Fig. 3.20). This correspondence of cycles around 14 and 29 days could be found in all investigated specimens, gamonts/schizonts and agamonts alike. When plotting those cycles on top of each other, the same pattern of interferences emerges as observed by Hohenegger & Briguglio (2014) (Figs. 12a & 13a, b). Besides these short-term cycles, some naturally grown specimens also show intermediate periods around 75 and 130 days (Fig. 12b). Agamonts and gamonts/schizonts from both localities exhibit 75 day cycles, while only gamonts/schizonts of both localities exhibit 130 day cycles. The most peculiar feature of these cycles is their corresponding phases and periods, also seen in short-term cycles.

The discrimination between ecological driven cycles and those created by analytical artifacts is hampered by the fact that long-term cycles might be actually the product of an artificial stacking effect of the 14 and 29 day cycles. The same is probably also true for long-term cycles around 170 to 180 days (Figs. 12c, 13c). Although further investigation on different localities with stronger and weaker seasonal changes in salinity, terrigenous influx and nutrients might allow to decipher more accuratly, which long-term cycles are genuine. Alas, the environmental and latitudinal similarity between Hawaii and Okinawa (oligotrophic carbonate plattforms) might additional hinder to see real differences in the periods of long-term cycles. Hence, further analysis from inner-tropic mesotrophic mixed siliciclastic settings, like Spermonde Archipelago, could result in different long-term cycles. This might be especially interesting for those taxa, that can adapt to a wider range of environmental parameters, like *H. depressa*. However, one of the most striking results presented here is that, in contrast to expectations, cultured specimens exhibit nearly the same periodic patterns as naturally living individuals.

This allows two possible interpretations: either growth cycles are a general characteristic of foraminiferal growth and are not environmentally controlled, or periodic growth patterns are inherited via epigenetics, but calibrated by ecological rhythmic signals as seen in pulse-coupled oscillators (Bélair, 1986; Mirollo and Strogatz, 1990).

This last interpretation considers that extrinsic rhythms, like lunar or tidal rhythm, might have positive or negative

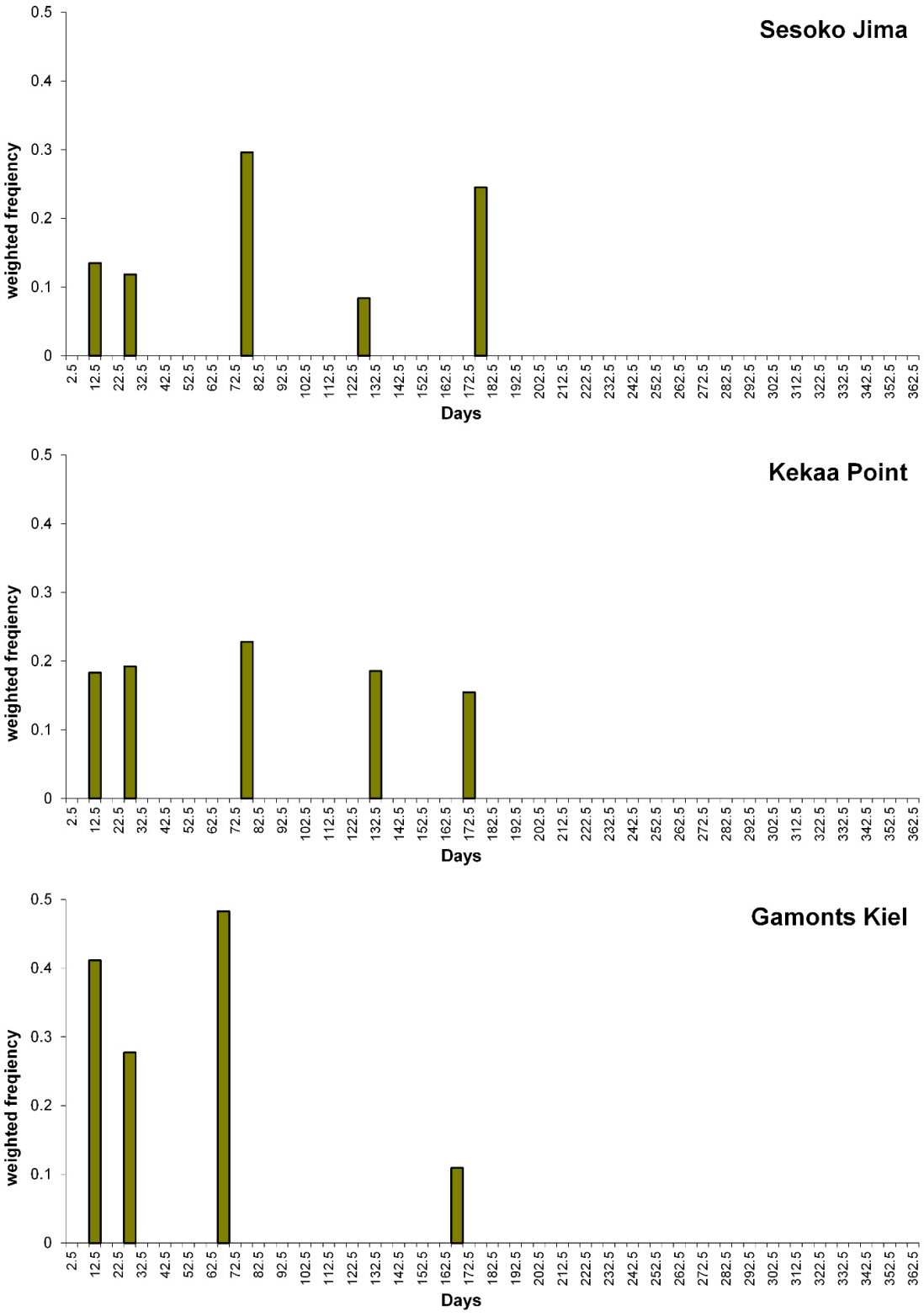

Figure 10 - Histograms of significant weighted periods for the naturally grown gamonts/schizonts of Kekaa Point and Sesoko-Jima.

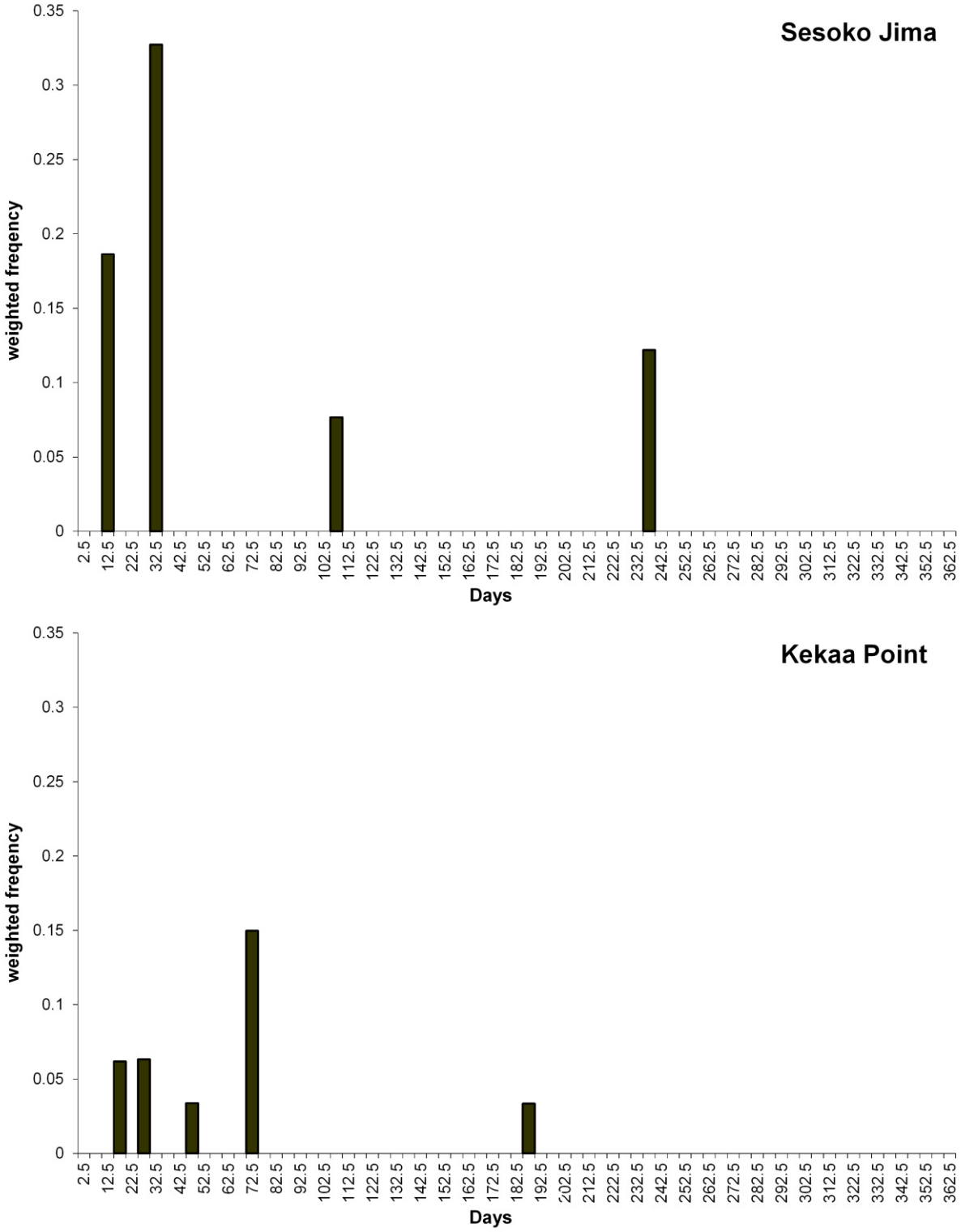

Figure 11- Histogram of weighted significant periods for the naturally grown Sesoko Jima agamont and for Kekaa Point agamonts.

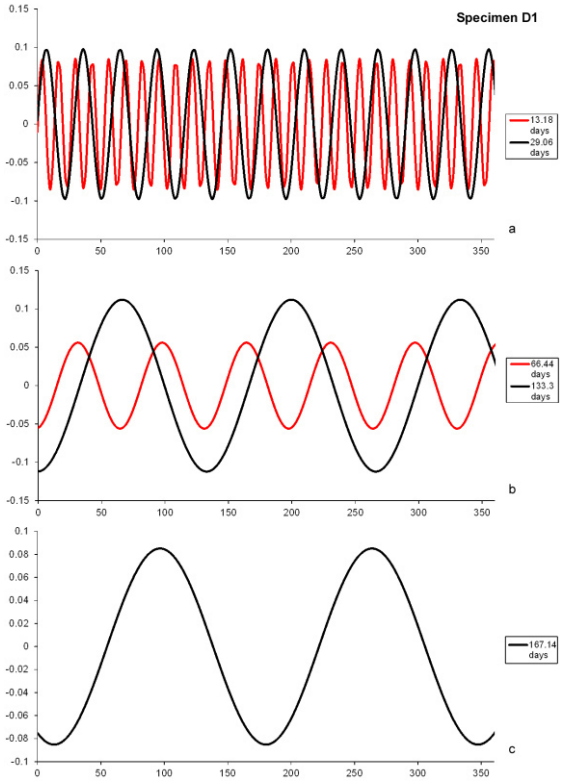

Figure 12 - Extracted cycles of specimen D1: a. short-term cycles around 14.5 and 29 days; b. in-phase long-term cycles around 70 and 130 days; c. long- term cycle around 180 days.

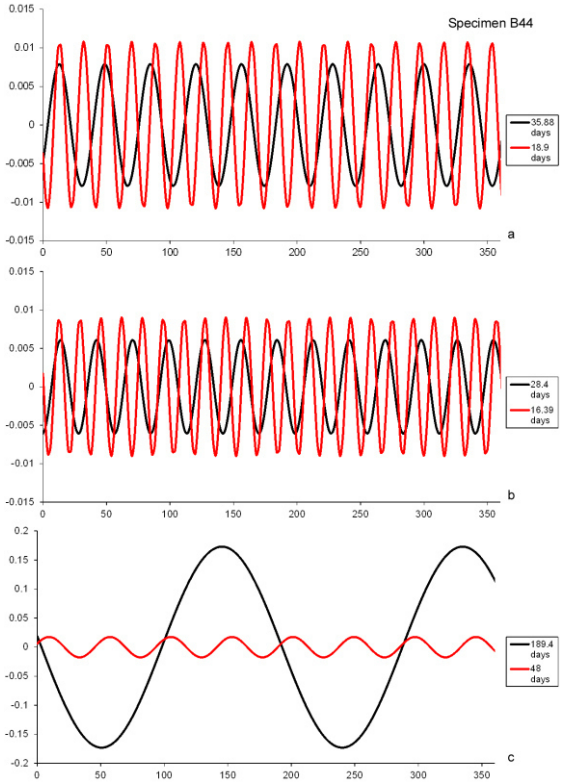

Figure 13 - Plot of separately extracted cycles of specimen B44: a & b short-term cycles around 14.5 days and 29 days, c. long- term cycles around 50 days and 180 days.

influence on the foraminiferal growth and therefore the organisms adapt and react in equilibrium with their "cyclic" environment. These reactions are afterwards inherited by an environmental maternal effect (Richards, 2006;

Räsänen and Kruuk, 2007; Richards et al., 2010) and transmitted to the next generation which still keep the cyclic growth pattern in a non-cyclic environment (e.g., petri-dish). In this way, environmentally induced cycles could become inherent growth cycles.

Furthermore, since individuals from the same locality and reproduction time should exhibit cycles with similar phases, the phase equality within the population should be discussed as well as they have been collected alive or from a living-"fresh" dead assemblage.

In Figure 14, the extracted 14 day cycles of gamonts/schizonts of each locality are plotted on top of each other to check for phase equality. For the gamonts/schizonts of Sesoko-Jima, which were sampled during the same reproduction time, the phases are either equal or complementary (Fig.14a). For the gamonts/schizonts of Hawaii, which seem to originate from different reproduction times, phases show a much more randomly scattered pattern than in Sesoko (Fig. 14b). Laboratory-cultured specimens should show aligned phases, since all of them are clones. However this is not the case, the phases seem to be scattered around a common centre (Fig 14c).

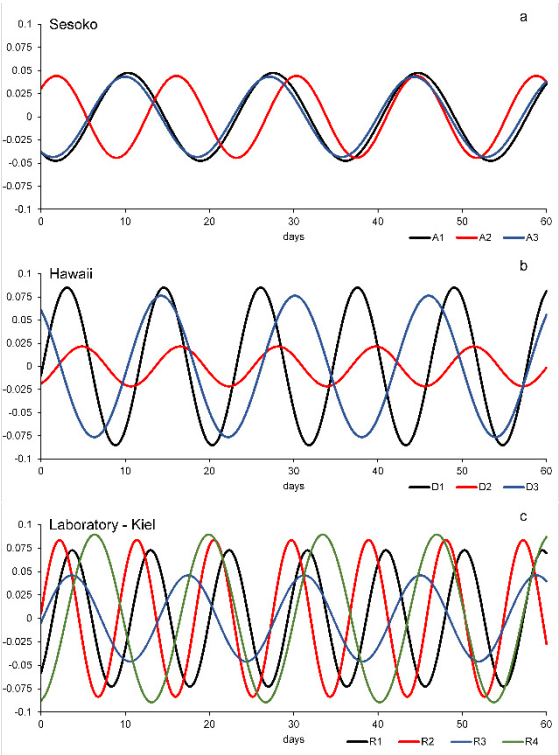

Figure 14 - Comparison of the 14 day cycles: The 14 day cycles of all gamonts/schizonts separated by localities to search for phase equality; a. Sesoko-Jima; b. Hawaii; c. Lab – Kiel.

Therefore these cycles cannot be plainly intrinsic and probably need an extrinsic pulse to calibrate them, as so-called pulsed-coupled biological oscillators. This mechanism is strongly discussed in biomathematics and it has been thoroughly researched how pulsating signals can influence it. Till now this process has been found in pacemaker neurons, the respiratory rhythm, circadian activity, and in the control of mitosis, but not yet in complex metabolitic activity of protists (Knight, 1972; Sachsenmeier et al., 1972; Buck and Buck, 1976; Petrillo, 1981; Bélair, 1986; Mirollo and Strogatz, 1990). In the given case the aforementioned seismic events during neap tides could pose as the gauging pulsatory signal, which implicates a gravitational-astronomical forcing on foraminiferal ontogeny. However, since this tidal influence on seismicity of rifting zones by Tolstoy (2015) has been discovered quite recently, no research on its influence on Earth's sea life has been done yet.

Finally, in direct comparison of growth functions in natural grown and laboratory-cultured specimens a clear

difference in the mode of cell growth is visible, as seen in Figure 9, confirming the assumption by Hohenegger et al. (2014) that the complexity of ecological variables affecting the growth of LBF cannot be substituted easily by laboratory conditions and should be always combined with field observations.

5. Conclusion

Computed micro-tomography and 3D reconstruction successfully quantifies the ontogeny of foraminiferal cells volumetrically, enabling the volumes of the whole chamber sequence to be accessed. *Heterostegina depressa* is a well-studied larger benthic foraminifera and thus represents an excellent model organism for the actuopalaeontological approach used in this work. The results on cell growth via volume analysis imply that not only embryonic size of larger benthic foraminifera give valuable information to reconstruct palaeoecology and biogeography, but also their growth rate might provide new insight in which way their local environment influences cell growth. So far, it can be concluded that embryonic size is a possible indicator to distinguish geographically isolated populations of this nummulitid taxon and maybe also other closely related taxa, as is has been found in other non-nummulitid groups. However, this effect might also be impaired by suboptimal environment conditions during laboratory culture.

The observations on the chamber volume revealed that LBF record, due to their longer lifetime, short- to long-term oscillations during their chamber formation, expressed in chamber size variation. Even though it is most likely that long-term cycles are only mathematical artifacts. Special attention should be given to the chamber-building rates, which are estimated using a power function instead of a Michaelis-Menten or Bertalanffy function, because these have a specific limit for each individual.

The results confirm that naturally grown foraminifera record oscillations in their chamber volume, which can possibly be induced by lunar and tidal cycles. Lunar cycles, and therefore light intensity oscillations, might affect the productivity of the photosynthetic symbionts hosted by the foraminiferal cell, probably causing a positive influence on photosynthetic activity during full moon nights. Certain growth oscillations point to tidal variation, which might reflect the effects of tidal currents (e.g., water turbidity, organic and inorganic nutrient availability) on the cell. Further comparison of specimens from different tidal regimes and/or localities with stronger and weaker seasonal influence might allow a better deciphering of growth cycles, especillay long-term cycles. Hence, research on latitudinal changes of long-term cycles has to been carried out in the future to inspect which fluctuating environmental factors influence LBF the most.

The occurrence of similar cyclicities in naturally grown and laboratory-cultured specimens implies that there are much more complex biologic mechanisms influencing these growth cycles. Therefore, a solely environmental cause is implausible and can probably be excluded. Detailed analysis and comparison of phase equality of specimens of each locality showed that the cyclic growth also cannot be only genetically controlled. Hence the theory of pulse-coupled biologic oscillators might apply to the oscillatory growth of LBF. Further and much more detailed research has to be done on cell growth and on growth cycles of these extraordinary protists to reveal the mechanisms of cyclic growth in larger benthic foraminifera.

Acknowledgment

This work was developed within the project “Breakthroughs in growth studies on larger benthic foraminifera” of the Austrian Science Fund (FWF; grant P26344-B25). We thank the Institute of Palaeontology, University of Vienna, for the use of the microCT, where all of the presented specimens have been scanned and for providing a dedicated working station for analysing the data sets. Furthermore, we thank Dr. Rudolf Röttger and Dr. Ralph Krüger for providing us with the material of their rigorous culturing experiments and their excellent pioneer work on culturing larger benthic foraminifera. Finally, we would like to thank Dr. Michael Stachowitsch for precisely proofreading this manuscript.

Valuable comments and suggestions of W. Renema, two anonymous reviewer and the Regional Editor Richard Jordan improved the former version of this manuscript.

References

Banner, F.T., Hodgkinson, R.L., 1991. A Revision of the Foraminiferal Subfamiliy *Heterostegininae*. Revista Espanola de Micropaleontologia 23, 101-140.

Beavington-Penney, S.J., Racey, A., 2004. Ecology of extant nummulitids and other larger benthic foraminifera: applications in palaeoenvironmental analysis. Earth-Science Reviews 67, 219-265.

Bélair, J., 1986. Periodic pulsatile stimulation of a nonlinear oscillator. Journal of Mathematical Biology 24, 217-232.

Bertalanffy, L., 1951. Zu einer allgemeinen Systemlehre. Biologia Generalis - Archiv für die allgemeinen Fragen der Lebensforschung.

Bijma, J., Erez, J., Hemleben, C., 1990. Lunar and semi-lunar reproductive cycles in some spinose planktonic foraminifers. J Foramin Res 20, 117-127.

Bijma, J., Hemleben, C., Wellnitz, K., 1994. Lunar-influenced carbonate flux of the planktonic foraminifer Globigerinoides sacculifer (Brady) from the central Red Sea. Deep-Sea Research 41, 511-530.

BouDagher-Fadel, M.K., 2008. Evolution and geological significance of larger benthic foraminifera. Elsevier.

Briguglio, A., Hohenegger, J., 2009. Nummulitids hydrodynamics: an example using Nummulites globulus Leymerie. Bollettino della societa paleontologica italiana 48, 105-111.

Briguglio, A., Hohenegger, J., 2011b. How to react to shallow water hydrodynamics: The larger benthic foraminifera solution. Marine Micropaleontology 81, 63-76.

Briguglio, A., Hohenegger, J., 2014. Growth oscillation in larger foraminifera. Paleobiology 40, 494-509.

Briguglio, A., Metscher, B., Hohenegger, J., 2011a. Growth rate biometric quantification by X-ray microtomography on larger benthic foraminifera: three-dimensional measurements push nummulitids into the fourth dimension. Turkish Journal of Earth Science 20, 683-699.

Briguglio, A., Hohenegger, J., Less, G., 2013. Paleobiological Applications of Three-Dimensional Biometry on Larger Benthic Foraminifera: A New Route of Discoveries. Turkish Journal of Earth Sciences 43, 72-87.

Buck, J., Buck, E., 1976. Synchronous fireflies. Scientific American 234, 74-85.

De Nooijer, L., Toyofuku, T., Kitazato, H., 2009. Foraminifera promote calcification by elevating their intracellular pH. Proceedings of the National Academy of Science of the United States of America 106, 15374-15378.

Ekman, S., 1953. Zoogeography of the Sea. Sidgwick & Jackson, London.

Erez, J., Almogi-Labin, A., Avraham, S., 1991. On the life history of planktonic foraminifera: lunar reproduction cycle in Globigerinoides sacculifer (Brady). Paleoceanography 6, 295-306.

Ferrandez-Canadell, C., Briguglio, A., Hohenegger, J., Woger, J., 2014. Test Fusion in Adult Foraminifera: A Review with New Observations of an Early Eocene *Nummulites* Specimen. J Foramin Res 44, 316-324.

Fujita, K., Hikami, M., Suzuki, A., Kuroyanagi, A., Kawahata, H., 2011. Effects of ocean acidification on calcification of symbiont-bearing reef foraminifers. Biogeosciences Discussion 8, 1809-1829.

Gompertz, B., 1825. On the nature of the function expressive of the law of human mortality, and on a new mode of determining the value of life contingencies. Philosophical transactions of the Royal Society of London, 513-583.

Görög, Á., Szinger, B., Tóth, E., Viszkok, J., 2012. Methodology of the micro-computer tomography on foraminifera. Paleontologia Electronica 15.

Hallock, P., 1984. Distribution of selected species of living algal symbiont-bearing foraminifera on two pacific coral reefs. J Foramin Res 14, 250-261.

Hallock, P., 1985. Why are larger foraminifera large? Paleobiology 11.

Hallock, P., 1988. The role of nutrient availability in bioerosion: consequences to carbonate buildups. Palaeogeography, Palaeoclimatology, Palaeoecology 63, 275-291.

Hallock, P., Pomar, L., 2008. Cenozoic evolution of larger benthic foraminifers: paleoceanographic evidence for changing habitats, Proceedings of the 11th International Coral Reef Symposium, Ft. Lauderdale, Florida, pp. 16-20.

Hallock, P., Lidz, B.H., Cockey-Burkhard, E.M., Donnelly, K.B., 2003. Foraminifera as bioindicators in coral reef assessment and monitoring: the FORAM index, Coastal Monitoring through Partnerships. Springer, pp. 221-238.

Hammer, Ø., Harper, D., Ryan, P., 2001. PAST: Paleontological statistics software package for education and data analysis. Palaeontologia Electronica 4.

Hauenschild, C., 1962. Die Zucht mariner Wirbelloser im Laboratorium (Methoden und Anwendung). Kieler Meeresforschungen 18, 1-98.

Hohenegger, J., 1999. Habitats of larger foraminifera on the upper reef slope of Sesoko Island, Okinawa, Japan. Marine Micropaleontology 36, 109-168.

Hohenegger, J., 2000. Coenoclines of larger foraminifera. Micropaleontology, 127-151.

Hohenegger, J., 2004. Depth coenoclines and environmental considerations of western Pacific larger foraminifera. The Journal of Foraminiferal Research 34, 9-33.

Hohenegger, J., 2009. Functional shell geometry of symbiont-bearing benthic Foraminifera. Galaxea, Journal of Coral Reef Studies 11, 81-89.

Hohenegger, J., 2011a. Larger foraminifera: Greenhouse Constructions and Gardeners in the Oceanic Microcosm. The Kagoshima University Museum, Japan, Kagoshima.

Hohenegger, J., 2011b. Growth-invariant meristic characters. Tools to reveal phylogenetic relationships in Nummulitidae (Foraminifera). Turkish Journal of Earth Sciences 20, 655-681.

Hohenegger, J., Briguglio, A., 2014. Methods for estimating growth pattern and lifetime of foraminifera on chamber volumes, in: Kitazato, H., Bernhard, J. (Eds.), Experimental Approaches in Foraminifera: Collection, Maintenance and Experiments. Springer book, Environmental Science Series, Tokyo, pp. 29-54.

Hohenegger, J., Briguglio, A., Eder, W., 2014. The natural laboratory of symbiont bearing benthic foraminifera: Studying individual growth and population dynamics under natural conditions, in: Kitazato, H., Bernhard, J. (Eds.), Experimental Approaches in Foraminifera: Collection, Maintenance and Experiments. Springer book, Environmental Science Series, Tokyo, pp. 13-27.

Hosono, T., Fujita, K., Kayanne, H., 2012. stimating photophysiological condition of endosymbiont-bearing Baculogypsina sphaerulata based on the holobiont color represented in CIE L*a*b color space. Marine Biology 159, 2663-2673.

Hottinger, L., 1982. Larger foraminifera, giant cells with a historical background. Naturwissenschaften 69.

Hottinger, L., 2000. Functional Morphology of Benthic Foraminiferal Shells, Envelopes of Cells beyond Measure. Micropaleontology 46, 57-86.

Hottinger, L., 2006b. The depth-depending ornamentation of some lamellar-perforate foraminifera. Symbiosis 42, 141-151.

Knight, B., 1972. Dynamics of encoding in a population of neurons. Journal of General Physiology 59, 734-766.

Krüger, R., 1994. Untersuchungen zum Entwicklungsgang rezenter Nummulitiden: Heterostegina depressa, Nummulites venosus und Cycloclypeus carpenteri. Christian–Albrechts–Universität Kiel, Kiel.

Lee, J., 2006. Algal symbiosis in larger foraminifera. Symbiosis 42, 63-75.

Lee, J., McEnery, M., Shilo, M., Reiss, Z., 1979. Isolation and cultivation of diatom symbionts from larger Foraminifera (Protozoa). Nature 280, 57-58.

Lee, J.J., Hallock, P., 1987. Algal Symbiosis as the Driving Force in the Evolution of Larger Foraminiferaa. Annals of the New York Academy of Sciences 503, 330-347.

Lončarić, N., Brummer, G.-J.A., Kroon, D., 2005. Lunar cycles and seasonal variations in deposition fluxes of planktic foraminiferal shell carbonate to the deep South Atlantic (central Walvis Ridge). Deep Sea Research Part I: Oceanographic Research Papers 52, 1178-1188.

Mercier, A., Sun, Z., Baillon, S., Hamel, J., 2011. Lunar rhythms in the deep sea: evidence from the reproductive periodicity of several marine invertebrates. Journal of Biological Rhythms 26, 82.86.

Michaelis, L., Menten, M., 1913. Die Kinetik der Invertinwirkung. Biochemische Zeitschrift 49, 333-369.

Mirollo, R., Strogatz, S., 1990. Synchronization of pulse-coupled biological oscillators. SIAM Journal on Applied Mathematics 50, 1645-1662.

Nobes, K., Uthicke, S., Henderson, R., 2008. Is light the limiting factor for the distribution of benthic symbiont bearing foraminifera on the Great Barrier Reef? Journal of Experimental Marine Biology and Ecology 363, 48-57.

Petrillo, G., 1981. Phase locking: a dynamic approach to the study of respiration. McGill University, Montreal.

Pomar, L., Morsilli, M., Hallock, P., Bádenas, B., 2011. Internal waves, an under-explored source of turbulence events in the sedimentary record. Earth-Science Reviews 111, 56-81.

Prazeres, M., Uthicke, S., Pandolfi, J.M., 2015. Ocean acidification induces biochemical and morphological changes in the calcification process of large benthic foraminifera. Proceedings of the Royal Society London B: Biological Sciences 282, 20142782.

Press, W., Teukolsky, S., Vetterling, W., Flannery, B., 1992. Numerical Recipes. Cambridge University Press 21, 10.1017/S0033583500004285.

Räsänen, K., Kruuk, L., 2007. Maternal effects and evolution at ecological time-scales. Functional Ecology 21, 408-421.

Renema, W., Troelstra, S., 2001. Larger foraminifera distribution on a mesotrophic carbonate shelf in SW Sulawesi (Indonesia). Palaeogeography, Palaeoclimatology, Palaeoecology 175, 125-147.

Richards, C., Bossdorf, O., Pigliucci, M., 2010. What role does heritable epigenetic variation play in phenotypic evolution? . BioScience 60, 232-237.

Richards, E., 2006. Inherited epigenetic variation – revisiting soft inheritance. Nature Reviews Genetic 7, 395-401.

Richards, F., 1959. "A Flexible Growth Function for Empirical Use". Journal of Experimental Botany 10, 290-300.

Ross, C., 1974. Evolutionary and ecological significance of large, calcerous Foraminifera (Protozoa), Great Barrier Reef. Proceedings of the 2nd International Coral Reef Symposium 1, 327-333.

Röttger, R., 1972. Analyse von Wachstumskurven von Heterostegina depressa (Foraminifera: Nummulitidae). Marine Biology 17, 228-242.

Sachsenmeier, W., Remy, V., Plattner-Schobel, R., 1972. Initiation of Synchronous mitosis in Physarum polycephalum. Experimental Cell Research 73, 41-48.

Schmidt, D., Rayfield, E., Cocking, A., Marone, F., 2013. Linking evolution and development: Synchrotron Radiation X-ray tomographic microscopy of planktic foraminifers. Palaeontology 56, 741-749.

Schulz, M., Mudelsee, M., 2002. REDFIT: estimating red-noise spectra directly from unevenly spaced paleoclimatic time series. Computers & Geosciences 28, 421-426.

Speijer, R.P., Van Loo, D., Masschaele, B., Vlassenbroeck, J., Cnudde, V., Jacobs, P., 2008. Quantifying foraminiferal growth with high-resolution X-ray computed tomography: New opportunities in foraminiferal ontogeny, phylogeny, and paleoceanographic applications. Geosphere 4, 760-763.

Spindler, R., Röttger, R., 1973. Der Kammerbauvorgang der Großforaminifere Heterostegina depressa (Nummulitidae). Marine Biology 18, 146-159.

Tolstoy, M., 2015. Mid-ocean ridge eruptions as a climate valve. Geophysical Research Letters 42, 1346-1351.

Tolstoy, M., Vernon, F., Orcutt, J., Wyatt, F., 2002. Breathing of the seafloor: Tidal correlations of seismicity at Axial volcano. Geology 30, 503-506.

Tyszka, J., 2004. Analysis of test ontogenesis (ATO) in small foraminifera: implications from Pseudonodosinella, in: Bubík, M., Kaminski, M. (Eds.), Proceedings of the Sixth International Workshop on Agglutinated Foraminifera. Grzybowski Foundation Special Publictaion, pp. 471-483.

Uthicke, S., Nobes, K., 2008. Benthic Foraminifera as ecological indicators for water quality on the Great Barrier Reef. Estuarine, Coastal and Shelf Science 78, 763-773.

Winter, A., Sammarco, P.W., 2010. Lunar banding in the scleractinian coralMontastraea faveolata: Fine-scale structure and influence of temperature. Journal of Geophysical Research 115.

Zuo, S., Zhang, N., Li, B., Zhang, Z., Zhu, X., 2009. Numerical simulation of tidal current and erosion and sedimentation in the Yangshan deep water harbor of Shanghai. International Journal of Sediment Research 24, 287-298.

Chapter 2 (accepted for publication in PALAIOS)

DEPTH-RELATED MORPHOCLINES OF MEGALOSPHERIC TESTS OF *HETEROSTEGINA DEPRESSA* D'ORBIGNY: BIOSTRATIGRAPHIC AND PALAEOBIOLOGICAL IMPLICATIONS

***Wolfgang Eder**[1] , Antonino Briguglio[2], Johann Hohenegger[1]

[1] University of Vienna, Department of Palaeontology, Althanstrasse 14, 1090, Vienna, Austria

[2] Universiti Brunei Darussalam, Faculty of Science, Jalan Tungku, BE1410, Brunei Darussalam

***corresponding author:** wolfgang.eder@univie.ac.at, +0043 1/427753563

Keywords – Foraminifera, Nummulitidae, biometry, biostratigraphy, palaeoecology

Abstract

Morphometric characters of equatorial sections have been widely applied to define species of larger benthic foraminifera for both biostratigraphic and evolutionary studies. In order to test the hypothesis that some of the observed morphological differences may reflect environmental conditions rather than evolutionary changes, we applied morphometric analysis to equatorial sections of megalospheric *Heterostegina depressa* tests from the reef slope of Sesoko-Jima, NW-Okinawa. Only living specimens were analyzed, thereby eliminating any postmortem alteration of the distribution of *H. depressa* along the water depth gradient. The analyses clearly differentiated two morphogroups corresponding to two megalospheric generations: gamonts with significantly larger proloculi and schizonts with smaller proloculi. Due to their asexual reproduction strategy, schizonts dominate in high-energy shallower environments. After a transition zone between 35 to 55 m, where both generations are present, schizonts are replaced by gamonts deeper on the slope. Both generations retain the characters of their initial tests regardless of depth. Where both megalospheric generations co-occur, the change in proportion of generations with depth results in an environmental morphological trend that matches apparent fossil evolutionary trends. These results are important for understanding relationships among fossil *Heterostegina* species, where continuous changes in morphological characters of the initial test part are interpreted as evolutionary trends.

1. Introduction

Larger benthic foraminifera (LBF) have populated tropical to warm temperate shallow marine environments over more than 300 million years. During this time they evolved in various lineages independently from smaller benthic foraminiferal groups by establishing a symbiotic relationship with diverse microalgae; thus, symbiosis became the group's unifying character (BouDagher-Fadel, 2008). Symbionts enabled LBF to develop test sizes >3mm, while restricting them to the photic zones of marine environments (Hohenegger, 2011a). Hosting and cultivating symbionts became the major intrinsic factors driving test morphology of LBF, specifically in developing microscopic "greenhouses." Physical factors, such as hydrodynamic energy and light attenuation, also constrain

test shapes (Hottinger, 2000; Hohenegger, 2004; Briguglio and Hohenegger, 2009; Briguglio and Hohenegger, 2011; Seddighi et al., 2015). Studying the factors controlling test shape of extant genera or species can provide essential information on the palaeoecology and palaeoenvironments of fossil larger benthic (Hottinger, 1977a; Reiss and Hottinger, 1984; Hallock et al., 1991; Beavington-Penney and Racey, 2004; Hohenegger, 2009, 2011b). LBF are significant carbonate producers in shallow marine environments (Langer and Lipps, 2003; Hohenegger, 2006) and are important index fossils (Serra-Kiel et al., 1998). To strengthen their biostratigraphic use, two-dimensional biometry based on equatorial sections has been extensively applied to differentiate species or subspecies within evolutionary lineages (Tan, 1937; Drooger, 1952; Schaub, 1981; Drooger and Roelofsen, 1982; Less, 1987; Drooger, 1993; Özcan et al., 2001; Less and Özcan, 2008; Less et al., 2008; Benedetti et al., 2010; Benedetti and Pignatti, 2013). In *Nummulites*, this has involved concentrating on the size of the embryonic apparatus, spiral-diagrams, and ornamentation (Schaub, 1963, 1981), whereas for other nummulitid subfamilies (e.g., Heterostegininae and Cycloclypeninae), additional characters have been introduced in accordance with their complex internal morphologies (Papp, 1954; Chaproniere, 1975; Drooger and Roelofsen, 1982). These approaches assumed that morphological variation within evolutionary lineages is greater than environmental and geographical variation within a species at any moment in time. Testing this assumption is one of the primary aims of this paper. Conflicting signals in major evolutionary trends, such as nepionic acceleration (Drooger, 1952) and a steady increase in body size (Cope, 1896) in some lineages, have been noted by different authors (Racey, 1992; Benedetti and Pignatti, 2013). In addition, critiques that the commonly used biometric approach does not correctly relate juvenile to adult test morphologies have been published (Reiss and Hottinger, 1984; Hohenegger, 2011b).

The nummulitid foraminifer *Heterostegina depressa* d'Orbigny 1826, as the single extant representative of the genus, is a cosmopolitan species of tropical to warm temperate shallow-water environments. The test is composed of a spiral arrangement of arched chambers. The chambers are subdivided into chamberlets by secondary septa (septula). Test coiling can be approximated by a modified logarithmic spiral (Hohenegger, 2011b). This morphology, present since the Eocene, is the diagnostic character of the heterosteginid subfamily (Banner and Hodgkinson, 1991). Heterostegininae are generally split into a *Heterostegina sensu stricto* lineage, which includes *H. depressa*, and a *Heterostegina sensu lato* group. The latter includes the fossil genera and subgenera *Heterostegina* (*Vlerkina*) Eames et al. 1968, *Spiroclypeus* Douvillé 1905, *Grzybowskia* Bieda (1949), and *Tansinhokella* Banner and Hodgkinson 1991.

Heterostegina depressa shows the broadest depth distribution among recent nummulitids, ranging from the shallowest subtidal down to ~100 m water depth under optimal light conditions (Banner and Hodgkinson, 1991; Hohenegger, 1994; Hohenegger et al., 1999; Hohenegger, 2000; Hohenegger et al., 2000; Hohenegger and Yordanova, 2001; Hohenegger, 2006). The range of different living morphotypes along environmental or geographic gradients within this single species might span the differences among fossil evolutionary lineages. Whereas earlier studies of this kind were based on assemblages that mixed live and dead individuals of *H. depressa* (Fermont, 1977a, 1977b; Biekart et al., 1985), the analysis presented here re-evaluates the current biometric system by applying it strictly to living specimens sampled along an environmental gradient. It demonstrates a change in test morphology with water depth and that the trimorphic life cycle of *H. depressa* (Röttger, 1974) influences the morphological change along gradients as proposed by (Leutenegger, 1977) and supported by (Biekart et al., 1985).

2. Material and Methods

196 specimens of *H. depressa* from 5 to 90 m water depth (collected by J. Hohenegger) were used for these analyses. All megalospheric specimens were collected offshore Sesoko-Jima (N 26° 39' 5.134" E 127° 51' 11.635" and N 26° 39' 38.776" N, 127° 51' 56.28") in 1993 and 1996. Samples down to 40 m were taken by SCUBA in 10-m intervals, whereas those from 50 to 90 m water depth were dredged. Sample from 80 and 90 meters have been grouped together due to small sample size. Only living specimens were picked from the sediments to obtain distribution patterns undisturbed by postmortem movement (for further information see Hohenegger, 1999). Sampling was done before the yearly typhoon season to exclude up- or downslope transport of living specimens.

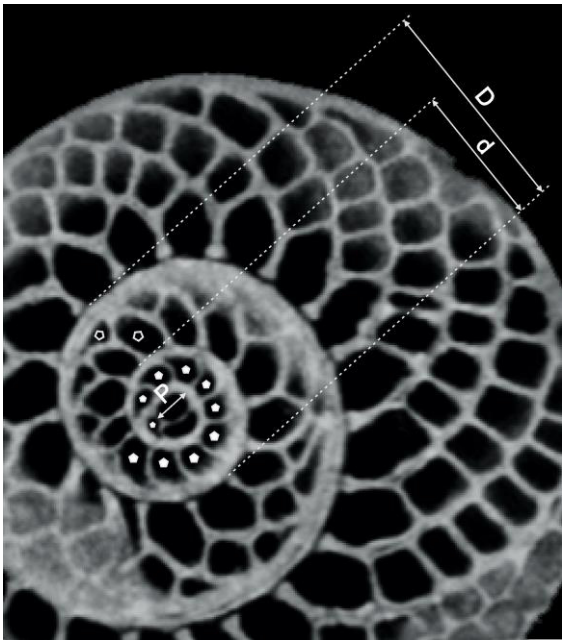

Figure 1 - The measured parameters are presented in a megalospheric equatorial section (see also Table 1). The proloculus diameter (P), , diameter of the first whorl (d), diameter of the first and a half whorl (D) are depicted as segments, while the number of operculinid chambers (Less et al., 2008) is marked by filled pentagons and number of chamberlets in the 14th chamber (S) is marked by empty pentagons.

To examine the internal structure of *H. depressa* more closely, specimens were investigated by micro-computed tomography (µCT). This visualization technique has been applied frequently in recent years to observe, quantify, and study foraminiferal shells non-destructively (Speijer et al., 2008; Briguglio and Hohenegger, 2011; Benedetti and Briguglio, 2012; Hohenegger and Briguglio, 2012; Briguglio et al., 2013; Schmidt et al., 2013; Ferrandez-Canadell et al., 2014). Accordingly, µCT has been used to obtain equatorial sections of *H. depressa* for measuring traditional biometric parameters. Images were taken with a Skyscan 1173 high-energy scanner (at a resolution between 5-8 µm) at the University of Vienna (Department of Palaeontology); equatorial sections were extracted from the three-dimensional datasets using DataViewer 1.4.4.0.

2.1. Statistical Analysis

The biometric characters used in this analysis (Table 1) use a two-dimensional morphometric system commonly applied in larger benthic foraminiferal research based on the system of Drooger and Roelofsen (1982) (Papp and Küpper, 1952; Papp, 1954; Chaproniere, 1980; Drooger and Roelofsen, 1982; Less and Özcan, 2008; Less et al., 2008).

The six parameters listed in table 1 were measured on all specimens and are further explained in figure 1. First, Pearson's *r* was calculated to check for correlation between each of the biometric parameters as well as water depth (Table 2). Then, a partial correlation was calculated to remove the effect of water depth (Table 2).

Additionally, a one-way ANOVA was applied to search for differences between transect intervals (Table 3). The P vs. X and X vs. S scatter plots from Less et al. (2008) were overlain with the corresponding scatter plots of the present data, showing 95.44 % confidence intervals for the standard error of the mean (Fig. 2 and 3).

biometric character	definition
P	the inner maximal diameter of the proloculus, omitting the wall
X	the number of undivided chambers until the first emergence of secondary septa, not counting embryonic chambers
S	the number of chamberlets at the 14th chamber. If it is an undivided chamber, the values were marked as 1, to avoid 0 values in shallower specimens
d	the diameter of the 1st whorl measured perpendicular to the axis of P
D	the diameter of the whorl at 1.5 revolutions
K	the index of spiral opening, which is calculated independently of P (Less et al. 2008)

Table 1 - In-text used abbreviations for the biometric characters and the corresponding definitions.

The confidence intervals of the present data were computed according to Less et al. (2008).
Proloculus size of the subsamples for every water depth was analyzed by one-way ANOVA and a post hoc least significant difference (LSD) multiple comparison to search for significant differences in proloculus size between the subsamples. Afterwards, canonical discriminant analysis was used to assign undetermined individuals into groups characterized by homogeneous character distributions. This re-sorting was based on the proloculus diameter P and the number of operculinid chambers X. The significance of difference and homogeneity of the reassigned groups was confirmed using analysis of variance (Table 4).
This grouping was mapped onto a nonmetric multidimensional scaling (nMDS) of all individual specimens using standardized Euclidean distances (Fig. 4)
The one-way ANOVAs, LSD multiple comparison, and discriminant analysis were calculated using IBM SPSS v. 22. All scatter plots and the nMDS were generated using PAST 3.10 (Hammer et al., 2001). The measurements were done using ImageJ 1.49.

3. Results

Table 2 presents the Pearson's *r* and partial correlation between each pair of biometric characters and depth of collection. The number of operculinid chambers (Less et al., 2008) shows the strongest negative correlation with water depth, followed by the proloculus size (P), which shows the strongest positive correlation, indicating that these two are the most informative depth-dependent parameters. After water depth was partialed out as a control variable, proloculus size becomes the most informative parameter. All other parameters correlate positively with proloculus size except operculinid chamber number, which shows the weakest negative correlation.

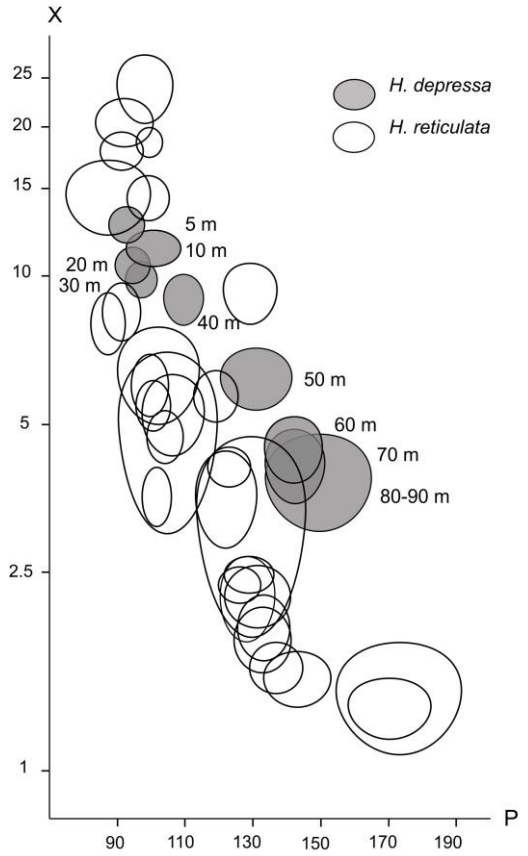

Figure 2 - Scatter plot of proloculus diameter (P) versus operculinid chambers (X of Less et al., 2008) overlain by scatter plots of the present data, revealing the coinciding evolutionary trend of the *H. reticulata* lineage and the depth transect of *H. depressa*.

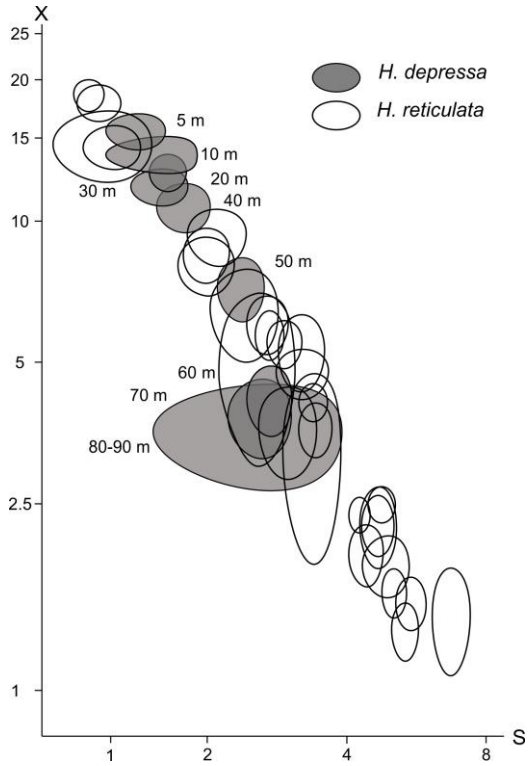

Figure - Scatter plot of number of chamberlets in the 14th chamber (S) versus operculinid chambers (X of Less et al., 2008) overlain by scatter plots of the present data, revealing the coinciding evolutionary trend of the *H. reticulata* lineage and the depth transect of *H. depressa*.

The number of chamberlets in the 14th chamber (S) displays a positive but slightly stronger correlation. The diameter of the 1st and 1 1/2st whorl show the strongest correlation with proloculus size. The spiral index (K) shows the weakest correlation with P.

Figures 2 and 3 are scatter plots of P vs X and X vs S from Less et al. (2008), overlain with the corresponding scatter plots of the present data, comparing the change of biometric parameters along the water depth gradient in *H. depressa* with inferred evolutionary change in the *H. reticulata* lineage.

Samples from 5 to 30 meters show a smaller proloculus size, while samples from 60 to 90 meters have a larger proloculus (Table 3). Only the samples from 40 and 50 meters differ significantly from both groups and were thus assigned to an intermediate group I. Boundaries for canonical discriminant analysis for classifying individuals belonging to group I were set according to the multiple comparison analysis: Samples from 5 to 30 meters were defined as preliminary group A_1 (interpreted as schizonts) and samples from 60 to 90 meters as preliminary group A_2 (interpreted as gamonts). The reclassification was done using operculinid chamber number in addition to proloculus size, because it shows the lowest correlation with the latter. (The spiral index was not used despite its lower correlation with proloculus size because it is a ratio between parameters d [diameter of whorl at one full revolution] and D [diameter of whorl at 1.5 revolutions].) Reclassification of group I is reported in Supplementary Data.

The ANOVA on proloculus size between the morphogroups (Table 4) shows homogeneity in both groups, indicating that neither the group with small proloculi, A_1, nor the group with larger proloculi, A_2, show a depth trend within either group. Figure 4 shows the nonmetric multidimensional scaling (nMDS) for all individuals based on all parameters; highlighted are the two morphogroups and the water depth gradient. Furthermore, figure 5 depicts the right skewed frequency distribution of proloculus size in relative abundance of the complete population.

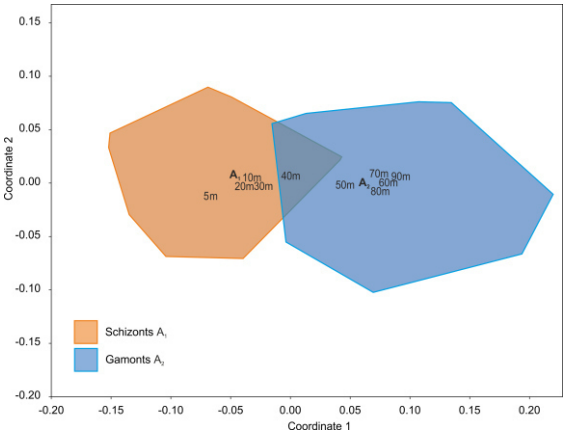

Figure 4 - Nonmetric multidimensional scaling (nMDS) using standardized Euclidean distances based on all measured parameters along the water depth gradient and the highlighted morphogroups A_1 and A_2. Note the overlapping area around 40-50 m water depth. The water depth and morphogroup markings indicate class centroids.

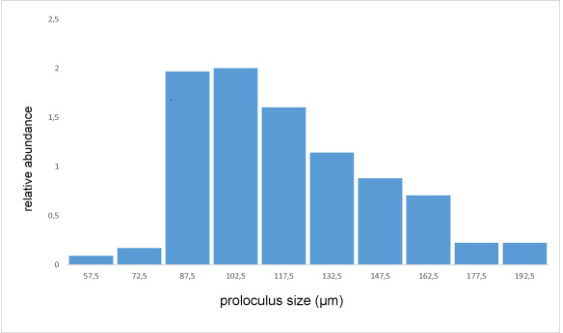

Figure 5 - Frequency distribution of the proloculus diameter for the complete population showing the right skewed distribution of proloculus size that results from mixing schizonts (A_1) and gamonts (A_2).

In summary, along transects from Sesoko-Jima, group A_1 contains individuals with smaller proloculus size that occur at shallower depths and group A_2 contains individuals with larger proloculi that are restricted to deeper depths. The turnover point between groups is located at 40-50 m depth (Fig. 2): A_1-individuals predominate from

5 to 40 m, declining at 50 m, while few A_2-individuals are present at 40 m, becoming dominant at 60 m and ranging down to 90 m.

4. Discussion

These results address a major question in larger benthic foraminifer biometry: Are the generations of schizonts (A_1), gamonts (A_2), and agamonts (B) expressed in a trimorphism (Leutenegger, 1977)? The possibility of morphologically different megalospheric A-forms is mostly ignored in biometric studies. Nonetheless, the present data set supports the suggestion of Leutenegger (1977) and studies by Biekart et al. (1985) that the two megalospheric generations of *H. depressa* show differences in internal test morphology. The proloculus diameter P and the number of operculinid chambers X are the most significant of the six biometric parameters used for differentiating generations. As postulated by Reiss and Hottinger (1984), parameters of the initial test represent only an early ontogenetic state, thus are irrelevant as depth-dependent indicators for the adult test. Especially in the case of the spiral index K, more detailed measurements over the whole equatorial section have to be done to correctly describe the complete spiral of *Heterostegina* (Hohenegger, 2011b). This is why parameter K was partially disregarded in this analysis, as was done by Less et al. (2008).

In addition, analyses of the Sesoko-Jima data are consistent with Leutenegger's (1977) claim that A_1 (schizonts) and A_2 (gamonts) show an uneven depth distribution similar to A (A_1 + A_2) and B (agamonts) forms (Hottinger, 1977a). Schizonts and gamonts show different morphologies in the initial part of the test (as seen in Fig. 6) and maintain a clear separation in frequency of occurrence along the water depth gradient, only overlapping between 35 to 55 m.

Furthermore, previously documented depth trends in *H. depressa* seem to result from the combination of the two megalospheric generations (Fermont, 1977b; Biekart et al., 1985).

Pearsons'r

		P	X	S	d	D	K
Depth	corr.	0.726	-0.819	0.572	0.613	0.639	0.541
	sig.	1.03E-33	5.27E-49	9.29E-19	6.91E-22	3.35E-24	1.29E-16
P	corr.		-0.789	0.692	0.893	0.886	0.517
	sig.		3.78E-43	1.45E-29	2.22E-69	6.22E-67	4.19E-15
X	corr.			-0.620	-0.746	-0.761	-0.516
	sig.			1.55E-22	2.06E-36	1.18E-38	5.01E-15
S	corr.				0.673	0.704	0.515
	sig.				1.80E-27	6.13E-31	5.63E-15
d	corr.					0.981	0.406
	sig.					1.04E-140	1.72E-09
D	corr.						0.559
	sig.						7.91E-18

partial correlation

control variable: Depth		X	S	D	d	K
P	corr.	-0.491	0.490	0.824	0.798	0.215
	sig.	1.51E-13	1.78E-13	7.83E-50	1.49E-44	0.001
X	corr.		-0.322	-0.539	-0.539	-0.150
	sig.		2.20E-06	2.25E-16	2.19E-16	0.018
S	corr.			0.497	0.536	0.298
	sig.			7.58E-14	3.38E-16	1.19E-05
D	corr.				0.970	0.112
	sig.				1.16E-120	0.059
d	corr.					0.330
	sig.					1.24E-06

Table 2 - Correlation tables for Pearson's *r* for water depth and the biometric parameters and the correlation table for the partial correlation. Note the strong correlation between the biometric parameters after water depth was partialed out. Degrees of freedom = 196 for all Pearson's *r* values; degrees of freedom = 193 for all partial correlation values.

When measuring cultured schizonts (A_1) and gamonts (A_2), Biekart et al. (1985) found differences in proloculus size similar to those observed in the populations at Sesoko-Jima. Biekart et al. (1985), however, were unable to detect bimodal distributions because the natural assemblages they examined represented a mixture of living and dead individuals. Generations could not be detected as bimodal distributions because the normal distributions of A_1 and A_2 strongly overlap when both generations are present. This results in a skewed rather than a bimodal frequency distribution when proportions are unequal, as is the case in the present data set (Fig. 5).

According to depth frequencies, apogamic schizogeny ($A_1 – A_1 – A_1$) can be assumed for shallow depth intervals from 5 to 35 m, whereas from 35 to 55 m an alternation of asexual and sexual reproduction (A – B – A) is more likely. Gametogamy ($A_2 – B – A_2$) is expected for individuals in deeper environments (Leutenegger, 1977).

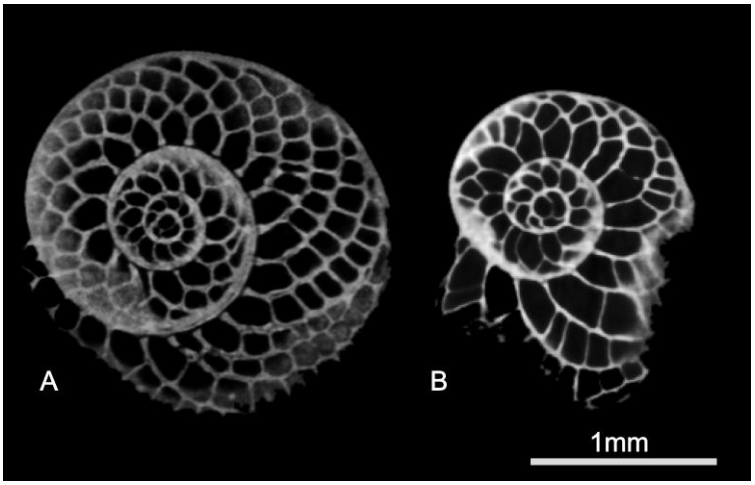

Figure 6 **-** Equatorial sections of *H. depressa*. A) Specimen 96-13-1_3 from 20 meters; morphogroup A_1. B) Specimen 93-3-3-2_4 from 60 meters; morphogroup A_2.

ANOVA

descriptive statistics

j	n	$\bar{x}$	s	s.e.	95% Confidence Interval for Mean		min.	max.
					lower l.	upper l.		
5	19	92.9	11.18	2.57	87.5	98.2	63.9	116.8
10	21	100.7	17.77	3.88	92.6	108.8	68.2	157.9
20	27	94.6	12.79	2.46	89.6	99.7	51.0	122.2
30	28	97.0	11.70	2.21	92.5	101.6	74.5	129.2
40	21	109.6	13.26	2.89	103.6	115.6	89.2	139.1
50	23	130.8	24.72	5.16	120.1	141.5	92.5	195.8
60	24	142.1	20.81	4.25	133.3	150.9	111.7	187.1
70	22	142.2	20.19	4.31	133.3	151.2	112.9	185.5
>80	11	149.2	25.49	7.68	132.1	166.3	113.0	192.3
Total	196	115.5	27.32	1.95	111.7	119.4	51.0	195.8

ANOVA

	Sum of Squares	Mean Square	F	sig.
Between Groups	86997.27	10874.66	34.759	3.2E-33
Within Groups	58504.59	312.86		
Total	145501.86			

LSD multiple comparison

	5	10	20	30	40	50	60	70	>80
5		0.163	0.740	0.430	**0.003**	**6.83E-11**	**1.72E-16**	**4.42E-16**	**1.02E-14**
10	7.85		0.238	0.471	0.105	**6.16E-08**	**3.58E-13**	**7.87E-13**	**5.34E-12**
20	1.76	6.09		0.615	**0.004**	**1.31E-11**	**6.78E-18**	**2.34E-17**	**2.61E-15**
30	4.16	3.69	2.40		**0.015**	**1.43E-10**	**9.33E-17**	**3.04E-16**	**2.11E-14**
40	16.73	8.88	14.97	12.57		**9.95E-05**	**4.67E-09**	**7.76E-09**	**9.02E-09**
50	37.97	30.12	36.21	33.81	21.23		**0.030**	**0.032**	**0.005**
60	49.22	41.37	47.46	45.06	32.49	11.25		0.976	0.269
70	49.38	41.53	47.62	45.22	32.64	11.41	0.16		0.286
>80	56.37	48.52	54.61	52.20	39.63	18.40	7.15	6.99	

Table 3 **-** Statistical summary of the ANOVA and LSD multiple comparison of the mean proloculus size per water depth *j*. Listed are the descriptive statistics of the biometric sample (size n_j , mean $\bar{x}_j$, standard deviation s_j, standard error $s.e._j$, minimum and maximum per water depth *j* (5-90 m)) followed by the ANOVA and the LSD multiple comparison. The upper triangle of the LSD analysis gives the significance (bold values: $p < 0.05$) for the specific comparisons and the lower triangle gives the mean difference.

ANOVA - between morphogroups

descriptive statistics

group	n	$\bar{x}$	s	s.e.	95% Confidence Interval for Mean		min.	max.
					lower l.	upper l.		
A1	119	98.1	13.33	1.22	95.7	100.6	51.0	157.9
A2	77	142.4	20.86	2.38	137.6	147.1	111.7	195.8
Total	196	115.5	27.32	1.95	111.7	119.4	51.0	195.8

Test of Homogeneity of Variances

Levene Statistic	sig.
21.374	6.88652E-06

ANOVA

	Sum of Squares	Mean Square	F	Sig.
Between Groups	91468.64	91468.64	328.408	1.3E-43
Within Groups	54033.22	278.52		
Total	145501.86			

Table 4 **-** Statistical summary for the ANOVA indicating significant differences in mean proloculus and homogeneity of morphogroups A_1 and A_2.

Of those ecological factors regarded as influencing the environmental distribution of larger benthic foraminifera (e.g., hydrodynamics, light attenuation, nutrients, and terrigenous influx), hydrodynamics along with topographic setting are the main factors influencing reproduction along the depth gradient. In general, fair-weather wave base (FWWB) at the sampling location in Okinawa lies around 15-20 m deep throughout the year, whereas storm waves during the typhoon season can influence the benthic communities down to 100 m and below (Hohenegger, 1999). Typhoons are instantaneous events transporting living individuals out of their survival range. Accordingly, the FWWB, ocean currents, and tidal currents are important factors constraining the depth occurrence of schizonts versus gamonts throughout the year. The hydrodynamic energy down to 35 m water depth seems to hinder gametogamy that would establish a sexual reproduction cycle (Lipps, 1982).

These relations are relevant for understanding fossil species. Some previous reports on distributions of embryonic size in fossil and mixed living/dead assemblages (e.g., the fossil *Nephrolepidina praemarginata* [Benedetti, et al., 2010] and the recent *H. depressa* [Fermont, 1977b]) imply a normal distribution along an environmental gradient (e.g., light intensity, water depth), with maximum embryonic size in optimal ecological conditions. This, however, could not be confirmed either in the living assemblages presented here or in studies on *Operculina* from Sesoko-

Jima (Yordanova and Hohenegger, 2004). Both studies used only living individuals that had been sampled shortly before the typhoon season, thereby excluding the influence of major transport mechanisms.

In Fermont's (1977a) study on recent *H. depressa*, he rejected any major influence of transport, even though the sediment was dried before picking, and thus probably represented a mixed living-dead assemblage as described in Hottinger (1977a). Furthermore, the bathymetric limit of *H. depressa* around Okinawa at 90 m water depth is much shallower than reported from the Gulf of Eilat by Fermont (1977b). Therefore, this study demonstrates the importance of using only living LBF and not empty tests in ecological research to correctly investigate distributional patterns and the influence of environmental factors of large benthic foraminifera.

Another issue is the way in which dimorphism interferes with biometric measurements on a population level. In general, an evolutionary trend toward larger test (Cope, 1896) and proloculus size (e.g., Tan, 1937) has been documented in different groups of larger foraminifera (Tan, 1937; Racey, 1992). Contradicting biometric data has been documented for *Nummulites*, where "more evolved" (large) species occurred together with unreworked "primitive" (small) species (Racey, 1992). Hence, this mixture of sizes could represent mixture of individuals from different environments rather than different evolutionary lineages.

This study has focused on a single taxon within one time horizon, so that morphological variability might be expected to be much lower than in the extensive fossil dataset of Less et al. (2008). However, the morphological variability of *H. depressa* along a water depth transect follows, with similar standard errors, closely following the evolutionary trend postulated for the *Heterostegina reticulata* lineage in the late Eocene (Figs. 2 and 3). Shallower specimens coincide with earlier representatives of the *H. reticulata* lineage, while deeper specimens coincide with later representatives of the lineage.

If a dimorphism in A-generations is assumed for *Heterostegina s.l.*, then the relative proportions of A_1 and A_2 as a function of water depth – thus of hydrodynamics – might influence the mean proloculus size in any biometric analysis that attempts to explain evolutionary trends. Based on depositional setting, autochthonous, parautochthonous, and allochthonous assemblages might lead to different biometric results, depending on the mixture of the two megalospheric generations. This calls for cautious biostratigraphic interpretations whenever proloculus size is used as an age indicator.

Finally, different proportions of megalospheric generations caused by postmortem transport and mixing can lead to different mean values of biometric parameters between localities from the same time horizon and water depth. More attention should be paid in the future to the palaeoenvironmental constrains of biometric parameters.

5. Conclusion

The large foraminifer *H. depressa* displays trimorphism composed of three generations: schizonts (A_1), gamonts (A_2), and agamonts (B). Statistical analyses demonstrate differences between megalospheres (A_1 and A_2) using the common biometric parameters proloculus diameter (P), operculinid chambers (Zuo et al.), number of chamberlets in the 14^{th} chamber (S), diameter of the first whorl (d), diameter of the first and a half whorl (D), and spiral-index (K, sensu Less et al., 2008). These analyses lead to a split of the megalospheric population into two morphogroups with significantly different proloculus sizes that do not change with depth. The two morphogroups, which can be interpreted as schizonts and gamonts, show overlapping distributions at depths between 35 and 55 m, with schizonts dominating above and gamonts below the mixing zone (Figs. 2 to 4).

In deciphering the ecological factors (light attenuation, terrigenous influx, nutrients, water energy, etc.) controlling the uneven depth distribution of morphogroups, hydrodynamic setting influences the distribution of schizonts and

gamonts along the water depth gradient most likely because strong water movement hinders sexual reproduction by destroying gametes.

Furthermore, the presence of morphologically different megalospheric tests and their change in proportion along environmental factors put strong constraints on the biostratigraphic use of morphospecies and subspecies. Puzzling evolutionary reversals that hinder biometric diagnosis of lineages and subspecies have been documented before (Racey 1992; Benedetti and Pignatti, 2013). Palaeogeographical differences (Hohenegger, 2014; Eder et al., 2016a), together with transport, reworking, and time averaging, can obscure the clear dependence of morphology on hydrodynamics, possibly leading to erroneous interpretations regarding evolutionary lineages.

In addition, the finding that the commonly used biometric parameters correlate highly with proloculus size indicates that they are determined too early in ontogeny to adequately reflect the morphological characteristics of adult specimens (Reiss and Hottinger 1984; Hohenegger, 2011b).

Finally, we highlight that actuopalaeontological studies should be based solely on living larger foraminifera taken concurrently at a single sampling location; otherwise the actual distributional patterns are not correctly represented or can be distorted.

Acknowledgements

We thank the Institute of Palaeontology, University of Vienna, for the use of the microCT, where all of the presented specimens were scanned, and for providing a dedicated working station for analyzing the data sets. This work was developed within the project “Breakthroughs in growth studies on larger benthic foraminifera” of the Austrian Science Fund (FWF; grant P26344-B25). Furthermore, we would like to thank Dr. Michael Stachowitsch for precisely proofreading this manuscript. Finally, we would like to thank our PALAIOS-Editor Dr. Thomas Olszewski, our Associate Editor Dr. Cesare Papazzoni, as well as two anonymous reviewers.

References

Banner, F.T., Hodgkinson, R.L., 1991. A Revision of the Foraminiferal Subfamiliy *Heterostegininae*. Revista Espanola de Micropaleontologia 23, 101-140.

Beavington-Penney, S.J., Racey, A., 2004. Ecology of extant nummulitids and other larger benthic foraminifera: applications in palaeoenvironmental analysis. Earth-Science Reviews 67, 219-265.

Benedetti, A., Briguglio, A., 2012. Risananeiza crassaparies n. sp. from the upper Chattian of Porto Badisco (southern Apulia, Italy). Bollettino della Società Paleontologica Italiana 51, 168.

Benedetti, A., Pignatti, J., 2013. Conflicting evolutionary and biostratigraphical trends in Nephrolepidina praemarginata (Douvillé, 1908)(Foraminiferida). Historical Biology 25, 363-383.

Benedetti, A., Di Carlo, M., Pignatti, J., 2010. Embryo size variation in larger foraminiferal lineages: stratigraphy versus paleoecology in Nephrolepidina praemarginata (R. Douvillé, 1908) from the Majella Mt.(Central Appennines). Journal of Mediterranean Earth Sciences 2, 19-29.

Biekart, J., Bor, T., Röttger, R., Drooger, C., Meulenkamp, J., 1985. *Megalospheric Heterostegina* depressa from Hawaii in sediments and laboratory cultures, Proceedings of the Koninklijke Nederlandse Akademie van Wetenschappen.

BouDagher-Fadel, M.K., 2008. Evolution and geological significance of larger benthic foraminifera. Elsevier.

Briguglio, A., Hohenegger, J., 2009. Nummulitids hydrodynamics: an example using Nummulites globulus Leymerie. Bollettino della societa paleontologica italiana 48, 105-111.

Briguglio, A., Hohenegger, J., 2011. How to react to shallow water hydrodynamics: The larger benthic foraminifera solution. Marine Micropaleontology 81, 63-76.

Briguglio, A., Hohenegger, J., Less, G., 2013. Paleobiological Applications of Three-Dimensional Biometry on Larger Benthic Foraminifera: A New Route of Discoveries. Turkish Journal of Earth Sciences 43, 72-87.

Chaproniere, G.C., 1975. Palaeoecology of Oligo-Miocene larger Foraminiferida, Australia. Alcheringa 1, 37-58.

Chaproniere, G.C.H., 1980. Biometrical studies of Early Neogene larger Foraminiferida from Australia and New Zealand. Alcheringa 4, 153-181.

Cope, E.D., 1896. The primary factors of organic evolution. Open Court.

Drooger, C., 1952. Study of American Miogypsinidae. Vonk.

Drooger, C., 1993. Radial foraminifera morphometrics and evolution, Verhandelingen der Koninklijke Nederlandse Akademie van Wetenschappen, Amsterdam, p. 242.

Drooger, C., Roelofsen, J., 1982. *Cycloclypeus* from Ghar-Hassan, Malta. Proceedings of the Koninklijke Nederlandse Akademie - Van Wetenschappen Series B -Palaeontology, Geology, Physics, Chemistry, Anthropology 85, 203-218.

Eder, W., Briguglio, A., Hohenegger, J., 2016a. Growth of *Heterostegina depressa* under natural and laboratory conditions. Marine Micropaleontology 122, 27-43.

Fermont, W., 1977a. Biometrical investigation of the genus *Operculina* in recent sediments of the Gulf of Elat. Utrecht Micropaleontological Bulletins 15, 171-204.

Fermont, W., 1977b. Depth-gradients in internal parameters of *Heterostegina* in the Gulf of Elat. Utrecht Micropaleontological Bulletin 15, 149-163.

Ferrandez-Canadell, C., Briguglio, A., Hohenegger, J., Woger, J., 2014. Test Fusion in Adult Foraminifera: A Review with New Observations of an Early Eocene *Nummulites* Specimen. J Foramin Res 44, 316-324.

Hallock, P., Röttger, R., Wetmore, K., 1991. Hypotheses on form and function in foraminifera. Biology of Foraminifera. Academic, 41-72.

Hammer, Ø., Harper, D., Ryan, P., 2001. PAST: Paleontological statistics software package for education and data analysis. Palaeontologia Electronica 4.

Hohenegger, J., 1994. Distribution of living larger Foraminifera NW of Sesoko-Jima, Okinawa Japan. Marine Ecology 15, 291-344.

Hohenegger, J., 2000. Coenoclines of larger foraminifera. Micropaleontology, 127-151.

Hohenegger, J., 2004. Depth coenoclines and environmental considerations of western Pacific larger foraminifera. The Journal of Foraminiferal Research 34, 9-33.

Hohenegger, J., 2006. The importance of symbiont-bearing benthic foraminifera for West Pacific carbonate beach environments. Marine Micropaleontology 61, 4-39.

Hohenegger, J., 2009. Functional shell geometry of symbiont-bearing benthic Foraminifera. Galaxea, Journal of Coral Reef Studies 11, 81-89.

Hohenegger, J., 2011a. Larger foraminifera: Greenhouse Constructions and Gardeners in the Oceanic Microcosm. The Kagoshima University Museum, Japan, Kagoshima.

Hohenegger, J., 2011b. Growth-invariant meristic characters. Tools to reveal phylogenetic relationships in Nummulitidae (Foraminifera). Turkish Journal of Earth Sciences 20, 655-681.

Hohenegger, J., 2014. Species as the basic units in evolution and biodiversity: recognition of species in the recent and geological past as exemplified by larger foraminifera. Gondwana Research 25, 707-728.

Hohenegger, J., Yordanova, E., 2001. Displacement of larger foraminifera at the western slope of Motobu Peninsula (Okinawa, Japan). 16 53-72.

Hohenegger, J., Briguglio, A., 2012. Axially oriented sections of nummulitids: A tool to interpret larger benthic foraminiferal deposits. J Foramin Res 42, 134-142.

Hohenegger, J., Yordanova, E., Hatta, A., 2000. Remarks on West Pacific Nummulitidae (foraminifera). J Foramin Res 30.

Hohenegger, J., Yordanova, E., Nakano, Y., Tatzreiter, F., 1999. Habitats of larger foraminifera on the upper reef slope of Sesoko Island, Okinawa, Japan. Marine Micropaleontology 36, 109-168.

Hottinger, L., 1977a. Distribution of larger Peneroplidae, *Borelis* and Nummulitidae in the Gulf of Elat, Red Sea. Utrecht Micropaleontological Bulletins 15, 35-109.

Hottinger, L., 2000. Functional Morphology of Benthic Foraminiferal Shells, Envelopes of Cells beyond Measure. Micropaleontology 46, 57-86.

Langer, M., Lipps, J., 2003. Foraminiferal distribution and diversity, Madang reef and lagoon, Papua New Guinea. Coral Reefs 22, 143-154.

Less, G., 1987. Paleontology and stratigraphy of the European Orthophragminids. Geologica Hungarica Series Paleontologica 51.

Less, G., Özcan, E., 2008. The late Eocene evolution of nummulitid foraminifer *Spiroclypeus* in the Western Tethys. Acta Palaeontologica Polonica 53, 303-316.

Less, G., Özcan, E., Papazzoni, C.A., Stockar, R., 2008. The middle to late Eocene evoltion of nummulitid foraminifer *Heterostegina* in the Western Tethys. Acta Palaeontologica Polonica 53, 317-350.

Leutenegger, S., 1977. Reproduction cycles of larger foraminifera and depth distribution of generations. Utrecht Micropaleontological Bulletins 15, 27-34.

Lipps, J., 1982. Biology/paleobiology of foraminifera. Foraminifera, Notes for a Short Course: Paleontological Society, University of Tennessee, 37-50.

Özcan, E., Sirel, E., Altiner, S.Ö., Çolakoğlu, S., 2001. Late Paleocene Orthophragminae (foraminfera) from the Haymana-Polath Basin, Central Turkey) and description of a new taxon, Orbitoclypeus haymanaensis. Micropaleontology 47, 339-357.

Papp, A., 1954. Morphologische-genetische Unterschungen an Foraminiferen. Paläontologische Zeitschrift 29, 74-78.

Papp, A., Küpper, K., 1952. Über die Entwicklung der Heterosteginen im Torton des Wiener Beckens. Anz. Österr. Akad. d. Wiss., mathem.-naturwiss. Kl 89.

Racey, A., 1992. The relative taxonomic value of morphological characters in the genus *Nummulites* (Foraminiferida). Journal of Micropalaeontology 11, 197-209.

Reiss, Z., Hottinger, L., 1984. The Gulf of Aqaba: ecological micropaleontology. Springer Science & Business Media.

Röttger, R., 1974. Larger foraminifera: Reproduction and early stages of development in *Heterostegina depressa*. Marine Biology 26, 5-12.

Schaub, H., 1963. Über einige Entwicklungsreihen von *Nummulites* und *Assilina* und ihre stratigraphische Bedeutung, in: von Koeningswald, G., Emeis, J., Buning, W. (Eds.), Evolutionary trends in Foraminifera. Elsvier, Philadelphia, pp. 282-297.

Schaub, H., 1981. Nummulites et Assilines de la Tethys Paléogène: taxinomie, phylogénesè et biostratigraphie. Birkhäuser.

Schmidt, D., Rayfield, E., Cocking, A., Marone, F., 2013. Linking evolution and development: Synchrotron Radiation X-ray tomographic microscopy of planktic foraminifers. Palaeontology 56, 741-749.

Seddighi, M., Briguglio, A., Hohenegger, J., Papazzoni, C.A., 2015. New results on the hydrodynamic behaviour of fossil Nummulites tests from two nummulite banks from the Bartonian and Priabonian of northern Italy. Bollettino della societa paleontologica italiana. Societa paleontologica italiana 54, 103-116.

Serra-Kiel, J., Hottinger, L., Caus, E., Drobne, K., Ferrandez, C., Jauhri, A.K., Less, G., Pavlovec, R., Pignatti, J., Samso, J.M., 1998. Larger foraminiferal biostratigraphy of the Tethyan Paleocene and Eocene. Bulletin de la Societé géologique de France 169, 281-299.

Speijer, R.P., Van Loo, D., Masschaele, B., Vlassenbroeck, J., Cnudde, V., Jacobs, P., 2008. Quantifying foraminiferal growth with high-resolution X-ray computed tomography: New opportunities in foraminiferal ontogeny, phylogeny, and paleoceanographic applications. Geosphere 4, 760-763.

Tan, S., 1937. Zur Kenntnis der Miogypsiniden. De Ingenieur in Nederlandsh-Indië (Mijnbouw en Geolgie) 4, 84-98.

Yordanova, E., Hohenegger, J., 2004. Morphoclines of living operculinid foraminifera based on quantitative characters. Micropaleontology 50, 149.

Zuo, S., Zhang, N., Li, B., Zhang, Z., Zhu, X., 2009. Numerical simulation of tidal current and erosion and sedimentation in the Yangshan deep water harbor of Shanghai. International Journal of Sediment Research 24, 287-298.

Chapter 3 (accepted for publication in the Proceedings of the 13th Int. Coral Reefs Symposium)

MORPHOMETRY OF THE LARGER FORAMINIFER *HETEROSTEGINA* EXPLAINING ENVIRONMENTAL DEPENDENCE; EVOLUTION AND PALAEOGEOGRPAHIC DIVERSIFIFCATION

***Wolfgang Eder[1]**, Johann Hohenegger[1], Ana I. Torres-Silva[1]. Antonino Briguglio[2]

[1] University of Vienna, Department of Palaeontology, Althanstrasse 14, 1090, Vienna, Austria

[2] Universiti Brunei Darussalam, Faculty of Science, Jalan Tungku, BE1410, Brunei Darussalam

***corresponding author:** wolfgang.eder@univie.ac.at, +0043 1/427753563

Keywords – larger foraminifera, palaeogeography, ecology, bathymetry, morphometry

Abstract

The cosmopolitan, symbiont-bearing, larger benthic foraminifer (LBF) *Heterostegina sensu lato* prefers oligotrophic environments in tropical and warm temperate seas. Harboring diatoms enables this species to be found across a wide illumination gradient from intertidal pools, where *H. depressa* protects against strongest illumination by occupying cryptic habitat, down to the base of the euphotic zone. Sheltered cryptic habitat, such as in holes of boulders, allows this species to live in highly energetic zones down to the fair weather wave base. Dependence on light for photosynthesis of its endosymbionts is managed by increasing surface/volume ratios of the test correlated with decreasing light, resulting in test flattening. Hydrodynamics also influences reproductive strategies. In high energy environments, asexual reproduction by schizogony dominates, while sexual reproduction (gametogony) is the dominant mode under low energy conditions. Thus, there is a shift in proportions between schizonts with smaller proloculi and gamonts with larger proluculi along the hydrodynamic gradient. Because there is a negative correlation between proloculus size and the number of chambers undivided by septula (operculinid chambers), the latter character shows negative dependence along the hydrodynamic gradient. Both proloculus size and number of operculinid chambers have been used as metric characters not only in the evolution of *Heterostegina* lineages starting in the middle Eocene, but also in many other nummulitds (e.g., *Nummulites*, *Spiroclypeus*, *Cycloclypeus*), totally neglecting the environmental dependence. Additionally, proloculus size can differ between biogeographically different populations (e.g., Okinawa and Hawaii) taken under similar hydrodynamic conditions. Using growth-independent and growth-invariant characters to describe the internal test morphology can enhance interpretation of evolutionary tendencies as distinct from environmental and palaeogeographic diversification.

1. Introduction

The genus *Heterostegina* d'Orbigny 1826 with first appearance in the Eocene (late Bartonian) belongs to the informal group of symbiont-bearing larger benthic foraminifera (LBF) with planispirally enrolled, chambered tests that follow a logarithmic spiral. The hyaline tests are characterized by a complete division of chambers into chamberlets, at least after an embryonal part (nepiont) consisting of a proloculus and deuteroloculus followed by a series of undivided 'operculinid' chambers. Whorls completely embrace the lateral test parts (involute tests) leading to alar chamber prolongations. Final

whorls can lose this complete embracement, then named 'maturo-evolute' (Banner and Hodgkinson, 1991). Beside molecular genetic differences (Holzmann et al., 2003), this test construction differentiates *Heterostegina* from the completely evolute genus *Planostegina* (Banner and Hodgkinson, 1991). In fossil representatives, the division into the subgenera *H. (Heterostegina)* and *H. (Vlerkina)* Eames et al. 1968 is solely based on the difference between maturo-evolute and involute tests (sensu Banner and Hodgkinson 1991), where the latter are regarded as typical for Paleogene representatives. The genus *Gryzbowskia* Bieda (1949) is characterized in equatorial sections by irregular-polygonal chamberlets, thus differentiated from *Heterostegina* possessing rectangular chamberlets (Banner and Hodgkinson, 1991; Lunt and Renema, 2014). The transition from complete involute into maturo-evolute tests in Paleogene species (e.g., Less et al., 2008) and the change from rectangular to polygonal chamberlets within one specimen makes a division based on chamberlet outline needless. This is followed by Less et al. (2008) in the work on the evolution of Paleogene Tethyan *Heterostegina*.

Today, the cosmopolitan single representative *Heterostegina depressa* d'Orbigny 1826 is restricted to oligotrophic tropical and warm temperate seas (Langer and Hottinger, 2000). It has reinvaded the Mediterranean as a Lessepsian immigrant (Hyams et al., 2002). Molecular genetic homogeneity of the species is documented by Holzmann et al. (2003) checking specimens from the Caribbean and Red Sea, and the Indian and Pacific Oceans.

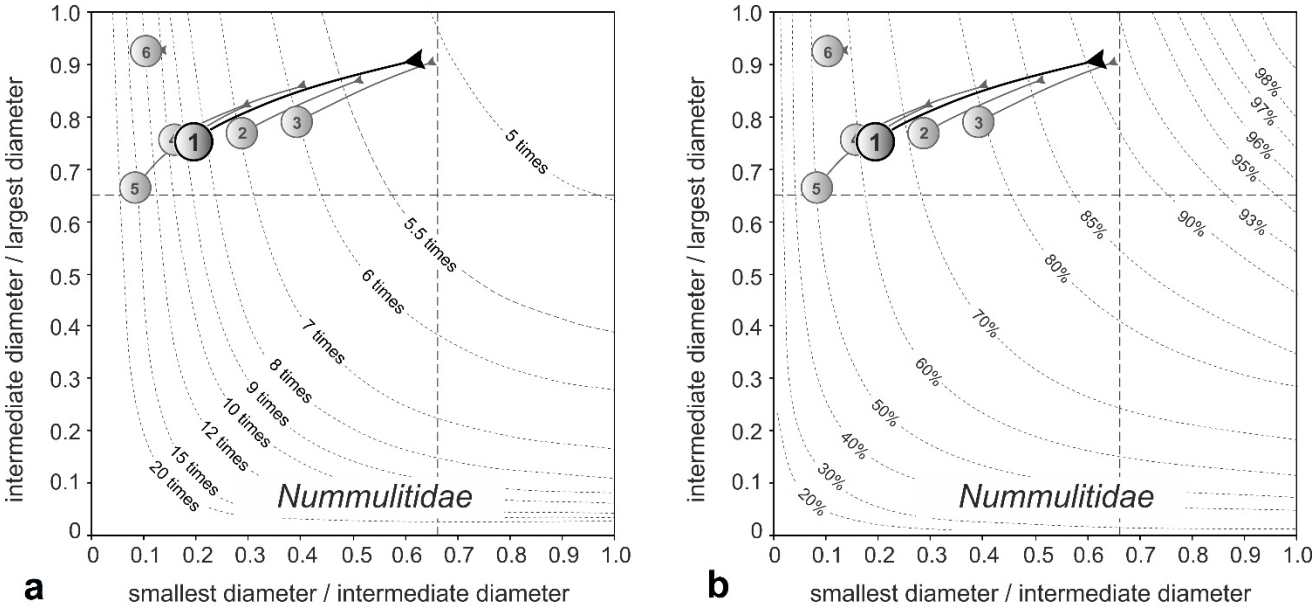

Figure 1 **-** The response of test shape in nummulitids to light and hydrodynamics represented in Zingg-diagrams. A) isolines represent surface/volume-ratios of triaxial ellipsoids with identical volumes. The surface/volume-ratio of a sphere is 4.836. B) isolines represent settling velocities expressed as percentages of the velocity of an equivalent sphere. Species are represented as trajectories indicating form changes, starting from thick lenticular to thin lenticular tests. 1. *Heterostegina depressa*, 2. *Operculinella cumingii*. 3. *Palaeonummulites venosus*, 4. *Operculina complanata*, 5. *Planostegina operculinoides*, 6. *Cycloclypeus carpenteri* modified after Hohenegger (2009)

2. Light

Specific *Thalassionema*-like diatoms harbored by *Heterostegina depressa* are clearly differentiated from related diatoms found in all other extant nummulitids (Holzmann et al., 2006), enabling one of the broadest distribution along the light gradient within diatom-bearing LBF. Best photosynthetic rates are obtained at low light levels with a maximum around 150 PAR µmol m^{-2} s^{-1} (Nobes et al., 2008). This allows the distribution from intertidal pools, where *H. depressa* protects

against strongest illumination in the shadow of boulders (cryptic habitat), to the deep euphotic zone (Hohenegger, 2004). The often used thickness/diameter-ratio (or the inverse D/T ratio) for determining the reaction to decreasing light intensities, is primarily understood as depth estimators (e.g., Hansen and Buchardt, 1977; Renema, 2005). But it can only be used for tests where flattening is obtained by thinning of the wall lamellae in combination with a constant test diameter, e.g., *Amphistegina* in Hallock (1979). This ratio is not useful where flattening is obtained by increasing test diameters and constant volumes (Röttger and Hallock, 1982). Here, the surface/volume ratios (e.g., Hohenegger, 2009) are better indicators to demonstrate the influence of decreasing light (Fig. 1a).

An equivalent parameter compared to the thickness/diameter ratio, but growth independent, is used to demonstrate the dependence of test flattening from light intensity. Measuring thickness at diverse radii for fitting a power function representing growth, thickness is calculated for the j^{th} specimen at a radius of 3000 µm by

$$th_j = a_j b_j^{3000} + c_j \qquad (1)$$

The correspondence of this growth invariant character with light intensity and depth are shown in Fig. 2.

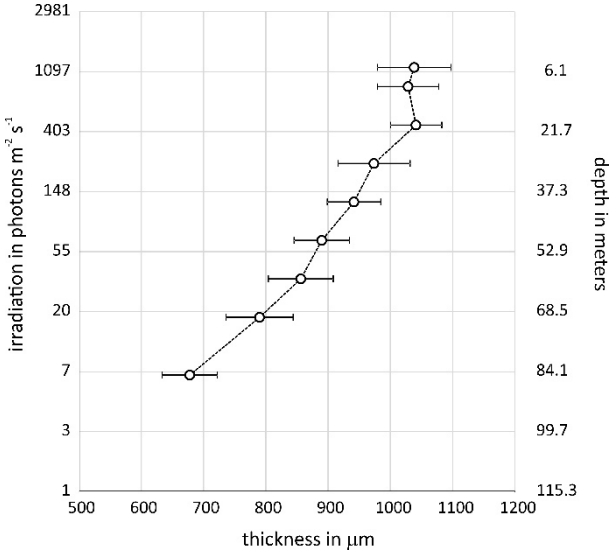

Figure 2 - Test thickness at a constant marginal radius of 3000 µm in dependence of light intensities correlating with depth. Bars indicate standard errors of the mean.

3. Hydrodynamics

While test flattening allows light absorption in low illuminated environments, because a large number of symbionts can be positioned in 'egg holders' of the test wall (Hottinger, 1977b), it weakens resistance against hydrodynamics (Fig. 1b). Therefore, thick lenticular *Heterostegina* can be found in high energy environments down to the fair-weather wave base protected in holes of coral rocks and boulders against entrainment and transport. The continuous flattening with depth allows settlement on middle to fine grained sand in deeper (i.e., more quiet) environments (e.g., Hohenegger, 2004).

Hydrodynamic is thus the second important factor for the distribution of *H. depressa*. Beside the effect of entrainment and transport of 'adult' tests, the hydrodynamic regime is extremely important for reproduction. A trimorphic life cycle in LBF as postulated by Leutenegger (1977) was first documented for LBF with *H. depressa* by Röttger et al. (1990). Morphological differences between the asexually reproduced schizonts and gamonts are expressed in proloculus size (Biekart et al., 1985), where prolocuti of schizonts are significantly smaller than prolocuti of gamonts. According to investigations at two depth transects NW of Sesoko Jima, Japan (Yordanova and Hohenegger, 2002), the test characters

'proloculus size' and 'number of operculinid chambers' (e.g., Less et al., 2008) are negatively correlated independent of their partial correlation with water depth. Decomposition of the bimodal frequency distribution of proloculus size combining all depth samples into normally distributed components resulted in two components, one with smaller and the other with larger proloculi, thus interpreted as schizonts and gamonts. Fitting depth samples using parameters of both distributions resulted in dominance of schizonts from 5 m to 35 m expressed in unimodal distributions, followed by bimodal distributions between 35 and 55 m, where both generations are present. Below 55 m the unimodal frequency distributions correspond to the distribution parameters of gamonts. Analyses of variance confirmed the stability in parameters of each generation with depth, thus explaining the depth trend as a sequence of two stable intervals - apogamic schizogeny at hydrodynamically exposed depths (5 to 35m) and gametogamy in quiet water (55 to 90 m) - connected by a transition zone where both reproduction modes are present showing decreasing schizogeny and increasing gametogamy (Eder et al., 2017). This distribution pattern can be explained by hydrodynamics hindering sexual reproduction in shallow environments exposed to strong water movement by destroying tiny gametes (Eder et al., 2017).

4. Evolutionary lineages

The depth trends in increasing proloculus size and decreasing number of undivided (operculinid) chambers of *H. depressa* perfectly mirrors the evolutionary lineages proposed by Less et al. (2008) for the Western Tethyan *Heterostegina armenica* and *H. reticulata* (Fig. 3; Eder et al., 2017). This is an argument for an intense environmental dependence of these lineages and may explain setbacks that have been documented also for *Nummulites*, where "more evolved" species occurred together with unreworked "primitive" species (Racey, 1992). Hence, the distributional pattern influenced by environmental factors might pose a problem for the explanation of continuous character changes as evolutionary tendencies.

Additionally, biogeographic differences may tangle the explanation as evolutionary lineages. Investigation on cell growth by chamber volumes using generalized logistic functions (Richards, 1959) showed that chamber growth in the initial test part up to chamber 25 can best be fitted by exponential function

$$V_{test} = ae^{bi} \qquad i = \text{chamber number} \qquad (2)$$

with the additive constant *a* explaining proloculus size and the multiplicative constant *b* determining the growth rate (Eder et al., 2016a).

Differences in initial growth between populations from Sesoko, Japan 20 m (collection Hohenegger) and Maui, Hawaii 40 m (collection Röttger) are expressed in proloculus size (constant *a* in equation 2), where individuals from Sesoko correspond to schizonts and individuals from Hawaii with larger proloculi correlate to gamonts (Fig. 4). Individuals from both natural populations have the same growth rates expressed in parameter *b* of equation 2. Cultured specimens originating from the natural population of Hawaii differ in both growth parameters from their natural population (Fig. 4; Eder et al., 2016a). This difference in parameter *a* indicates that they are also schizonts. Hence, schizonts from Hawaii have larger proloculi than those from Japan. Parameter *a* has to be studied on a larger scale to establish a reliable biogeographic trend, while parameter *b* gives more information about individual growth.

The above mentioned difficulties in explaining evolutionary lineages by a small set of internal test characters as used for stratigraphic purpose (e.g., Less et al., 2008) can be avoided using growth-independent and growth-invariant characters enabling a more or less general description of the complete test (Hohenegger, 2011b; Hohenegger and Torres-Silva, 2017). Using these methods, constants of equations fitting the character change during growth act as "supergenes" (Thompson

and Jiggins, 2014). Their effect on individuals can then be used as characters to classify fossil individuals in populations by multivariate. After determining populations using classification analyses, they can be interpreted as populations within an evolutionary lineage or as palaeobiogeographically separated populations (Hohenegger, 2014). Significant differences between populations can be obtained by discriminant analysis. The Late Eocene *Heterostegina ocalana* Cushman 1921 from Cuba and Panama (Cole, 1952) can be used as an example for interpretation of populations.

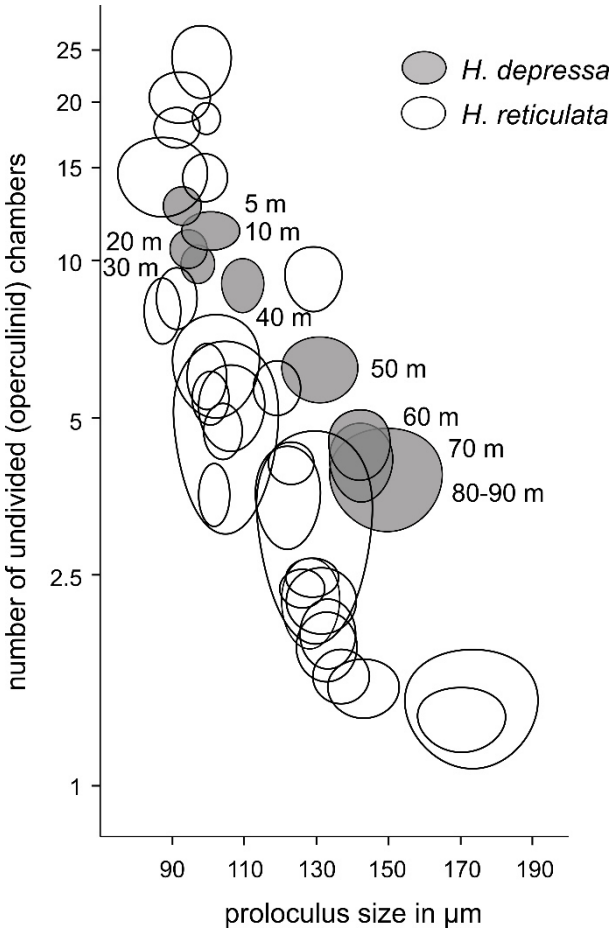

Figure 3 - Depth trend in proloculus size versus number of undivided postembryonic chambers in *Heterostegina depressa* from Sesoko Island, Okinawa with ellipses marking standard errors (95%). This depth trend completely fits the proposed evolutionary lineage of the late Eocene *Heterostegina reticulata* with the subspecies (from top to the bottom) *H. reticulata tronensis*, *H. reticulata hungarica*, *H. reticulata multifida*, *H. reticulata helvetica*, *H. reticulata reticulata*, *H. reticulata mossanensis* and *H. reticulata italica* (modified after Less et al., 2008).

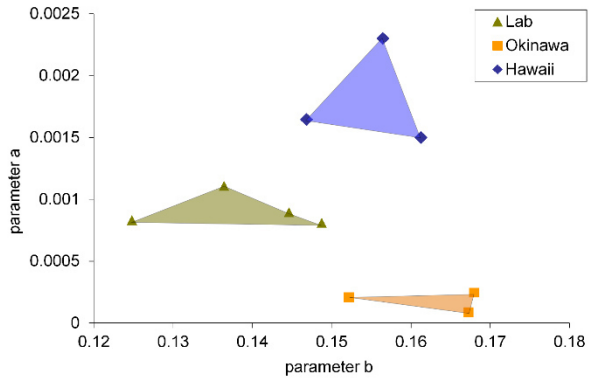

Figure 4 - Scatter plot of the constants *a* (indicating proloculus volume) and *b* (indicating growth rate) for the exponential fit of the first 25 chambers comparing megalospheres from Sesoko and Maui with laboratory cultures (after Eder et al., 2016a).

Evolutionary tendencies in populations from Cuba that are stratigraphically supported are also demonstrated in the first axis by a weak increase in the number of operculinid chambers, but strongly documented by the second discriminant axis with decreases in the "expansion rate of the marginal spiral", the "number of chamberlets" and the "backward bend angle of chambers" (Fig. 5). This evolutionary tendency is not coupled with an increase in "proloculus size" (here proloculus

height and width), yet regarded as one of the most prominent indicator for evolutionary changes in heterostegines (Less et al., 2008).

Palaeogeographical differences leading to subspecies together with transport, reworking and time-averaging could obscure

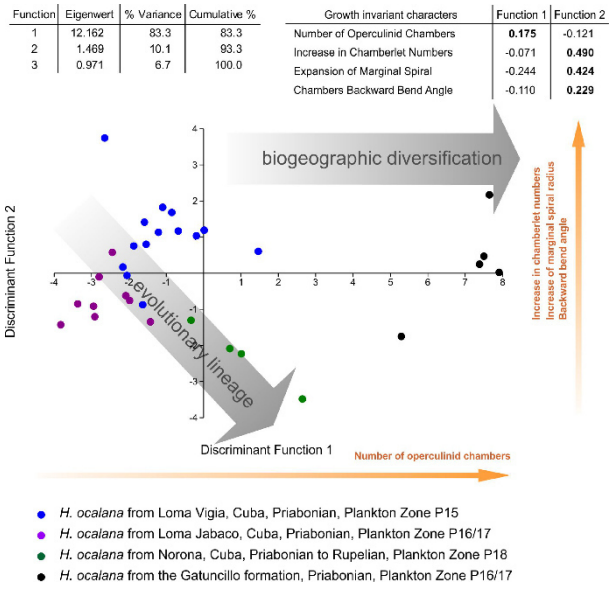

Figure 5 - Discriminant analysis of Heterostegina ocalana populations from Cuba and Panama based on growth independent and growth invariant characters, where loadings of the important characters are shown altered from Hohenegger and Torres-Silva (2017)

the clear dependence of fossil *Heterostegina* species on hydrodynamics and light, possibly leading to erroneous interpretations regarding evolutionary lineages. Using growth-independent and growth-invariant characters describing the internal test morphology more or less completely allows a much better interpretation of evolutionary tendencies separated from palaeogeographic diversification.

Acknowledgements

These investigations were funded by the FWF (Austrian Science Fund) project P 23459-B17 'Functional Shell Morphology of Larger Benthic Foraminifera', the FWF project P 26344-B25 'Breakthroughs in growth studies on larger benthic foraminifera' and by the North-South Dialogue scholarship of the Austrian Exchange Service (OeAD). We would like to thank our responsible Editor Dr. Pamela Hallock and further two anonymous reviewers and Dr. Ben Ross for helping to improve this manuscript.

References

Banner, F.T., Hodgkinson, R.L., 1991. A Revision of the Foraminiferal Subfamiliy *Heterostegininae*. Revista Espanola de Micropaleontologia 23, 101-140.

Biekart, J., Bor, T., Röttger, R., Drooger, C., Meulenkamp, J., 1985. *Megalospheric Heterostegina* depressa from Hawaii in sediments and laboratory cultures, Proceedings of the Koninklijke Nederlandse Akademie van Wetenschappen.

Cole, W., 1952. Eocene and Oligocene larger foraminifera from the Panama Canal Zone and vicinity. : U.S. Geol Survey Professional Paper 244, 1-41.

Eder, W., Briguglio, A., Hohenegger, J., 2016a. Growth of *Heterostegina depressa* under natural and laboratory conditions. Marine Micropaleontology 122, 27-43.

Eder, W., Hohenegger, J., Briguglio, A., 2017. Depth-related morphoclines of megalospheric test of Heterostegina depressa d'Orbigny: biostratigraphic and palaeobiological implications. PALAIOS.

Hallock, P., 1979. Trends in test shape with depth in large, symbiont-bearing foraminifera. J Foramin Res 9, 61-69.

Hohenegger, J., 2004. Depth coenoclines and environmental considerations of western Pacific larger foraminifera. The Journal of Foraminiferal Research 34, 9-33.

Hohenegger, J., 2009. Functional shell geometry of symbiont-bearing benthic Foraminifera. Galaxea, Journal of Coral Reef Studies 11, 81-89.

Hohenegger, J., 2011b. Growth-invariant meristic characters. Tools to reveal phylogenetic relationships in Nummulitidae (Foraminifera). Turkish Journal of Earth Sciences 20, 655-681.

Hohenegger, J., 2014. Species as the basic units in evolution and biodiversity: recognition of species in the recent and geological past as exemplified by larger foraminifera. Gondwana Research 25, 707-728.

Hohenegger, J., Torres-Silva, A., 2017. Growth-invariant and growth-independent characters in equatorial sections of Heterostegina shells relieve phylogenetic and paleobiogeographic interpretations. PALAIOS.

Holzmann, M., Hohenegger, J., Pawlowski, J., 2003. Molecular data reveal parallel evolution in nummulitid foraminifera. J Foramin Res 33, 277-284.

Holzmann, M., Berney, C., Hohenegger, J., 2006. Molecular identification of diatom endosymbionts in nummulitid Foraminifera, Symbiosis. Balaban Publishers, pp. 93-101.

Hottinger, L., 1977b. Foraminifères operculiniformes. Éditions du Muséum.

Hyams, O., Almogi-Labin, A., Benjamini, C., 2002. Larger foraminifera of the South Eastern Mediterranean shallow continental shelf off Israel. Isreal Journal of Earth Sciences 51, 169-179.

Langer, M., Hottinger, L., 2000. Biogeography of selected "larger" foraminifera. Micropaleontology 46, 105-126.

Less, G., Özcan, E., Papazzoni, C.A., Stockar, R., 2008. The middle to late Eocene evoltion of nummulitid foraminifer *Heterostegina* in the Western Tethys. Acta Palaeontologica Polonica 53, 317-350.

Leutenegger, S., 1977. Reproduction cycles of larger foraminifera and depth distribution of generations. Utrecht Micropaleontological Bulletins 15, 27-34.

Nobes, K., Uthicke, S., Henderson, R., 2008. Is light the limiting factor for the distribution of benthic symbiont bearing foraminifera on the Great Barrier Reef? Journal of Experimental Marine Biology and Ecology 363, 48-57.

Racey, A., 1992. The relative taxonomic value of morphological characters in the genus *Nummulites* (Foraminiferida). Journal of Micropalaeontology 11, 197-209.

Richards, F., 1959. "A Flexible Growth Function for Empirical Use". Journal of Experimental Botany 10, 290-300.

Röttger, R., Hallock, P., 1982. Shape Trends in Heterostegina-Depressa (Protozoa, Foraminiferida). J Foramin Res 12, 197-204.

Röttger, R., Krüger, R., de Rijk, S., 1990. Trimorphism in foraminifera (Protozoa)—verification of an old hypothesis. European journal of protistology 25, 226-228.

Thompson, M., Jiggins, C., 2014. Supergenes and their role in evolution. Heredity 113, 1-8.

Yordanova, E., Hohenegger, J., 2002. Taphonomy of larger foraminifera: relationships between living individuals and empty tests on flat reef slopes (Sesoko Island, Japan). Facies 46, 169-204.

Chapter 4 - ready for submission

TEST FLATTENING IN THE LARGER FORAMINIFERA *HETEROSTEGINA DEPRESSA*: PREDICTING BATHYEMTRY FROM AXIAL SECTIONS

***Wolfgang Eder**[1], Johann Hohenegger[1], Antonino Briguglio[2]

[1] University of Vienna, Department of Palaeontology, Althanstrasse 14, 1090, Vienna, Austria

[2] Universiti Brunei Darussalam, Faculty of Science, Jalan Tungku, BE1410, Brunei Darussalam

***corresponding author:** wolfgang.eder@univie.ac.at, +0043 1/427753563

Keywords - morphometry, thin sections, bathymetry, light intensity, hydrodynamics

Highlights - quantification methods for test flattening in *Heterostegina* - palaeoenvironment reconstruction of larger foraminifera – light intensity and hydrodynamics influence test shape of larger foraminifera

Abstract

Previous attempts to quantifying the test flattening trend in *Heterostegina depressa* with water depth have been rather unsuccessful. Due to its broad depth distribution, *H. depressa* is a perfect model species to calibrate test flattening as a bathymetric signal for fossil assemblages. This might enable us to better reconstruct palaeoenvironments of fossil larger foraminiferal communities or even provide clues on the degree of transport in allochthonous deposits. In this study we used growth-independent functions to describe the change of test thickness throughout ontogeny. Four growth-invariant characters, deriving from these functions, clearly quantify a transition of individuals with thicker to thinner central parts along the water depth gradient. This is probably controlled by light intensity because the photosymbionts of *H. depressa* (diatoms) are most effective at low irradiation levels, and hydro-dynamics.hydrodynamics Thus, shallower specimens grow thicker to reduce light penetration, whereas specimens living deeper than the light optimum increase their surface to obtain a better light exposure.

1. Introduction

Larger benthic foraminifera (LBF) are a non-taxonomic group of benthic protists unified by their symbiotic relationship with photosynthetic microalgae. They, have developed from smaller benthic forms multiple times throughout earth history. Due to their symbionts, they can attain larger test sizes, but are restricted to the photic zone of tropical to warm-temperate shallow marine environments (Hallock, 2000; BouDagher-Fadel, 2008).

In the past decades, larger foraminifera have been highlighted as important index fossils (Cahuzac and Poignant, 1997; Serra-Kiel et al., 1998) and especially nummulitids have been distinguished as highly informative facies fossils (Hallock et al., 1986; Beavington-Penney and Racey, 2004). These inferences on the ecology of fossil nummulitids were possible due to thorough actuopalaeontological research on the intricate ecological constraints of larger foraminifera test morphology (Reiss and Hottinger, 1984; Hallock et al., 1991; Hottinger, 2000; Hohenegger, 2009, 2011b; Prazeres et al., 2015; Eder et al., 2016b; Eder et al., 2017). Their shape and function is strongly influenced by two major factors – first, the intrinsic need to provide and shelter their symbionts, developing so-called “microscopic greenhouses” (sensu Hohenegger, 2011a) and second, the need to adapt to

physical factors of their immediate environment, mainly light attenuation and hydrodynamic energy (Hottinger, 2000; Hohenegger, 2004; Briguglio and Hohenegger, 2009; Hohenegger, 2009; Seddighi et al., 2015). The importance of the ecological adaptation of test thickness to water depth as a palaeoecological indicator has been thoroughly studied (Haynes, 1965; Hottinger, 1977a; Hallock, 1979; Röttger and Hallock, 1982; Hallock, 1988; Beavington-Penney and Racey, 2004; Cosovic et al., 2004; Hohenegger, 2004, 2009, 2011b), whereby the most commonly used indicator is the thickness/diameter (T/D) ratio. Several authors, however, have reported the T/D ratio's limited applicability as a water depth indicator (Reiss and Hottinger, 1984; Hallock and Glenn, 1986; Renema, 2005; Hohenegger, 2011b). This is mainly because its significance is restricted to species whose flattening is obtained by thinning of the lamellae (Hallock, 1979).

The nummulitid *Heterostegina depressa* d'Orbigny 1826 is the only extant representative of the heterosteginine subfamily (Banner and Hodgkinson, 1991; Holzmann et al., 2003). Generally, its test coiling is characterized by an approximated logarithmic spiral and arched chambers, which are subdivided into chamberlets by complete secondary septa (septula) (Hottinger, 1977b; Hohenegger, 2011b). It is a cosmopolitan species of tropic to warm-temperate shallow marine environments and shows the broadest depth distribution within the recent nummulitids: it occurs from the uppermost subtidal down to around 100 m water depth (Banner and Hodgkinson, 1991; Hohenegger, 2004). This species hosts *Thalassionema*-type diatom symbionts, which clearly differ from the diatoms of all other recent nummulitids (Holzmann et al., 2006); their highest photosynthetic rates are achieved at an optimal photosynthetic active radiation around 150 $\mu mol/m^{-2}\ s^{-1}$ (Nobes et al., 2008). Thus, *H. depressa* reacts to suboptimal light conditions by test modification (flattening), which, however, weakens resistance against high water energy and entrainment (Reiss and Hottinger, 1984; Hohenegger, 2009).

In the present study we use *H. depressa* to apply a new methodology to measure and model test thickness in nummulitids based on Hohenegger (2011b). This analysis demonstrates, that the growth functions, introduced here, can be used to describe the ontogenetic change of thickness in *H. depressa*. Furthermore, growth-invariant characters deriving from these function can be used to illustrate the continuous change in test shape with water depth. Finally, we discuss how the hydrodynamic regime, light intensity and attenuation, as well as habitat properties can influence these observed growth patterns.

2. Material and Methods

We used 127 specimens of *H. depressa* from depths of 5 to 90 m water depth (coll. J. Hohenegger). All selected specimens have megalospheric tests and were collected offshore Sesoko-Jima (N 26° 39' 5.134" E 127° 51' 11.635" and N 26° 39' 38.776" N, 127° 51' 56.28") in 1993 and 1996. Samples down to 40 m were collected by SCUBA, whereas deeper samples were dredged. Undisturbed distribution patterns were recorded by picking only living specimens from the sediments (for more information refer to Hohenegger, 1999). Sampling was done before the annual typhoon season to rule out down- or upslope transport of living specimens.

Axial sections were obtained by micro-computed tomography (µCT) visualisation. MicroCT is frequently used to observe, quantify and model foraminiferal test morphology in a non-destructive way (Speijer et al., 2008; Briguglio et al., 2011a; Hohenegger and Briguglio, 2012; Briguglio et al., 2013; Ferrandez-Canadell et al., 2014; Eder et al., 2016a). The images used in this study were taken with the high-energy scanner Skyscan 1173 at the University of Vienna (Department of Palaeontology). DataViewer 1.4.4.0 was used to extract the axial sections from the three-dimensional datasets.

2.1 Statistical analysis

Two growth functions (Hohenegger, 2011b) describing the ontogenetic development in thickness of *H. depressa* were used in this study.

The mediolateral thickness (*MlTh*) represents the test thickness at the radius centre of the whorl, which can be used to approximate the test shape in axial view. The change in mediolateral thickness during ontogeny can be shown by relating the mediolateral thickness with the corresponding marginal radius *MR*. We therefore measured *MlTh* at five locations on each shell's axial section (Fig. 1). These positions were chosen to represent the embryonic, juvenile, and adult spiral.

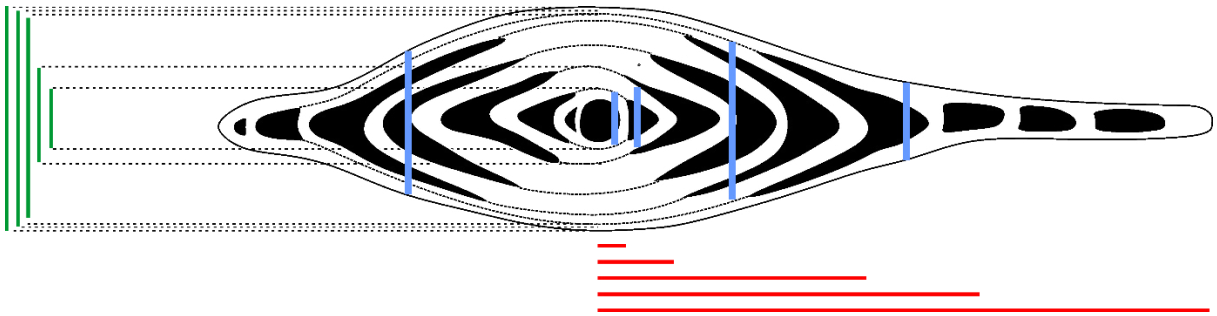

Figure 1 - *H. depressa* in axial view – Measurements of mediolateral thickness (MlTh) are indicated in blue, total thickness (Th) in green and corresponding radii in red.

Based on these measurements, the *MlTh* of the whole test was computed by,

$$MlTh = b_0(MR + b_3)^{b_1}\, e^{b_2(MR+b_3)} \qquad (1)$$

which is a composite function consisting of a power and exponential function. The parameters b_0 - the multiplicative constant, b_1 - the allometric constant, b_2 - the restriction rate and b_3 - an additive radius constant were estimated by non-linear regression using IBM-SPSS. The constants b_0 and b_1 control the power function, and b_2 determines the decrease in the exponential function.

In addition, the thickness (*Th*) at the test centre was measured in axial sections, at the same five positions mentioned above (Fig. 1). Its increase depends on the radius and can be approximated by the power function

$$Th = a \cdot MR^b + c \qquad (2)$$

where *a* is the multiplicative constant, *b* the growth rate and *c* the offset from the equatorial plane. This function describes how the thickness/diameter "ratio" changes during growth, thus discouraging the use of a fixed *T/D* ratio for depth estimation in *Heterostegina* and in all LBF with similar growth geometry.

Figure 2 displays regressions lines for equations 1 and 2 for one specimen from each water depth interval. Figure 3 illustrates the progression of the growth functions in an axial section to demonstrate how the mediolateral and total thickness change with test size. Based on these functions, the following growth-independent characters can describe flattening tendencies in *H. depressa.*

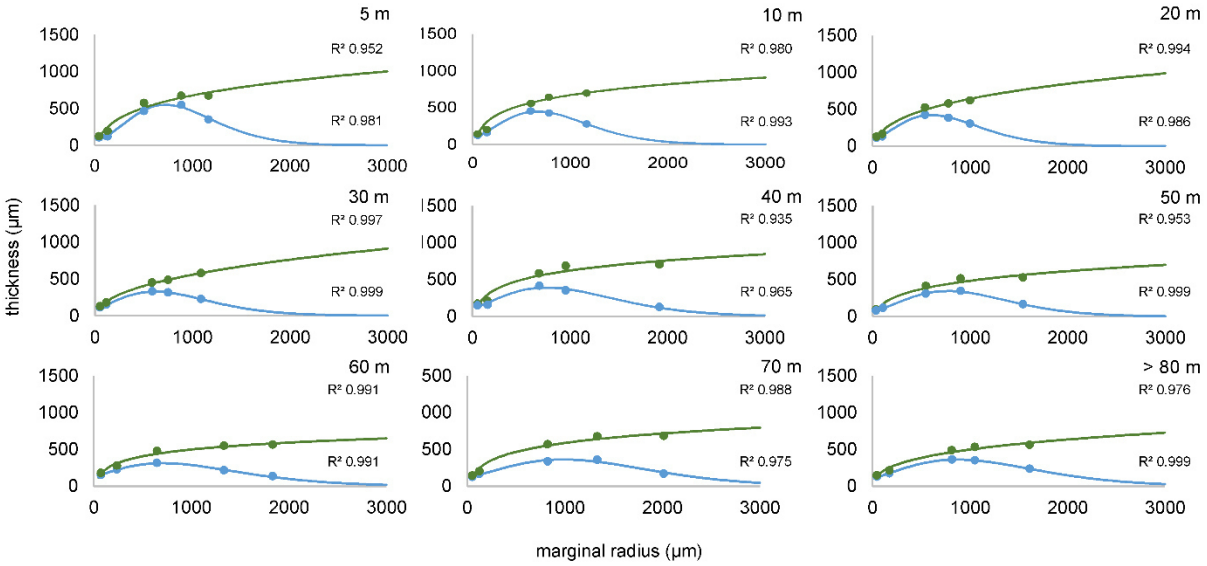

Figure 2 - Illustration of the two growth function for one specimen of *H. depressa* at each water depth interval. The mediolateral thickness is indicated in blue and total thickness in green. Filled dots represent the measurements depicted in Fig. 1. The corresponding functions of *MlTh* and *Th* are given along with their coefficient of determination R².

Using equation 2, the thickness *ThMR3* is calculated at 6 mm diameter or 3 mm marginal radius. This parameter characterizes the same relation as the thickness/diameter ratio, but allows comparison between individuals of different size due to the fixed radius (3 mm), thus becoming a growth-independent character.

The radius at the point of maximal mediolateral thickness (*MRmax*) is positioned at the inflection point of the function determining mediolateral thickness (equation 1). Computing the maximum mediolateral thickness (*MaxMlTh*) requires cal-culating *MRmax*. Hence, the first derivative of equation 1 must be set to zero.

$$MlTh' = b_0(b_3\,MR)^{b_1-1}(b_2\,MR + b_2b_3 + b_1)\,e^{b_2\,MR+b_2b_3} \quad (3)$$

By inserting parameters b_1, b_2 and b_3, the marginal radius *MRmax* can then be computed by

$$MRmax = -(b_2b_3 + b_1)/b_3 \quad (4)$$

Consequently, the maximal mediolateral thickness *MaxMlTh* can be calculated fitting *MRmax* into equation 1.

In maturo-evolute species, such as *H. depressa*, the test shape in axial section combines two shapes: an initial thick ellipse transferring into a final thin one. Thus, the maximal mediolateral thickness *MaxMlTh* in relation to its marginal radius *MRmax* describes the transfer point between these two different shapes and, therefore, marks the onset of test flattening. This is best described by the flattening ratio *F*, which is the ratio between *MaxMlTh* and *MRmax*. The linear relationship between numerator and denominator running through the origin manifests a correct use of the ratio and was tested by Pearson's correlation coefficient.

The two growth functions and four derived growth-invariant characters (i.e., radius at the point of maximal mediolateral thickness *MRmax*, maximal mediolateral thickness *MaxMlTh*, thickness at 3 mm marginal radius *ThMR3* and the flattening ratio *F*) (see Fig. 3) were computed for all specimens of *H. depressa* at 5 m depth and from 10 m to 70 m in 10m intervals; 80 and 90 m were merged due to their small sample sizes. Differences of the

characters between depths were checked by Kruskal-Wallis tests followed by a post-hoc Nemenyi multiple comparison (after Dunn, 1964). Additionally, Pearson's *r* was calculated for the four growth-invariant characters and proloculus size (taken from Eder et al., 2017) along the depth gradient. Finally, a partial correlation omitting water depth as control variable was calculated to check for correlation between the calculated characters and proloculus size.

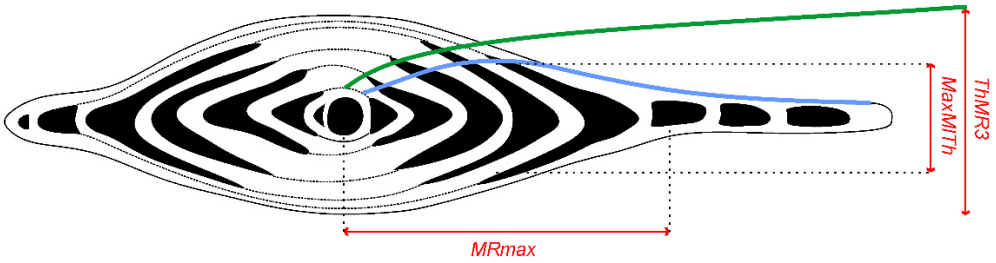

Figure 3 - The growth function for mediolateral thickness (blue) and for total thickness (green) plotted over an axial section. The unidimensional growth-invariant characters *ThMR3*, *MRmax* and *MaxMlTh* are depicted in red.

3. Results

Sample size n_j, mean $\bar{x}_j$, standard error se_j, and the ranges are given for the characters *MRmax*, *MaxMlTh*, *ThMR3* and *F* at every water depth *j* in table 1. The constants b_0, b_1, b_2, b_3 of equation 1, and *a*, *b*, *c* for equation 2, are given in the Supplementary data.

The correlations (Pearson's r and partial correlation) between the four growth-independent characters, the proloculus size and water depth are given in table 2. The ratio *F* correlates strongest with water depth, followed by *ThMR3* and *MaxMlTh*, while *MRmax* shows the weakest correlation. After water depth has been partialized, the four characters correlate with each other, while proloculus size shows no significant correlation with any of the growth-independent characters characterizing test flattening (Table 2).

Differences between depths proven for *MaxMlTh*, *ThMR3* and *F* by the Kruskal-Wallis test are significant, while those for *MRmax* are not (Tab. 3). Results of the post-hoc Nemenyi tests are also presented in Table 3.

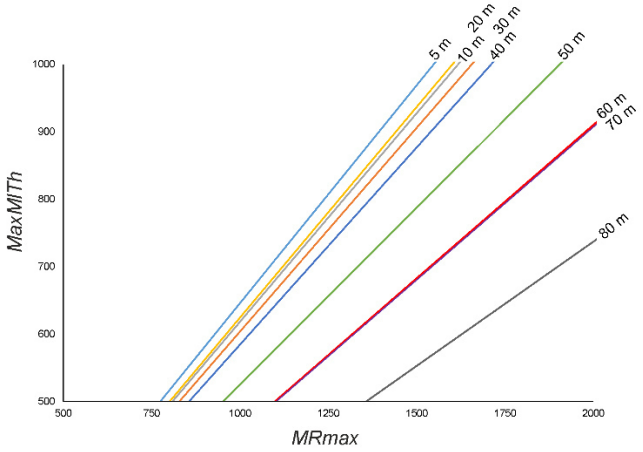

Figure 4 - Regression lines between *MRmax* and *MaxMlTh* following $y = kx$ (running through the origin) manifesting the correct use of the flattening ratio *F* for every investigated water depth.

The radius at the maximal mediolateral thickness *MRmax* shows no apparent trend, while a more or less consecutive depth trend is evident for the maximal mediolateral thickness *MaxMlTh*. Interestingly, a distinct excursion to thicker values occurs between 30 to 40 m. For the thickness at *MR* = 3mm (*ThMR3*), thickness decreases constantly. Based on multiple comparison, *ThMR3* can be differentiated into 5 to 20, 30 to 40, 50 to 60, 70 and >80 m intervals. For the flattening ratio *F,* intervals from 5 to 30, 40, 50 and 60 to 80 m are recognizable.

depth	*n*	$\bar{x}$	*se*	*min*	*max*	$\bar{x}$	*se*	*min*	*max*
5	13	725.0	26.55	636.1	617.4	473.6	22.91	328.4	617.4
10	15	766.1	28.65	590.2	562.0	467.5	13.60	368.3	562.0
20	15	724.7	31.91	553.1	565.7	453.7	15.67	360.3	565.7
30	15	673.0	41.30	415.0	679.5	423.1	30.04	292.4	679.5
40	15	802.6	38.85	570.5	699.6	471.4	25.12	306.6	699.6
50	15	847.9	70.97	504.3	747.7	450.3	38.56	264.2	747.7
60	15	884.8	55.76	664.6	549.6	419.5	25.32	274.7	549.6
70	15	841.2	82.36	373.3	639.2	388.9	38.01	198.2	639.2
80	9	819.7	133.63	348.9	433.3	332.6	29.87	199.6	433.3
		ThMR3				***F***			
depth	*n*	$\bar{x}$	*se*	*min*	*max*	$\bar{x}$	s_e	*min*	*max*
5	13	1038.3	59.24	772.4	1501.3	0.7	0.02	0.5	0.8
10	15	1028.6	49.04	813.8	1518.0	0.6	0.02	0.5	0.7
20	15	1041.3	41.32	788.2	1364.3	0.6	0.02	0.5	0.8
30	15	973.8	57.98	638.0	1434.0	0.6	0.03	0.4	0.8
40	15	941.7	42.96	698.5	1234.8	0.6	0.02	0.5	0.7
50	15	889.9	44.58	686.2	1178.5	0.5	0.02	0.4	0.7
60	15	856.2	52.15	588.9	1244.0	0.5	0.03	0.3	0.7
70	15	789.8	54.00	465.3	1207.7	0.5	0.02	0.3	0.6
80	9	677.8	44.37	433.8	867.5	0.4	0.04	0.3	0.6

Table 1- Sample size n_j, mean $\bar{x}_j$, standard error s_e, minimum and maximum for the characters *MRmax*, *MaxMlTh*, *ThMR3* and *F* for every water depth *j*.

Pearson's r						
		MRmax	***MaxMlTh***	***ThMR3***	***F***	***P***
depth	corr.	0.225	-0.29	-0.491	-0.599	0.747
	p	0.006	4.67E-04	2.23E-09	6.38E-14	3.40E-24
MRmax	corr.		0.623	0.219	-0.384	0.203
	p		2.56E-15	0.007	4.49E-06	0.011
MaxMlTh	corr.			0.689	0.418	-0.237
	p			1.61E-19	5.53E-07	0.004
ThMR3	corr.				0.537	-0.442
	p				4.56E-11	1.02E-07
F	corr.					-0.473
	p					1.11E-08

control variable: water depth		***MaxMlTh***	***ThMR3***	***F***	***P***
Mrmax	corr.	0.761	0.406	-0.345	-0.009
	p	4.02E-25	1.35E-06	3.98E-05	0.462
MaxMlTh	corr.		0.657	0.317	-0.042
	p		4.70E-17	1.61E-04	0.320
ThMR3	corr.			0.350	-0.132
	p			3.10E-05	0.071
F	corr.				-0.055
	p				0.272

Table 2 - Pearson's correlations for water depth, growth-invariant characters and proloculus size. Note the significant correlation between some characters and proloculus size before water depth is partialized. Degrees of freedom = 127 for all Pearson's r values; degrees of freedom = 124.

Finally, table 4 provides the statistics proving the linear relationship between *MRmax* and *MaxMlTh*. The coefficient of correlation *k* steadily decreases towards deeper samples, except a short excursion at 10 m, whereas p-values and coefficients of variation remain similar between samples. Figure 4 plots the regression lines illustrating the linear relationship between *MRmax* and *MaxMlTH* for every water depth interval *j*.

4. Discussion

The presented methodology solves a problem in quantifying thickening and flattening tendencies in larger benthic foraminiferal tests in relation to water depth. The ontogenetic development of test thickness in *H. depressa* can be approximated by a power function correlating test thickness to the marginal radius (or diameter), and its value continuously changes with increasing growth.

Based on this function, thickness was computed for every specimen at a marginal radius of 3 mm (3000 µm), which bypasses the problem of growth dependence by comparing specimens using this fixed thickness. The thickness *ThMR3* gives accurate results on water depth, showing a clear depth trend (Fig. 5c). Using this parameter is particularly convenient also because it simplifies the comparison of differently sized specimens (by considering only the first 3 mm).

Thickness, however, provides no direct information on the degree of flattening, which is especially interesting for the so-called maturo-evolute shape of *H. depressa* (Banner and Hodgkinson, 1991) and for other nummulitids showing similar flattening tendencies. Tests with thickened centres and thinner periphery occur in several fossil (e.g., *Spiroclypeus, Heterotegina*) and recent nummulitid genera (e.g., *Palaeonummulites, Operculinella, Cycloclypeus*). To describe and quantify such geometry, we have introduced the maximal mediolateral thickness (*MaxMlTh*), the corresponding marginal radius (*MRmax*) and the flattening ratio (*F*). From 5 to 30 m water depth the maximal mediolateral thickness (*MaxMlTh*) remains more or less constant, while at 40 m the trend shows a sudden excursion to thicker values before decreasing constantly towards deeper samples (Fig. 5b). This distinctive setback in the trend seems to record the change from reef-associated to sandy habitats because specimens become thicker on sandy bottoms to resist entrainment by orbital wave movement (Briguglio and Hohenegger, 2011b). The similar ratios from 5 to 30 m correlate with reef-associated habitats, which are built-up of highly diverse

structures (e.g., shaded areas, tide pools, reef crevices) (Fig. 5d). Samples from 40 and 50 m correspond to the transition zone between reef-associated habitats and sandy bottoms. This zone is characterized by an intercalation of reef debris and few living corals (Hohenegger, 2004, in Fig. 4). The deepest samples (60 to >80 m) correlate with sandy bottoms in a low energy setting. This habitat-related change is also reflected in the flattening ratio *F*.

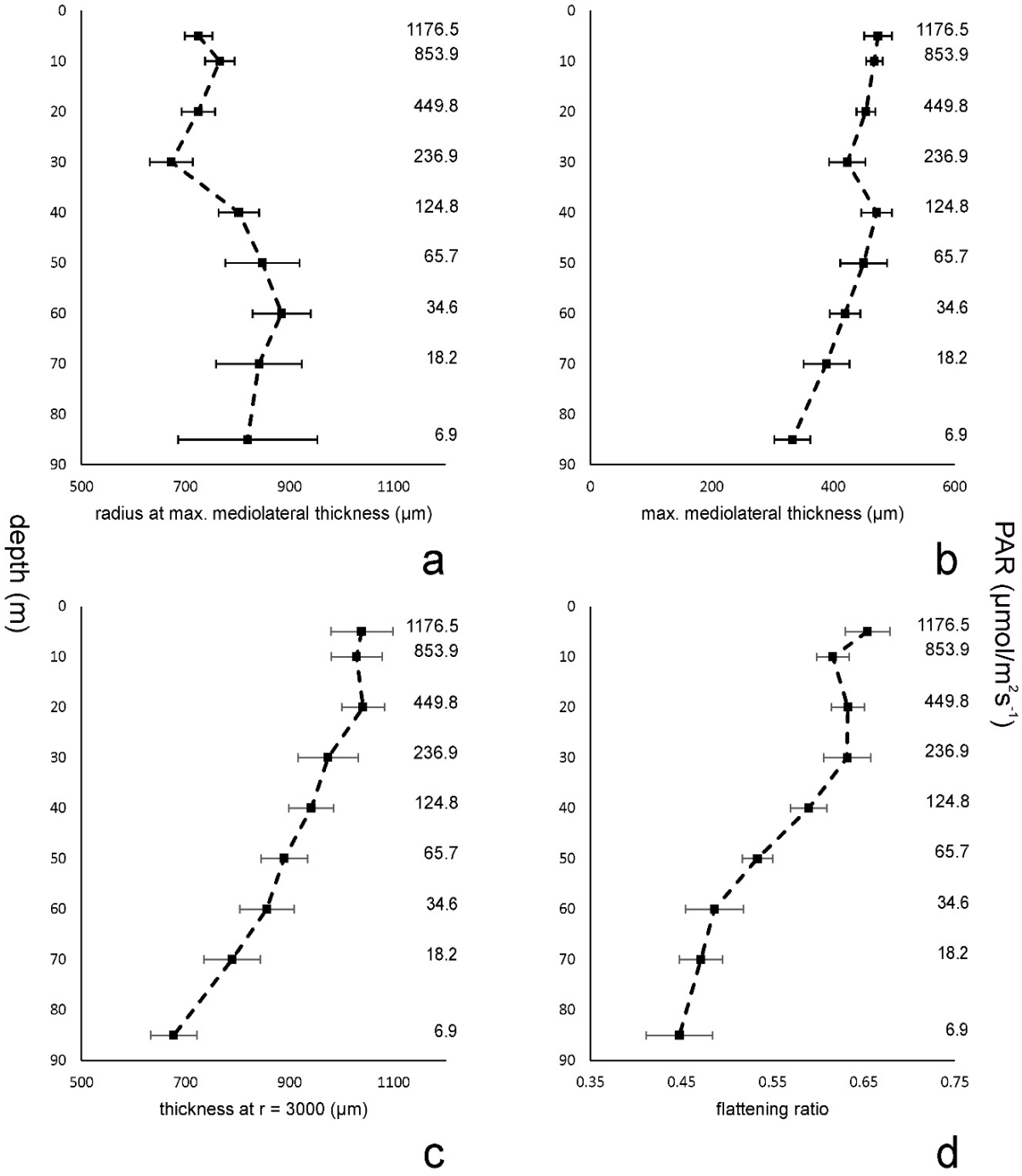

Figure 5 - The mean and standard error of the growth-invariant characters plotted against water depth (left ordinate) and light intensity (right ordinate). a) Marginal radius at the maximal mediolateral thickness (*MRmax*); b) Maximal mediolateral thickness (*MaxMlTh*); c) Thickness at 3000 µm (*ThMR3*); d) Flattening ratio *F*.

Kruskal-Wallis

	MRmax	***MaxMlTh***	***ThMR3***	***F***
χ^2	13.192	15.580	31.851	50.843
df	8	8	8	8
p	0.105	0.049	9.90E-05	2.81E-08

grouping Variable: water depth

Ranks

	depth	*n*	Mean Rank
MRmax	5	13	54.15
	10	15	65.73
	20	15	53.73
	30	15	42.07
	40	15	71.73
	50	15	71.53
	60	15	83.67
	70	15	67.80
	80	9	64.44
	Sum	127	
MaxMlTh	5	13	77.54
	10	15	77.27
	20	15	71.07
	30	15	56.87
	40	15	75.67
	50	15	64.67
	60	15	59.07
	70	15	51.47
	80	9	31.00
	Sum	127	
ThMR3	5	13	81.62
	10	15	81.27
	20	15	86.40
	30	15	70.33
	40	15	67.87
	50	15	58.80
	60	15	51.80
	70	15	41.73
	80	9	21.56
	Sum	127	
F	5	13	92.38
	10	15	80.53
	20	15	86.87
	30	15	85.73
	40	15	70.40
	50	15	49.53
	60	15	39.60
	70	15	32.20
	80	9	28.22
	Sum	127	

Nemenyi (after Dunn)									
MaxMlTh	5	10	20	30	40	50	60	70	80
5		0.089	2.121	**6.775**	0.613	**4.218**	**6.054**	**8.545**	**11.647**
10	accept		2.188	**7.200**	0.565	**4.447**	**6.424**	**9.106**	**12.247**
20	accept	accept		**5.012**	1.624	2.259	**4.235**	**6.918**	**10.606**
30	**reject**	**reject**	**reject**		**6.635**	2.753	0.776	1.906	**6.847**
40	accept	accept	accept	**reject**		**3.882**	**5.859**	**8.541**	**11.824**
50	**reject**	**reject**	accept	accept	**reject**		1.976	**4.659**	**8.912**
60	**reject**	**reject**	**reject**	accept	**reject**	accept		2.682	**7.429**
70	**reject**	**reject**	**reject**	accept	**reject**	**reject**	accept		**5.418**
80	**reject**	**reject**	**reject**	reject	**reject**	**reject**	**reject**	**reject**	
ThMR3	5	10	20	30	40	50	60	70	80
5		0.114	1.568	**3.697**	**4.506**	**7.477**	**9.771**	**13.071**	**15.031**
10	accept		1.812	**3.859**	**4.729**	**7.929**	**10.400**	**13.953**	**15.806**
20	accept	accept		**5.671**	**6.541**	**9.741**	**12.212**	**15.765**	**17.165**
30	**reject**	**reject**	**reject**		0.871	**4.071**	**6.541**	**10.094**	**12.912**
40	**reject**	**reject**	**reject**	accept		**3.200**	**5.671**	**9.224**	**12.259**
50	**reject**	**reject**	**reject**	**reject**	**reject**		2.471	**6.024**	**9.859**
60	**reject**	**reject**	**reject**	**reject**	**reject**	accept		**3.553**	**8.006**
70	**reject**	**reject**	**reject**	**reject**	**reject**	**reject**	**reject**		**5.341**
80	**reject**	**reject**	**reject**	**reject**	**reject**	**reject**	**reject**	**reject**	
F	5	10	20	30	40	50	60	70	80
5		**3.884**	1.808	2.180	**7.205**	**14.044**	**17.299**	**19.724**	**16.058**
10	**reject**		2.235	1.835	**3.576**	**10.941**	**14.447**	**17.059**	**13.847**
20	accept	accept		0.400	**5.812**	**13.176**	**13.176**	**19.294**	**15.524**
30	accept	accept	**reject**		**5.412**	**12.776**	**16.282**	**18.894**	**15.224**
40	**reject**	**reject**	**reject**	**reject**		**7.365**	**10.871**	**13.482**	**11.165**
50	**reject**	**reject**	**reject**	**reject**	**reject**		**3.506**	**6.118**	**5.641**
60	**reject**	**reject**	**reject**	**reject**	**reject**	**reject**		2.612	1.053
70	**reject**	**reject**	**reject**	**reject**	**reject**	**reject**	accept		1.053
80	**reject**	**reject**	**reject**	**reject**	**reject**	**reject**	accept	accept	

Table 3 - Kruskal-Wallis tests proving homogeneity for each growth-invariant character. Sample size n and mean ranks for each depth interval j are given, followed by a post-hoc Nemenyi test after Dunn. The results of the multiple comparison are presented as triangular matrices. The upper triangle gives the significance (underlined: $q < q^{(0.05,8)}$) and the lower triangle shows the acceptance of H_0 (sample median is the same).

The reason for a decrease in thickness has been thoroughly discussed, and it is widely accepted that hydrodynamic energy and light intensity have a synergetic influence on test thickness (Larsen and Drooger, 1977; Hallock, 1979; Hohenegger, 2004). Nonetheless, our results on test flattening show that specimens from different depths are influenced by these factors in a different way. A clear shift in test flattening is evident from the high-energetic reef-associated samples to the transitional zone and to deeper, low-energy samples. This implies that, in shallower environments, mechanical strengthening of the test is more important, whereas in deeper slope environments, light intensity is the major factor controlling test shape. The differences in internal morphology of the two

bathymetrically separated megalospheric generations (gamonts and schizonts), as reported in Eder et al. (2017), are not reflected in test thickness and flattening (Table 2, partial correlation).

Furthermore, the rather stable values of the characters *ThM3* and *F* (Fig 5c-d) in shallower samples proposes a realized maximal limit of total test thickness around the efficiency optimum of the host's symbionts (~ 300 PAR). This limitation in morphological plasticity seems to be around 30 m water depth, coinciding with the maximal abundance of *Heterostegina* in oligotrophic environments (Hohenegger, 2000). Structured reef-associated habitats may allow *Heterostegina* to settle in even shallower water depths because they can populate shaded areas and holes to counteract high light intensities and entrainment (Hohenegger, 2004).

	Pearson's r		
depth	*k*	*R*	*p*
5	0.646	0.646	0.009
10	0.604	0.587	0.022
20	0.618	0.723	0.002
30	0.625	0.752	0.001
40	0.585	0.766	0.009
50	0.525	0.923	9.41E-07
60	0.455	0.715	0.003
70	0.454	0.841	8.63E-05
80	0.369	0.865	0.003

Table 4 - The slope k_j, the correlation coefficient R_j and its probability p_j for the linear regression between *MRmax* and *MaxMlTh* at water depth intervals *j*.

While hydrodynamic and light intensity are the general factors controlling thickness, other factors like water transparency, sedimentary compositions and structure of habitats additionally affect test shape.. Therefore, structured habitats (e.g., reefs and reef debris) diminish the influence of light intensity and hydrodynamic energy on the test of *H. depressa*, while in unstructured habitats (e.g., sandy to silty bottoms) the exposure to physical influences is stronger. Vice versa, the sediment distribution along the slope is primarily influenced by hydrodynamic energy and submarine topography, hence encountering complex synergetic effects.

Therefore, absence/presence of reef environments and the topography of the slope (e.g., steep drop-offs) must be taken into account when considering test thickness and flattening as depth indicators. Especially for palaeontological application, different paleoenvironmental indicators must be integrated to cross-correlate with the information obtained from test thickness and test flattening in nummultids. Ramp-like slope morphologies, typical of Paleogene shallow marine environments, lacking any major bioherms might be a key factor in the emergence of secondary growth in thickness as an adaption to highly illuminated, high energy environments. In these taxa lateral chambers have to be strictly differentiated between lateral chamberlets (e.g., *Heterostegina* sensu lato, *Tansinhokella* and *Grzybowskia*) and "real" lateral chambers or orbitoid type "cubicula" (e.g., *Spiroclypeus*) (Banner and Hodgkinson, 1991). Only for the first case, where spiral and lateral growth steps take place simultaneously, the present methodology can be applied.

5. Conclusion

The ontogenetic development of thickness in *H. depressa* can either be described by a power function for thickness or by a complex function for mediolateral thickness. From these functions, four growth-invariant characters can be obtained, enabling a detailed quantification of trends in test thickness and flattening.

The character *Th3* describes the theoretical thickness at the fixed size of *MR* = 3000 µm, while the maximal mediolateral thickness *MaxMlTh* describes the thickness at the onset of test flattening, which is especially important for "maturo-evolute" nummulitid taxa. The relation between the marginal radius *MRmax* and the maximal mediolateral thickness can be exemplified as the flattening ratio *F*.

Furthermore, the presented results hint that the thickness *Th3* and the flattening ratio *F* allow the best bathymetric estimation. The generally accepted factors influencing test shapes in larger foraminifera are light intensity and hydrodynamic energy; although they show complex synergetic effects with terrigenous influx, sediment composition and proportion. Shallower samples from reef-associated habitats show no distinct changes in their degree of flattening down to 30 meters water depth, since extrinsic factors are partially cancelled out due to the three-dimensional structure of the micro-habitat in firm substrates. Thus, test thickness seems to be a habitat-independent indicator for bathymetric changes, with a continuous decrease in thickness along water depth. In contrasts, the flattening ratio incorporates additional information on the sediment composition of the habitat.

A connection between internal morphology in the different megalospheric generations (e.g., proloculus size) and test thickness or flattening could not be detected, while a similar tendency of flattening in microspheric generation has yet to be tested.

Since similar ecological constraint can be assumed for fossil heterostegenid taxa, the dependence on water depth expressed in different test thickness established in this study allows reconstructing bathymetric distributions of autochthonous fossil populations. Further, this might give a hint on the degree of transport in allochthonous deposits and permits a more detailed reconstruction of paleoenvironments of fossil larger foraminiferal communities. However, in case of a secondary growth in thickness it has to be strictly differentiated between lateral chamberlets and cubicula.

Acknowledgements

This work was performed at the micro-CT Facility, which is part of the Department of Palaeontology at the University of Vienna, Austria. This study was exercised within the project "Breakthroughs in growth studies on larger benthic foraminifera" of the Austrian Science Fund (FWF; grant P26344-B25).

References

Banner, F.T., Hodgkinson, R.L., 1991. A Revision of the Foraminiferal Subfamiliy *Heterosteginae*. Revista Espanola de Micropaleontologia 23, 101-140.

Beavington-Penney, S.J., Racey, A., 2004. Ecology of extant nummulitids and other larger benthic foraminifera: applications in palaeoenvironmental analysis. Earth-Science Reviews 67, 219-265.

BouDagher-Fadel, M.K., 2008. Evolution and geological significance of larger benthic foraminifera. Elsevier.

Briguglio, A., Hohenegger, J., 2009. Nummulitids hydrodynamics: an example using Nummulites globulus Leymerie. Bollettino della societa paleontologica italiana 48, 105-111.

Briguglio, A., Hohenegger, J., 2011b. How to react to shallow water hydrodynamics: The larger benthic foraminifera solution. Marine Micropaleontology 81, 63-76.

Briguglio, A., Metscher, B., Hohenegger, J., 2011a. Growth rate biometric quantification by X-ray microtomography on larger benthic foraminifera: three-dimensional measurements push nummulitids into the fourth dimension. Turkish Journal of Earth Science 20, 683-699.

Briguglio, A., Hohenegger, J., Less, G., 2013. Paleobiological Applications of Three-Dimensional Biometry on Larger Benthic Foraminifera: A New Route of Discoveries. Turkish Journal of Earth Sciences 43, 72-87.

Cahuzac, B., Poignant, A., 1997. Essai de biozonation de l'Oligo-Miocène dans les bassins européens à l'aide des grands foraminifères néritiques. Bulletin de la Société géologique de France 168, 155-169.

Cosovic, V., Drobne, K., Moro, A., 2004. Paleoenvironmental model for Eocene foraminiferal limestones of the Adriatic carbonate platform (Istrian Peninsula). Facies 50, 61-75.

Dunn, O.J., 1964. Multiple Comaprisons using rank sums. Technometrics 6, 241-252.

Eder, W., Briguglio, A., Hohenegger, J., 2016a. Growth of *Heterostegina depressa* under natural and laboratory conditions. Marine Micropaleontology 122, 27-43.

Eder, W., Hohenegger, J., Briguglio, A., 2017. Depth-related morphoclines of megalospheric test of Heterostegina depressa d'Orbigny: biostratigraphic and palaeobiological implications. PALAIOS.

Eder, W., Hohenegger, J., Torres-Silva, A.I., Briguglio, A., 2016b. Morphometry of the larger foraminifera Heterostegina explaining environmental dependence, evolution and paleogeographic diversification. Proceedings of the 13th International Corel Reefs Symposium.

Ferrandez-Canadell, C., Briguglio, A., Hohenegger, J., Woger, J., 2014. Test Fusion in Adult Foraminifera: A Review with New Observations of an Early Eocene *Nummulites* Specimen. J Foramin Res 44, 316-324.

Hallock, P., 1979. Trends in test shape with depth in large, symbiont-bearing foraminifera. J Foramin Res 9, 61-69.

Hallock, P., 1988. The role of nutrient availability in bioerosion: consequences to carbonate buildups. Palaeogeography, Palaeoclimatology, Palaeoecology 63, 275-291.

Hallock, P., 2000. Symbiont-bearing foraminifera: harbingers of global change? Micropaleontology, 95-104.

Hallock, P., Glenn, E.C., 1986. Larger Foraminifera: A Tool for Paleoenvironmental Analysis of Cenozoic Carbonate Depositional Facies. PALAIOS 1, 55-64.

Hallock, P., Forward, L.B., Hansen, H.J., 1986. Influence of Environment on the Test Shape of Amphistegina. J Foramin Res 16, 224-231.

Hallock, P., Röttger, R., Wetmore, K., 1991. Hypotheses on form and function in foraminifera. Biology of Foraminifera. Academic, 41-72.

Haynes, J., 1965. Symbiosis, wall structure and habitat in foraminifera. Contributions from the Cushman Foundation for Foraminiferal Research 16, 40-43.

Hohenegger, J., 1999. Habitats of larger foraminifera on the upper reef slope of Sesoko Island, Okinawa, Japan. Marine Micropaleontology 36, 109-168.

Hohenegger, J., 2000. Coenoclines of larger foraminifera. Micropaleontology, 127-151.

Hohenegger, J., 2004. Depth coenoclines and environmental considerations of western Pacific larger foraminifera. The Journal of Foraminiferal Research 34, 9-33.

Hohenegger, J., 2009. Functional shell geometry of symbiont-bearing benthic Foraminifera. Galaxea, Journal of Coral Reef Studies 11, 81-89.

Hohenegger, J., 2011a. Larger foraminifera: Greenhouse Constructions and Gardeners in the Oceanic Microcosm. The Kagoshima University Museum, Japan, Kagoshima.

Hohenegger, J., 2011b. Growth-invariant meristic characters. Tools to reveal phylogenetic relationships in Nummulitidae (Foraminifera). Turkish Journal of Earth Sciences 20, 655-681.

Hohenegger, J., Briguglio, A., 2012. Axially oriented sections of nummulitids: A tool to interpret larger benthic foraminiferal deposits. J Foramin Res 42, 134-142.

Holzmann, M., Hohenegger, J., Pawlowski, J., 2003. Molecular data reveal parallel evolution in nummulitid foraminifera. J Foramin Res 33, 277-284.

Holzmann, M., Berney, C., Hohenegger, J., 2006. Molecular identification of diatom endosymbionts in nummulitid Foraminifera, Symbiosis. Balaban Publishers, pp. 93-101.

Hottinger, L., 1977a. Distribution of larger Peneroplidae, *Borelis* and Nummulitidae in the Gulf of Elat, Red Sea. Utrecht Micropaleontological Bulletins 15, 35-109.

Hottinger, L., 1977b. Foraminifères operculiniformes. Éditions du Muséum.

Hottinger, L.C., 2000. Functional Morphology of Benthic Foraminiferal Shells, Envelopes of Cells beyond Measure. Micropaleontology 46, 57-86.

Larsen, A., Drooger, C., 1977. Relative thickness of the test in the Amphistegina species of the Gulf of Elat. Utrecht Micropaleontological Bulletin 15, 225-239.

Nobes, K., Uthicke, S., Henderson, R., 2008. Is light the limiting factor for the distribution of benthic symbiont bearing foraminifera on the Great Barrier Reef? Journal of Experimental Marine Biology and Ecology 363, 48-57.

Prazeres, M., Uthicke, S., Pandolfi, J.M., 2015. Ocean acidification induces biochemical and morphological changes in the calcification process of large benthic foraminifera. Proceedings of the Royal Society London B: Biological Sciences 282, 20142782.

Reiss, Z., Hottinger, L., 1984. The Gulf of Aqaba: ecological micropaleontology. Springer Science & Business Media.

Renema, W., 2005. Depth estimation using diameter-thickness ratios in larger benthic foraminifera. Lethaia 38, 137-141.

Röttger, R., Hallock, P., 1982. Shape Trends in Heterostegina-Depressa (Protozoa, Foraminiferida). J Foramin Res 12, 197-204.

Seddighi, M., Briguglio, A., Hohenegger, J., Papazzoni, C.A., 2015. New results on the hydrodynamic behaviour of fossil Nummulites tests from two nummulite banks from the Bartonian and Priabonian of northern Italy. Bollettino della societa paleontologica italiana. Societa paleontologica italiana 54, 103-116.

Serra-Kiel, J., Hottinger, L., Caus, E., Drobne, K., Ferrandez, C., Jauhri, A.K., Less, G., Pavlovec, R., Pignatti, J., Samso, J.M., 1998. Larger foraminiferal biostratigraphy of the Tethyan Paleocene and Eocene. Bulletin de la Societé géologique de France 169, 281-299.

Speijer, R.P., Van Loo, D., Masschaele, B., Vlassenbroeck, J., Cnudde, V., Jacobs, P., 2008. Quantifying foraminiferal growth with high-resolution X-ray computed tomography: New opportunities in foraminiferal ontogeny, phylogeny, and paleoceanographic applications. Geosphere 4, 760-763.

Collective Conclusion

The presented work highlights the importance of actuopalaeontological studies to expand the knowledge on ecological dependence of larger foraminiferal test morphology. These studies on volumetric growth, the morphology of *Heterostegina depressa* in equatorial and axial view and their comparison to fossil relatives have revealed some uncertainties of classical palaeontological approaches towards the morphometry of larger foraminifera. Therefore, biometric-taxonomic studies should be interpreted more cautiously in the future, incorporating the vast pool of actuopalaeontological information available.

The studies presented in the first chapter on volumetric growth yielded unique results on the environmentally forced and still enigmatic processes of chamber formation. Similar to other nummulitid genera, *Heterostegina* shows short- to long-term oscillation in their volumetric growth. Even though this experimental approach is quite new and requires better fine tuning (e.g., more accurate chamber building rates), the presented data give good hints towards the controlling factors. Short-term growth cycles around 15 days and 30 days, exhibited by many LBF, seem to be induced by lunar rhythms (e.g., tidal and full moon cycles). The cause of long-term cycles around 75, 140 and 180 days has to be approached more carefully and should be observed together with the complete environmental background of the sampling habitat. However, most recent investigations, not included in this thesis, hint towards reproductive cycles as the cause for long-term growth oscillations.

In addition, during analysis of the chamber volume, peculiar intraspecific patterns in proloculus size were revealed. The results were tentatively interpreted as biogeographic differences, which lead to further studies of the inner morphology of *H. depressa* and fossil relatives within this thesis.

Detailed analysis of equatorial sections of *H. depressa* were thus conducted. The studied specimens, sampled along a water depth transect from 5 to 90 meters depth, were analysed by classical biometric measurements. This revealed a significant change in the important characters proloculus diameter (P) and the number of operculinid chambers (X) with water depth. However, Pearson's correlation shows significant dependence between all measured biometric characters operculinid chambers (X), number of chamberlets in the 14^{th} chamber (S), diameter of the first whorl (d), diameter of the first and a half whorl (D), spiral-index (K) and proloculus diameter (P). Further, a detailed analysis of frequency distribution regarding proloculus size and number of operculinid chambers revealed the presence of two morphologic groups with constant distributions at water depths (A_1: 5 to 30 m and A_2: 60 to 90 m). The mixture of these two groups A_1 and A_2 at depth intervals between 35 and 55 m results in the apparent bathymetric trend of biometric characters. Furthermore, the morphological variability of *H. depressa* along a water depth transect follows, with similar standard errors, the evolutionary trend postulated for the *H. reticulata* lineage in the late Eocene of the Tethys. Hence, the use of these characters to interpret evolutionary tendencies and phylogenetic relationships should be questioned and closely revised. The ecological dependence of early ontogenetic morphologies of larger foraminifera tests is yet too understudied and, therefore, the test in its completeness should be studied to interpret palaeoecological and biostratigraphical trends.

One possible approach for this, is the application of growth-invariant meristic characters to describe the inner morphology of *Heterostegina* test. By this, the complete ontogenetically change of test morphologies can be described by growth-independent functions, where function constants can be used as growth-invariant characters. These constants define the form of each individual test, enabling the classification of morphological different groups by multivariate statistics. Classified groups can be later interpreted as palaeogeographically separated populations or different species. This methodology can be modified and applied on axial section of larger foraminifera.

Based on the same specimens sampled along the water depth transect from chapter two, the hypothesized but untested test flattening of *H. depressa* was quantified. This has been done using four growth-invariant characters (i.e., radius at the point of maximal mediolateral thickness *MRmax*, maximal mediolateral thickness *MaxMlTh*, thickness at 3 mm marginal radius *ThMR3* and the flattening ratio *F*) derived from two growth functions. Especially, thickness at 3 mm marginal radius *ThMR3* and the flattening ratio *F* have been revealed to be significant in quantifying the bathymetric trends. *ThMR3* seems to be a rather habitat-independent indicator for changes in light intensities, with a continuous decrease in thickness along water depth, while the flattening ratio incorporates additional information on the sediment composition of the habitat. Especially the flattening ratio *F* is extremely important in the genus *Heterostegina*, because the degree of involution (maturo-evolute to involute) is often used as discriminator between subgenera and/or subgroups. However, *H. depressa* rather shows a transition between both caused by ecological adaption.

In summary, since many ecological constrains of recent *Heterostegina depressa* can be transferred to fossil heterosteginid taxa, the presented thesis increases the knowledge of ecological dependence expressed in different test modifications. By getting a better grip on ecological requirements of extant taxa more detailed interpretations and reconstructions in terms of palaeobiogeography and palaeoenvironment is possible. Further, the insights on ecological dependence of internal morphology presented here call for a much more tentative approach towards interpreting morphological change through time with evolutionary tendencies. Although classical biometric systematic works with several parameters to describe equatorial test morphologies, most of these characters are dropped in recent studies in favor of those that have been supposed to be of stratigraphic importance. This approach is completely valid to describe and define chronospecies for biostratigraphic zonation. However, it describes phenotypic plasticity only superficially and resulting homogenous populations or groups shouldn't be interpreted as distinct species. Most recent results on species recognitions show that larger foraminifera exhibit reticulate evolution, complicating morphological diagnosis due to intraspecific biogeographic and ecological variance. Within stratigraphic ranges major regional to global changes in physical environment (e.g., transgressive-regressive cycle) or biotic interaction (e.g., emergence of ecological competitors) might lead to disappearance and reemergence of ecophenotypes. Later on, these ecophenotypes might be ascribed as new species and/or genera. The definition of distinct morphotypes as species along a stratigraphic sequence should be done in context with palaeonvironmental data to avoid interpreting ecomorphotypes as distinct species. Hence, the reconstruction of evolutionary tendencies and phylogenetic relationships should not be based on few significant characters, but rather on the complete morphology of the test.

Acknowledgements

First and foremost my thanks go to my supervisor Johann Hohenegger aka “King Jon Lackland”. He is the master mind behind all of this work, who knows exactly how to push and pull each of his students into the right direction. Thank you for letting me tap into your vast pool of knowledge on larger foraminifera, statistics and all those other scientific and non-scientific topics. I don’t even try to hide the fact, that I possibly just read half of your publications and probably understood even less. Yet again, I have to thank you for opening my eyes towards the beauty and importance of statistics, an area I especially despised throughout my early studies.

Further, I want to thank Antonino Briguglio, who initially invited me to be part of this working group and initiated my deep connection to good Italian coffee, food and wine. In addition, I am grateful for his seemingly never-ending inventiveness in applied palaeontology, as well as his continuously urge to question existing doctrines. Thank you for being my always contactable Skypevisor.

I would also like to thank Rudolf Röttger for providing some of his sampled and cultured material for the first part of this work, as well as for the insight he gave me into his extensive laboratory studies. His studies are the foundation of all laboratory observations on larger foraminifera done today.

My thanks and remembrance go to Peter Pervesler, he taught me the importance of detailed observation and description and the art of carrying around a two-meter long leveling board. Special thanks go to Martin Zuschin, who always treated me like one of his own students and showed me that nothing good happens at university after 10 AM.

I also would like to thank my colleauges; Julia Wöger and Shunichi Kinoshita with whom I shared a room, the craziness of doing a PhD, as well as the dreams, trials and disappointment of organising a scientific project. Erik Wolfgring, the saddest girl on the dancefloor, for his scientific and emotional support throughout. Ana I. Torres-Silva, who taught me and keeps reminding me how important it is to think out of the box.

Further, I would like to thank all those brilliant, amazing and sometimes eccentric researchers I was able to meet during my PhD. In addition, I extend my best regards towards the anonymous and known reviewers, co-editors and editors of the published papers within this work, as well as the reviewer of this thesis.

My personal gratitude goes to the Department of Palaeontology of the University of Vienna and all of its staff members; to Doris Nagel and Petra Heinz, the Heads of Department during my time here. Kai-Uwe Hochhauser, who always had an open ear for my IT problems, doomsday prophecies and microsoft conspiracies and our ever ingenious preparation team (Valentin Perlinger, Franz Mayer and Roland Mayer).

Special thanks goes to our µCT-Team, Jürgen Kriwet, Cathrin Pfaff and Gerlinde Kaineder. Thank you for providing me with the opportunity to scan my material and gain such amazing results.

At this point I have and want to thank my family, who encouraged me throughout the progression of this work, buffered my disappointment and supported me how only family is able to. Finally, special credit goes to my girlfriend, Doris Weißenböck; without her I would have quit half-way through this thesis.

Kurzfassung

Die kosmopolite Großforaminifere *Heterostegina depressa* bevorzugt marine oligotrophische Küstenregionen tropischer bis gemäßigt warmen Meeren. Innerhalb der Familie der Nummulitidae zeigt sie die weiteste Wassertiefenverteilung und weist darüber eine starke ökologische Anpassungsfähigkeit, basierend auf Gehäusemodifikationen, auf. Dies ermöglicht ihr diverse ökologische Nischen zu besetzen, welche überwiegend nur durch Lichtintensität und das hydrodynamische Regime begrenzt werden. *Heterostegina depressa* stellt als einzige rezenter Vertreter der heterostegeniden Unterfamilie einen perfekten Modellorganismus dar, um die durch aktuopaläontologische Studien gewonnenen Information auf ihre fossilen Verwandten umzulegen.

Um das Volumetrische Wachstum von *H. depressa* zu studieren, wurden megalospherische Gehäuse von Exemplaren aus natürlichen Populationen und Laborkulturen mittels microCT-Scans und 3D Visualisierung analysiert. Ähnlich wie in vorrangehenden Untersuchungen über das volumetrische Wachstum von Großforaminiferen, konnte in dieser Arbeit gezeigt werden, dass die Kammervolumensequenz von *H. depressa* um eine theoretische Wachstumsfunktion oszilliert. Die beinahe idente Periodizität in allen untersuchten Exemplaren, deutet auf einen gemeinsamen intrinsischen oder extrinsischen beeinflussenden Faktor hin. Kurzzeit Zyklen um 15 bzw. 30 Tage belegen wahrscheinlich einen gezeitenbezogenen und lunaren Einfluss, während Langzeit Zyklen um 70 bzw. 180 Tage schwerer interpretierbar sind, jedoch möglichweise eine klimatisch-saisonale Ursache haben. Überraschenderweise wurden analoge Zyklizitäten in den Exemplaren der natürlichen Population und der Laborkulturen entdeckt. Jedoch, konnte ein rein genetischer Hintergrund der Wachstumszyklen nicht belegt werden. Darüber hinaus, zeigten die volumetrischen Messungen der Proloculusgrößen eine intraspezifisches Variation, welche auf eine ökologische bzw. biogeographische Abhängigkeit dieses häufig verwendeten biometrischen Parameters hindeutet. Dies führte zu einer detaillierten zweidimensionalen biometrischen Analyse von äquatorialen Schnitten. Um die Hypothese zu überprüfen, dass die beobachteten morphologischen Variationen unterschiedliche ökologische Bedingungen widerspiegeln, wurden Gehäuse von *H. depressa* aus schrittweise gewählten Intervallen zwischen 5 und 90 Meter Wassertiefe untersucht. Diese Analyse zeigt eine eindeutige Präsenz zweier Morphogruppen, welche als Gamonten (mit signifikant größeren Proloculi) und als Schizonten (mit signifikant kleineren Proloculi) interpretiert werden können. Während asexuale Reproduktion (Schizogonie) unter hydrodynamisch hoch-energetischen Bedingungen stattfinden kann, findet unter niedrig-energetischen Bedingungen überwiegend sexuelle Reproduktion (Gametogonie) statt. Daher stellt sich ein fließender Übergang der Proportion von Schizonten zu Gamonten entlang des hydrodynamischen Gradienten ein. Auf Grund von wechselnden Proportionen der beiden Generationen entlang der Wassertiefe entsteht ein scheinbarer umweltbedingter morphologischer Trend, welcher sich mit evolutiven Trends der fossilen Heterostegina Linie deckt. Des Weiteren, ergab die durchgeführte Studie, dass viele der häufig verwendeten biometrischen Parameter mit der Proloculusgröße korrelieren und daher nur einen geringen Informationswert besitzen. Um die ökologischen und biogeographische Differenzierung der Gehäusemorphologie von *Heterostegina depressa* zu untersuchen, wurden verschiedene biometrische Ansätze kombiniert. Zunächst, wurden an äquatoriale Schnitten von Heterostegina bestimmte häufig angewendete biometrischer Parameter vermessen. Darunter, Proloculusgröße und Zahl der operculiniden Kammern, welche nicht nur in Studien über evolutive Reihen von Heterostegina, sondern auch anderer Nummulitiden verwendet werden (z.B. *Nummulites, Spircoclypeus, Cylcoclypeus*). Dies jedoch meist ohne eine umweltbedingte Abhängigkeit in Betracht zu ziehen. Darüber hinaus, zeigt die Proloculusgröße von *Heterostegina depressa*, aus ähnlichen hydrodynamischen Bedingungen, eine biogeographische Differenzierung (hier: Okinawa und Hawaii). Durch die Anwendung von

biometrischen Parameter, welche entweder Wachstum unabhängig oder unveränderlich sin, können interne Gehäusemorphologie besser beschrieben werden. Wodurch die Unterscheidung von umweltbedingter, biogeographischer und stratigraphischer Diversifikation vereinfacht und evolutionäre Tendenzen klarer hervorgehoben werden können. Auf Grund ihrer Endosymbiose zeigt *H. depressa* eine starke Lichtabhängigkeit. Um niedrigere Lichtintensität in tiefer liegenden Habitaten entgegen zu wirken kommt es zu einer Erhöhung der Oberflächen-Volums Ratio durch ein verstärktes Abflachen des Gehäuses. Dadurch wird die Belichtung der Symbionten verbessert, während jedoch ein gewisser mechanischer Widerstand gegen die hydrodynamischen Bedingungen nicht unterschritten wird. Auf Grund dieser Adaption stellt *H. depressa* eine perfekte Modellspezies dar, um umweltbedingte Gehäusemodifikation innerhalb der Nummulitiden zu untersuchen. Vier wachstumsunveränderliche Parameter wurden benutzt um die Abflachung von Gehäusen zu beschreiben und diese Morphologie als bathymetrischen Indikator für fossile Vergesellschaftungen nutzbar zu machen. Die hier präsentierte Analyse quantifiziert einen eindeutigen Übergang von Individuen mit dickeren Gehäusezentren zu Individuen mit Dünneren. Dies erlaubt *H. depressa* Habitate unterhalb des Lichtoptimums ihrer Symbiont zu besiedeln.

Appendix

Chapter 1

Code	*Origin*	*SampleNo.*	*Depth (m)*
D1-68	Maui, Kekaa Point	#68	40
D2-68	Maui, Kekaa Point	#68	40
D3-68	Maui, Kekaa Point	#68	40
A1	Sesoko-Jima	Transect A	20
A2	Sesoko-Jima	Transect A	20
A3	Sesoko-Jima	Transect A	20
B13	Maui, Kekaa Point	P.1.10.91	n.n
B30	Maui, Kekaa Point	P.1.10.91	n.n
B44	Maui, Kekaa Point	P.1.10.91	n.n
B69	Maui, Kekaa Point	P.1.10.91	n.n
B1	Sesoko-Jima	Transect A	20
R1	Universität Kiel	F1.27.1.91	n.n.
R2	Universität Kiel	F1.27.1.92	n.n.
R3	Universität Kiel	F1.27.1.93	n.n.
R6	Universität Kiel	F1.27.1.94	n.n.

List of the used specimens; origin and water depth.

Code	*Amplitude*						
	α1	α2	α3	α4	α5	α6	α7
D1-68	0,085	0,098	0,056	0,112	0,085		
D2-68	0,022	0,039	0,069	0,070			
D3-68	0,076	0,055	0,103	0,074			
A1	0,048	0,068	0,128	0,108			
A2	0,044	0,012	0,062	0,084			
A3	0,043	0,038	0,106	0,137			
B13	0,005	0,007	0,068	0,069			
B30	0,014	0,010	0,020	0,014	0,016	0,016	
B44	0,009	0,011	0,006	0,008	0,018	0,173	
B69	0,004	0,009	0,003	0,006	0,012		
B1	0,090	0,097	0,071	0,119	0,137	0,077	0,122
R1	0,741	0,246	0,180				
R2	1,130	0,300	0,117				
R3	1,220	0,760	0,701				
R6	0,674	0,335	0,380				

Amplitude for each cycle of every specimen used in chapter 1.

Code	*Phase*						
	φ1	φ2	φ3	φ4	φ5	φ6	φ7
D1-68	1,69	1,52	2,96	3,12	-2,65		
D2-68	2,63	-2,49	1,49	-3,10			
D3-68	-0,64	-0,61	2,57	3,10			
A1	-2,51	2,20	-3,04	-2,55			
A2	0,81	0,75	-0,23	-2,11			
A3	-2,63	-2,64	-1,65	-2,31			
B13	-1,03	1,54	3,11	-0,27			
B30	-1,60	-2,09	-2,44	-3,04	2,01	1,33	
B44	-1,38	-1,92	3,06	2,24	1,22	-1,46	
B69	-2,90	-1,95	-2,77	2,23	-0,62		
B1	-2,01	0,00	1,73	0,84	2,15	-0,75	2,70
R1	-2,45	0,22	-2,13				
R2	1,70	1,23	-2,58				
R3	-2,13	-2,55	1,24				
R6	-2,73	1,75	-2,64				

Phase for each cycle of every specimen used in chapter 1.

Code	*Period*							*R²*	*p*
	τ1	τ2	τ3	τ4	τ5	τ6	τ7		
D1-68	13,2	29,1	66,4	133,3	167,1			0,666	2,64E-05
D2-68	14,3	28,3	60,3	182,1				0,376	1,71E-03
D3-68	15,2	25,2	92,9	126,4				0,376	7,98E-03
A1	14,7	28,4	67,3	178,6				0,472	2,09E-05
A2	15,1	29,3	83,4	129,8				0,432	1,27E-03
A3	14,5	28,8	82,0	174,6				0,678	4,03E-07
B13	14,3	34,9	74,6	75,0				0,431	2,09E-10
B30	13,9	16,4	22,3	27,8	46,4	185,5		0,41	9,79E-06
B44	16,4	18,9	28,4	35,9	48,0	189,4		0,460	1,18E-04
B69	11,8	20,8	28,2	34,8	65,1			0,581	4,52E-06
B1	12,1	13,2	24,5	35,2	39,5	105,9	239,5	0,661	3,48E-11
R1	290,1	52,0	37,0					0,870	6,25E-11
R2	275,3	55,1	21,3					0,983	2,40E-10
R3	336,5	47,4	43,8					0,903	1,02E-07
R6	146,4	30,4	40,4					0,837	4,31E-14

Period for each cycle of every specimen and R^2 and *p* for the summed-up sinusoidal regression function.

	Generalized logistic function							*Exponential function*	
	A	K	Q	B	M	v	R^2	a	b
D1-68	-0,0065	101,8920	0,2494	0,0201	121,6899	0,1439	0,999	0.0023	0.156
D2-68	-0,0088	150,5193	1,2730	0,2075	105,3852	2,2504	0,999	0.0015	0.161
D3-68	0,0054	1,8001	0,8004	0,0400	-147,0962	0,0002	0,999	0.0016	0.147
A1	-0,0004	28,7916	1,5800	0,0183	-31,4507	0,0568	0,997	0.0002	0.152
A2	0,0002	10,4920	13,5455	0,0205	-368,1446	0,0006	0,999	0.0002	0.168
A3	-0,0013	15,7221	2,3210	0,0172	-425,6429	0,0001	0,999	0.0001	0.167
B13	-0,0100	212,9922	0,3881	0,0117	83,4902	0,0574	0,999		
B30	0,0154	2,6544	0,2177	0,1274	107,3800	1,3492	0,979		
B44	-0,0022	39,8364	0,3024	0,0290	136,1007	0,2428	0,999		
B69	-0,0006	83,9361	12,1258	0,2217	118,4094	2,2883	0,999		
B1	-9,4370E-08	6,2796	9,6824	0,0558	5,1892	0,1481	0,911		
R1	0,0021	0,2866	11,5879	0,1334	10,7629	0,4806	0,999	0.0009	0.145
R2	0,0000	0,2100	1,6400	0,0700	-114,9000	0,0000	0,998	0.0008	0.149
R3	0,0010	0,9070	2,0880	0,0410	-35,6320	0,0480	0,999	0.0011	0.136
R6	0,0013	0,6292	2,1275	0,0492	-14,3389	0,0785	0,999	0.0008	0.1248

Functional parameters of the Richard's curve for all specimens and the exponential function for the initial spiral of all megalospheric specimens.

A-Forms	*D1-68*	*D2-68*	*D3-68*	*A1*	*A2*	*A3*
chamber	chamber volumina in mm^3					
3	0,00014777	0,000160287	0,00012501	0,00000700	0,00003300	0,00001000
4	0,000436856	0,000295345	0,00032075	0,00001000	0,00005200	0,00000000
5	0,000675647	0,000376972	0,00024723	0,00000100	0,00005300	0,00002000
6	0,000867258	0,000524088	0,00041187	0,00003200	0,00003400	0,00001200
7	0,000812289	0,000619815	0,00051187	0,00008000	0,00004400	0,00001300
8	0,000861917	0,000715172	0,00064392	0,00007600	0,00006700	0,00002000
9	0,001127413	0,000769714	0,00085781	0,00006400	0,00006000	0,00002000
10	0,001143214	0,000846704	0,00074225	0,00004100	0,00013900	0,00002200
11	0,000303997	0,001200672	0,00067781	0,00009400	0,00009200	0,00001900
12	0,001472581	0,001526812	0,00115690	0,00016800	0,00006300	0,00003900
13	0,003757895	0,001245567	0,00139098	0,00019300	0,00019400	0,00004700
14	0,003295447	0,000977865	0,00151006	0,00020000	0,00026100	0,00006400
15	0,003342404	0,00082574	0,00167915	0,00031000	0,00023500	0,00003600
16	0,003731413	0,002664779	0,00363089	0,00032400	0,00043300	0,00011800
17	0,002550366	0,002820429	0,00409999	0,00021000	0,00034700	0,00008500
18	0,000789145	0,003508329	0,00354126	0,00019600	0,00047100	0,00007800
19	0,006641412	0,003713141	0,00256474	0,00029400	0,00052300	0,00037800
20	0,006363008	0,003566768	0,00192471	0,00064600	0,00086500	0,00033800
21	0,006886211	0,004137606	0,00268252	0,00071200	0,00138900	0,00038100
22	0,008110876	0,006839118	0,00203046	0,00047200	0,00154300	0,00034100
23	0,006391939	0,008004727	0,01482303	0,00054900	0,00213300	0,00056200
24	0,006960986	0,004110892	0,00243640	0,00081900	0,00270200	0,00075000
25	0,008292251	0,006960076	0,00321902	0,00088300	0,00329000	0,00076200

26	0,008650993	0,008536978	0,00388090	0,00222200	0,00394000	0,00048000
27	0,011204252	0,01034652	0,00403462	0,00181800	0,00355800	0,00146900
28	0,009591913	0,010523689	0,00785996	0,00313700	0,00459100	0,00177400
29	0,013013543	0,009659176	0,01013728	0,00140000	0,00490500	0,00161100
30	0,009977361	0,008464811	0,01160660	0,00240400	0,00434300	0,00074600
31	0,010998398	0,013154704	0,01053526	0,00227900	0,00164900	0,00093000
32	0,005831348	0,018027704	0,01078231	0,00126100	0,00142200	0,00301800
33	0,009339325	0,017731616	0,00769662	0,00107200	0,00600600	0,00327100
34	0,004106624	0,015249944	0,01293832	0,00168100	0,00562500	0,00444700
35	0,017674304	0,018872366	0,01783575	0,00102500	0,00531500	0,00414600
36	0,009958445	0,01572524	0,01380577	0,00448100	0,00805900	0,00322100
37	0,01628451	0,01208408	0,01148604	0,00441500	0,00833200	0,00414600
38	0,013842523	0,004172484	0,01240330	0,00521300	0,00802000	0,00322100
39	0,015014891	0,012787379	0,02066235	0,00504400	0,01026500	0,00242800
40	0,025508556	0,00784277	0,01805243	0,00383900	0,00908300	0,00236100
41	0,008921385	0,027670554	0,01606605	0,00048000	0,00498000	0,00236600
42	0,033012108	0,035792528	0,02378563	0,00560400	0,00559600	0,00381200
43	0,03066715	0,031705196	0,01317778	0,00715100	0,01207400	0,00421100
44	0,045799768	0,023078614	0,02901030	0,00567100	0,01831300	0,00414500
45	0,045127904	0,024239586	0,02224964	0,00162100	0,01230700	0,00884600
46	0,032017108	0,063843948	0,01827688	0,00691900	0,01212900	0,00812800
47	0,04604034	0,045031692	0,03105446	0,00887000	0,01282200	0,00602100
48	0,027694616	0,075177792	0,02586646	0,00972900	0,01668200	0,01064300
49	0,021046084	0,06562288	0,02157887	0,01081200	0,01467500	
50	0,040091264	0,055790804	0,00052484	0,00548300	0,01749300	
51	0,033851324	0,059136804	0,03059851	0,00910100	0,01847600	
52	0,037962176	0,067325568		0,009812	0,004828	
53	0,03087612	0,065615644		0,010102		
54	0,075296552			0,019955		
55	0,076450448			0,012361		
56	0,048333664			0,018923		
57	0,100243848			0,011795		
58	0,078815216			0,007544		
59	0,02445347			0,020809		
60				0,021929		
61				0,024735		
62				0,018694		

Chamber volumina of all naturally grown megalospheric specimen in mm³.

A-Forms	*R1*	*R2*	*R3*	*R6*
chamber	chamber volumina in mm³			
3	0,00006599	0,00004650	0,00006909	0,00003685
4	0,00011604	0,00008991	0,00000177	0,00005482
5	0,00018358	0,00014128	0,00009190	0,00011093
6	0,00021945	0,00007197	0,00026751	0,00011112

7	0,00016010	0,00007551	0,00037402	0,00015797
8	0,00028876	0,00037048	0,00043270	0,00014686
9	0,00032752	0,00041920	0,00051862	0,00015241
10	0,00050445	0,00056513	0,00044444	0,00021760
11	0,00025156	0,00066788	0,00065260	0,00033983
12	0,00044732	0,00034590	0,00044090	0,00057447
13	0,00059082	0,00055295	0,00070309	0,00027705
14	0,00075291	0,00085832	0,00093251	0,00026594
15	0,00084193	0,00060078	0,00093561	0,00055502
16	0,00086519	0,00127110	0,00090682	0,00082596
17	0,00113911	0,00136012	0,00144847	0,00045872
18	0,00133775	0,00042562	0,00207671	0,00091930
19	0,00168210	0,00105120	0,00123943	0,00117783
20	0,00234134	0,00200341	0,00125537	0,00065484
21	0,00293924	0,00200740	0,00168431	0,00141358
22	0,00640464	0,00354534	0,00366403	0,00146358
23	0,00230679	0,00341579	0,00305373	0,00231880
24	0,00390518	0,00708669	0,00381926	0,00411166
25	0,00366558		0,00303203	0,00306217
26	0,00241508	0,00359095	0,00458081	0,00161803
27	0,00231853	0,00441761	0,00461492	0,00258585
28	0,00856660	0,00191218	0,00354002	0,00318347
29	0,00745938	0,00247332	0,00705989	0,00397702
30	0,01498386	0,00343484	0,00266399	0,00312050
31	0,01046151	0,00379734	0,00610214	
32	0,01124432	0,00307189	0,00785953	0,00065392
33	0,01476729	0,00480735	0,00879270	0,00155507
34	0,01054389	0,00370655	0,01275746	0,00185582
35	0,00703133		0,00932284	0,00017501
36	0,00208048	0,00312481	0,01149455	0,00056410
37	0,01634088	0,00112826	0,00326499	0,00108634
38	0,01253357	0,00089929		0,00072688
39	0,01361688	0,00347935	0,00794612	0,00034835
40		0,00244387	0,01598325	0,00492632
41	0,00382414	0,01407328	0,02260667	0,00485706
42	0,01569027	0,00383831	0,00011205	0,00975208
43	0,00780550	0,00395014	0,01613604	
44	0,01593342	0,00322158	0,00675806	0,00490984
45	0,01070045	0,00090106	0,00397871	0,01308185
46	0,00917403	0,00172572	0,00640309	0,00998376
47	0,00621619	0,00077617	0,00079521	0,00700863
48	0,00174056	0,00036893	0,00009301	0,00208472
49	0,00601954	0,02158713	0,00217038	0,01728184
50	0,00433700	0,01459523	0,00308982	0,01001765
51		0,01148902	0,00157248	0,01524861
52	0,00219275		0,01555874	0,00118227
53	0,00113513	0,02601360		0,01225070

54	0,00387706	0,00506224	0,01768306	0,01734703
55	0,01265869		0,00572569	0,01229941
56	0,00839366		0,01576645	0,01155141
57	0,04070981		0,03124414	0,02750079
58	0,03147377		0,02507534	0,01358335
59	0,01396632		0,00897894	0,02524070
60	0,01094183		0,00241043	0,00891464
61	0,00533948			
62	0,00576643			
63	0,00070552			

Chamber volumina of all laboratory grown megalospheric specimen in mm³.

B-Forms	*B1*	*B13*	*B30*	*B44*	*B69*
chamber	chamber volumina in mm³				
3					
4				0,00000158	
5				0,00000211	
6				0,00000816	
7				0,00000553	
8				0,00001185	
9				0,00001554	
10				0,00001975	
11				0,00002950	
12		0,00001264		0,00002950	
13	0,00000400	0,00001554		0,00003766	0,00000948
14	0,00000100	0,00001791	0,00000000	0,00004161	0,00001870
15	0,00000200	0,00003081	0,00001335	0,00004662	0,00002423
16	0,00000400	0,00003556	0,00002382	0,00009640	0,00004161
17	0,00000600	0,00003398	0,00003970	0,00012589	0,00004714
18	0,00001300	0,00005742	0,00003646	0,00014881	0,00005610
19	0,00001300	0,00006769	0,00005667	0,00014565	0,00007533
20	0,00003500	0,00006848	0,00044685	0,00023625	0,00008270
21	0,00003100	0,00013616	0,00030031	0,00024863	0,00010219
22	0,00005000	0,00019779	0,00066991	0,00025495	0,00010482
23	0,00006100	0,00020359	0,00044613	0,00022835	0,00014117
24	0,00009200	0,00017699	0,00034940	0,00037162	0,00020333
25	0,00010400	0,00018963	0,00029670	0,00011852	0,00018199
26	0,00008000	0,00020991	0,00019094	0,00007901	0,00021781
27	0,00005900	0,00020859	0,00031150	0,00026785	0,00027997
28	0,00026900	0,00053992	0,00059700	0,00025416	0,00033528
29	0,00014800	0,00057442	0,00032160	0,00075562	0,00015223
30	0,00021200	0,00048197	0,00049305	0,00085123	0,00026627
31	0,00017600	0,00084543	0,00029345	0,00089574	0,00059286
32	0,00029200	0,00089837	0,00088576	0,00049093	0,00065712
33	0,00038600	0,00135084	0,00096914	0,00021096	0,00059312

34	0,00056900	0,00144539	0,00187114	0,00103296	0,00081146
35	0,00076000	0,00212648	0,00145317	0,00132188	0,00077248
36	0,00063800	0,00209751	0,00203537	0,00193528	0,00130924
37	0,00101200	0,00249915	0,00117343	0,00259345	0,00040217
38	0,00084500	0,00211647	0,00192528	0,00184731	0,00147885
39	0,00085800	0,00225237	0,00178415	0,00192316	0,00099503
40	0,00255000	0,00195660	0,00291572	0,00205617	0,00203036
41	0,00245000	0,00301695	0,00254755	0,00184336	0,00211306
42	0,00235500	0,00260161	0,00379245	0,00248178	0,00134953
43	0,00160100	0,00153310	0,00362245	0,00141090	0,00080856
44	0,00321900	0,00218363	0,00355315	0,00345706	0,00209172
45	0,00286700	0,00195687	0,00299585	0,00307095	0,00118940
46	0,00241900	0,00212095	0,00417181	0,00150097	0,00449870
47	0,00209400	0,00028207	0,00296914	0,00052043	0,00155971
48	0,00896300	0,00226528	0,00201732	0,00163266	0,00232955
49	0,00364700	0,00004214	0,00281321	0,00787938	0,00024494
50	0,00403600	0,00021597	0,00137376	0,00507734	0,00349209
51	0,00751100	0,00552189	0,00833820	0,00810904	0,00243569
52	0,00523900	0,00346942	0,00568922	0,00538285	0,00360929
53	0,00791900	0,00811955	0,00833820	0,00918072	0,00576685
54	0,00872800	0,00724936	0,00833640	0,00863632	0,00453610
55	0,00830500	0,00965159	0,00891391	0,00532939	0,00406282
56	0,00845000	0,00795362	0,00747446	0,01331385	0,00627938
57	0,00980200	0,00963948	0,00970691	0,01090687	0,00575052
58	0,00958800	0,00656775	0,00525645	0,00807270	0,00437518
59	0,01119500	0,01094607	0,00747446	0,00496409	0,00231085
60	0,00887400	0,01073933	0,00792456	0,02387307	0,00353660
61	0,01006500	0,00874480	0,00976321	0,02693770	0,00958052
62	0,00814800	0,01216260	0,00549431	0,01258826	0,00813169
63	0,00557500	0,00970690	0,00328027	0,02155538	0,01064245
64	0,00404000	0,00975642	0,00474318	0,01901328	0,01068221
65	0,01105200	0,00952412	0,01378126	0,01804854	0,00543763
66	0,02321100	0,00285155	0,01570437	0,02756664	0,02168390
67	0,01905600	0,02567419	0,02441651	0,02322912	0,02732407
68	0,02714800	0,02545243	0,01848798	0,02707492	0,01820393
69	0,00463000	0,01810220	0,02318894	0,02868256	
70	0,02138200	0,02018417	0,01596786	0,01266595	
71	0,02685600	0,01864475	0,02035443	0,00076853	
72	0,03816700	0,01811511	0,02260276	0,04429383	
73	0,02246000	0,01216971	0,01860674	0,01293433	
74	0,00927400	0,01799553	0,02625372	0,02292097	
75	0,01013100	0,02112204	0,02395703	0,01348478	
76	0,00338800	0,04753658	0,02477854	0,04794183	
77	0,15319200	0,05526660	0,01860674	0,02997862	
78	0,00633900	0,00000000	0,01219923	0,04940014	
79	0,00254700	0,05221805	0,00813968	0,06294418	
80	0,10866000	0,05018665	0,03113696	0,03116276	

81	0,09045300	0,05832726	0,03743942	0,09115056
82	0,13841700	0,01245652	0,00134380	0,12022475
83	0,12014100	0,01778352	0,04827609	0,07801790
84	0,04309600	0,01403018	0,04182563	0,06950590
85	0,14600200	0,07708105	0,04416384	0,06617474
86	0,17611900	0,04823610	0,07030603	0,11389033
87	0,16968300	0,00401566	0,07486946	0,06391446
88	0,14674900	0,00000000	0,05704056	0,04802058
89	0,20122200	0,05638936	0,08352168	0,01586991
90	0,22254300	0,06128100	0,06152748	0,04140013
91	0,34339100	0,09088183	0,08698098	0,20415462
92	0,21842600	0,04433106	0,08863195	0,11673056
93	0,13597700	0,04226963	0,10015586	0,15843226
94	0,29096100	0,01744614	0,09310659	0,05640196
95		0,06901049	0,13099322	0,09844050
96		0,04047500	0,00801876	0,16258146
97		0,07940216	0,15252181	
98		0,08905402	0,09099722	
99		0,06990675	0,07142821	
100		0,01311180	0,05293192	
101		0,05120511	0,06869188	
102		0,11748942	0,05228980	
103		0,07998132	0,03786173	
104		0,06473278	0,02764806	
105		0,04814102	0,00325970	
106		0,03905648	0,00207580	
107		0,16379026	0,02382240	
108		0,12516123	0,17956456	
109		0,20521946		
110		0,13851427		
111		0,13549259		
112		0,09341470		
113		0,23179491		
114		0,15638523		
115		0,01512055		
116		0,10898640		
117		0,18599950		

Chamber volumina of all microspheric specimen in mm^3.

ANOVA

		Sumo f Squares	df	Mean Square	F	Sig.
parameter_a	Between Groups	0	2	0,0000	32,53	0,000
	Within Groups	0	7	0,0000		
	Total	0	9			
parameter_b	Between Groups	0,001	2	0,0010	6,112	0,029
	Within Groups	0,001	7	0,0000		
	Total	0,002	9			

Post-Hoc-Tests

dependent variable		Group I	Group J	Mean difference (I-J)	s.e.	sig	95%- confidence lower limit	Upper limit
parameter a	LSD	Kiel	Hawaii	0,00073	0,00019	0,006	0,00028	0,00118
			Sesoko	-0,00090	0,00019	0,002	-0,00135	-0,00046
		Hawaii	Kiel	-0,00073	0,00019	0,006	-0,00118	-0,00028
			Sesoko	-0,00163	0,00020	0,000	-0,00211	-0,00115
		Sesoko	Kiel	0,00090	0,00019	0,002	0,00046	0,00135
			Hawaii	0,00163	0,00020	0,000	0,00115	0,00211
	Bonferroni	Kiel	Hawaii	0,00073	0,00019	0,019	0,00014	0,00132
			Sesoko	-0,00090	0,00019	0,006	-0,00150	-0,00031
		Hawaii	Kiel	-0,00073	0,00019	0,019	-0,00132	-0,00014
			Sesoko	-0,00163	0,00020	0,000	-0,00227	-0,00100
		Sesoko	Kiel	0,00090	0,00019	0,006	0,00031	0,00150
			Hawaii	0,00163	0,00020	0,000	0,00100	0,00227
parameter b	LSD	Kiel	Hawaii	-0,02384	0,00708	0,012	-0,04058	-0,00710
			Sesoko	-0,01622	0,00708	0,056	-0,03296	0,00052
		Hawaii	Kiel	0,02384	0,00708	0,012	0,00710	0,04058
			Sesoko	0,00762	0,00757	0,348	-0,01027	0,02551
		Sesoko	Kiel	0,01622	0,00708	0,056	-0,00052	0,03296
			Hawaii	-0,00762	0,00757	0,348	-0,02551	0,01027
	Bonferroni	Kiel	Hawaii	-0,02384	0,00708	0,036	-0,04598	-0,00170
			Sesoko	-0,01622	0,00708	0,167	-0,03836	0,00592
		Hawaii	Kiel	0,02384	0,00708	0,036	0,00170	0,04598
			Sesoko	0,00762	0,00757	1,000	-0,01605	0,03129
		Sesoko	Kiel	0,01622	0,00708	0,167	-0,00592	0,03836
			Hawaii	-0,00762	0,00757	1,000	-0,03129	0,01605

ANOVA, LSD and Bonferroni post-hoc tests for parameter *a* and *b* of the exponential functions fitted to the first 25 chambers of all gamonts/schizonts.

Chapter 2

Depth (m)	P	X	S	d	D	K	A1/2
5	92,0	14	1	425,4	595,9	33,8	1
5	63,9	13	1	329,6	458,6	32,7	1
5	97,8	16	1	405,2	564,7	34,2	1
5	85,6	14	1	360,4	511,2	35,4	1
5	106,0	16	1	424,3	570,5	31,5	1
5	100,0	14	1	427,3	605,3	35,2	1
5	84,6	15	1	302,2	431,6	37,3	1
5	94,9	10	1	424,5	583,3	32,5	1
5	99,8	14	1	374,5	535,1	36,9	1
5	93,2	11	2	383,9	537,1	34,5	1
5	98,9	14	1	409,1	576,5	35,0	1
5	84,0	13	2	365,4	520,4	35,5	1
5	91,4	11	2	382,3	620,1	45,0	1
5	91,3	8	2	364,3	520,4	36,4	1
5	94,1	12	2	400,0	542,6	31,8	1
5	85,8	13	2	369,6	522,3	35,0	1
5	116,8	11	2	436,3	601,0	34,0	1
5	81,1	9	2	368,0	539,6	37,4	1
5	103,1	12	2	461,4	645,9	34,0	1
10	110,7	9	2	445,7	661,3	39,2	1
10	78,8	16	1	328,1	480,6	38,0	1
10	68,2	16	1	227,0	328,1	38,9	1
10	104,7	13	2	440,4	702,7	43,9	1
10	87,7	15	3	322,1	488,6	41,5	1
10	157,9	12	3	741,8	1045,3	34,2	1
10	83,2	11	1	359,5	495,0	32,9	1
10	109,9	9	1	514,3	728,0	34,6	1
10	92,5	10	1	378,9	526,9	34,1	1
10	93,8	11	1	390,2	537,5	33,2	1
10	95,0	11	1	403,6	601,3	39,0	1
10	100,2	9	2	413,3	613,2	39,0	1
10	106,0	11	2	357,1	554,7	44,0	1
10	100,5	11	2	431,6	601,6	33,9	1
10	104,3	10	2	459,7	670,8	37,3	1
10	106,1	9	1	473,1	683,6	36,4	1
10	112,2	10	2	464,5	656,4	35,3	1
10	116,3	11	2	487,2	694,9	35,9	1
10	87,7	13	1	365,4	503,8	33,3	1
10	105,2	11	2	454,0	675,5	38,8	1
10	94,0	10	3	369,3	537,7	37,9	1
20	92,8	7	1	387,7	547,4	35,1	1
20	99,1	11	1	424,5	634,0	39,2	1

20	97,9	10	2	422,9	632,0	39,2	1
20	96,5	11	2	424,7	614,2	36,6	1
20	94,6	9	2	369,1	523,3	36,0	1
20	83,5	8	2	336,9	477,8	35,7	1
20	92,4	8	1	383,2	532,0	33,9	1
20	94,9	13	1	420,5	606,6	36,4	1
20	102,9	8	2	466,3	709,9	40,1	1
20	98,0	10	2	462,7	662,6	35,4	1
20	107,9	10	1	417,8	640,8	41,8	1
20	93,0	12	1	390,6	522,8	30,8	1
20	122,2	6	2	602,6	846,8	33,7	1
20	93,2	11	2	396,9	564,4	35,5	1
20	100,0	8	2	445,1	677,9	40,3	1
20	107,6	9	2	521,9	783,4	38,7	1
20	92,6	11	1	389,9	555,7	35,8	1
20	115,1	9	2	429,7	635,6	39,6	1
20	97,6	10	2	368,1	545,0	39,5	1
20	51,0	14	2	237,4	343,4	36,3	1
20	91,0	13	2	394,5	526,8	30,4	1
20	84,3	12	2	348,9	487,7	34,4	1
20	96,1	11	2	431,8	634,8	37,7	1
20	98,1	14	2	420,6	618,4	38,0	1
20	82,3	11	2	366,4	539,3	37,8	1
20	79,2	13	2	336,4	466,4	33,6	1
20	91,3	14	2	405,5	567,0	34,0	1
30	109,4	8	2	524,2	822,2	41,8	1
30	105,4	5	2	470,3	677,3	36,2	1
30	74,5	12	1	321,1	500,6	42,1	1
30	112,1	8	2	531,2	840,9	42,5	1
30	88,6	13	1	393,7	580,7	38,0	1
30	102,6	9	1	408,2	582,1	36,3	1
30	95,7	11	2	441,5	627,2	34,9	1
30	102,8	9	2	433,1	633,8	37,8	1
30	81,4	10	2	341,9	469,6	32,9	1
30	88,6	12	1	339,8	498,4	38,7	1
30	87,4	11	2	304,3	479,0	44,6	1
30	91,6	7	1	405,1	568,3	34,2	1
30	110,2	10	2	484,1	685,4	35,0	1
30	93,0	12	1	397,9	549,7	33,2	1
30	109,3	11	2	412,5	582,9	36,0	1
30	109,7	10	2	471,4	663,5	34,7	1
30	83,1	10	1	322,6	447,4	34,3	1
30	96,8	9	2	375,0	558,9	39,8	1
30	88,7	10	1	358,9	507,1	35,4	1
30	97,2	9	2	503,2	666,1	28,6	1
30	90,2	13	2	461,8	681,4	37,1	1
30	105,1	8	2	448,1	602,9	31,1	1

30	129,2	5	4	504,4	802,1	44,2	1
30	87,9	12	1	398,8	591,0	38,2	1
30	91,9	13	2	376,4	521,1	33,7	1
30	96,1	9	1	423,6	576,7	31,9	1
30	101,8	9	1	403,6	600,8	39,5	1
30	86,4	10	2	362,0	546,6	40,1	1
40	113,7	8	2	470,5	760,4	44,8	1
40	95,2	11	2	390,4	596,9	41,2	1
40	135,8	4	3	609,3	900,0	38,0	2
40	117,3	8	1	449,9	638,3	36,2	1
40	96,2	13	1	328,7	486,9	40,5	1
40	118,7	9	2	451,4	674,3	40,1	1
40	116,3	10	2	443,0	702,3	44,2	1
40	103,8	11	2	462,8	688,9	38,6	1
40	104,7	7	2	375,1	521,1	35,1	1
40	110,3	11	3	476,7	703,5	38,2	1
40	99,9	10	2	349,9	511,0	39,2	1
40	114,9	7	1	463,2	661,7	36,3	2
40	106,8	12	1	479,1	688,8	36,0	1
40	119,8	7	2	536,8	771,4	36,0	2
40	113,1	8	2	454,3	726,6	44,4	1
40	90,8	9	2	455,5	676,6	37,7	1
40	117,8	10	3	476,3	767,9	44,9	1
40	97,1	11	2	416,5	588,7	35,0	1
40	100,9	8	2	423,6	603,2	35,8	1
40	89,2	9	1	407,5	579,3	35,1	1
40	139,1	5	2	588,9	964,7	45,5	2
50	195,8	2	4	823,5	1267,3	41,4	2
50	157,9	5	3	627,0	911,3	37,7	2
50	144,1	3	4	651,0	963,3	38,1	2
50	160,2	4	2	635,7	922,4	37,6	2
50	142,8	5	4	646,3	1024,4	42,9	2
50	103,7	10	3	347,5	507,8	39,7	1
50	127,8	7	3	505,5	798,9	43,7	2
50	140,4	6	3	560,1	864,1	42,0	2
50	103,7	9	2	459,6	663,8	36,5	1
50	129,5	6	3	517,0	705,3	32,7	2
50	93,2	8	2	493,5	744,8	38,6	1
50	151,6	4	2	652,3	1005,3	41,4	2
50	110,3	10	1	430,6	604,6	35,2	1
50	115,7	5	2	445,7	677,6	41,3	2
50	120,6	9	2	378,6	566,8	42,2	1
50	141,7	5	3	500,6	726,0	38,6	2
50	118,1	6	2	438,5	611,8	35,1	2
50	92,5	7	2	374,3	566,8	40,6	1
50	156,6	6	3	636,0	923,4	37,5	2
50	114,2	7	3	522,7	837,9	43,5	2

50	138,5	6	2	561,5	843,5	40,0	2
50	137,6	5	3	594,2	906,5	40,6	2
50	112,4	8	2	497,6	753,6	39,9	1
60	145,3	7	3	524,5	809,2	42,9	2
60	187,1	4	5	849,0	1500,1	49,6	2
60	168,3	3	4	723,0	1076,3	38,9	2
60	122,3	3	2	539,9	826,7	40,7	2
60	182,7	2	5	902,5	1417,8	41,7	2
60	144,6	6	3	648,8	1005,3	41,4	2
60	127,1	6	4	387,2	546,0	37,9	2
60	157,9	3	3	735,8	1277,8	48,4	2
60	121,9	7	2	327,8	485,6	43,4	2
60	125,5	5	3	541,8	872,7	44,3	2
60	118,5	4	2	526,6	809,0	40,9	2
60	129,0	7	3	575,8	893,3	41,5	2
60	162,4	6	3	613,3	885,7	37,7	2
60	144,0	3	2	578,2	872,9	40,4	2
60	159,7	4	3	673,7	950,5	35,0	2
60	128,8	7	3	524,8	828,6	43,4	2
60	150,6	5	3	617,3	957,1	42,1	2
60	131,8	4	2	610,9	931,6	40,1	2
60	111,7	6	3	497,7	804,2	44,3	2
60	148,4	3	2	663,0	1050,1	42,9	2
60	163,0	3	4	744,7	1135,1	40,2	2
60	129,8	2	3	564,4	859,5	40,4	2
60	130,5	4	3	605,6	938,3	41,2	2
60	118,8	4	2	612,7	1021,3	45,3	2
70	162,8	4	1	568,2	858,2	41,7	2
70	121,8	7	1	442,9	653,3	39,6	2
70	126,3	5	2	515,2	808,5	43,0	2
70	147,8	6	2	620,1	882,2	35,7	2
70	120,1	6	3	570,3	883,1	41,0	2
70	185,5	4	4	712,5	1067,5	40,2	2
70	125,8	5	2	485,7	712,2	38,6	2
70	140,2	3	2	477,8	706,1	40,3	2
70	135,0	6	3	478,4	714,0	40,7	2
70	148,7	5	3	569,0	941,2	47,0	2
70	126,6	5	2	393,6	596,1	43,1	2
70	117,0	5	3	494,6	786,5	43,6	2
70	112,9	6	2	414,3	645,8	43,4	2
70	172,4	2	4	572,7	962,0	49,3	2
70	156,5	4	3	629,2	992,0	43,4	2
70	127,5	2	3	606,4	963,8	42,7	2
70	128,7	3	3	579,2	856,9	38,1	2
70	154,4	3	4	689,3	1115,4	44,3	2
70	142,0	3	3	600,0	986,2	45,7	2
70	161,7	5	6	593,8	933,5	44,0	2

70	142,9	2	3	642,1	981,5	40,5	2
70	172,6	1	4	664,0	1127,8	48,6	2
80	165,9	6	2	683,4	1010,1	38,7	2
80	130,8	6	3	510,5	787,2	42,1	2
80	167,9	4	3	623,5	889,4	36,8	2
80	148,5	5	3	550,2	804,0	38,7	2
80	122,3	4	3	485,1	724,5	39,7	2
80	113,0	3	3	483,7	695,5	36,3	2
80	137,9	4	5	602,5	916,2	40,3	2
80	141,3	1	3	607,4	990,0	45,1	2
90	136,6	4	1	479,4	654,9	33,9	2
90	185,0	3	4	715,8	1138,0	44,3	2
90	192,3	3	3	520,3	845,5	49,8	2

The biometric datamatrix of all megalospheric specimen investigated regarding proloculus diameter (P), operculinid chamber number (X), number of chamberlets in the 14th chamber (S), diameter of the first whorl (d), diameter of the first and a half whorl (D) and the spiral index (K), as well as the assignment into morphogroup A_1 or A_2 is given.

Discriminant analysis

Group Statistics

Group		Mean	Std. Deviation	Valid N (listwise)	
				Unweighted	Weighted
A1	P	96,3	13,54	95	95
	X	10,9	2,37	95	95
A2	P	143,5	21,33	57	57
	X	4,3	1,59	57	57
Total	P	114,0	28,43	152	152
	X	8,4	3,85	152	152

Summary of Canonical Discriminant Functions

Eigenvalues

Function	Eigenvalue	% of Variance	Cumulative %	Canonical Correlation
1	3,129[a]	100,0	100,0	,871

Wilks' Lambda

Test of Function(s)	Wilks' Lambda	Chi-square	df	Sig.
1	,242	211,292	2	,000

Standardized Canonical Discriminant Function Coefficients

	Function 1
P	-,533
X	,680

Structure Matrix

	Function 1
X	,866
P	-,771

Pooled within-groups correlations between discriminating variables and standardized canonical discriminant functions
Variables ordered by absolute size of correlation within function.

Functions at Group Centroids

Group	Function 1
A1	1,361
A2	-2,269

Unstandardized canonical discriminant functions evaluated at group means

Classification Statistics

Classification Processing Summary

Processed		196
Excluded	Missing or out-of-range group codes	0
	At least one missing discriminating variable	0
Used in Output		196

Prior Probabilities for Groups

Group	Prior	Cases Used in Analysis	
		Unweighted	Weighted
A1	,500	95	95,000
A2	,500	57	57,000
Total	1,000	152	152,000

Classification Results[a,c]

	Group		Predicted Group Membership		Total
			1,00	2,00	
Original	Count	A1	92	3	95

		A2	0	57	57
		Ungrouped cases	24	20	44
	%	A1	96,8	3,2	100
		A2	0	100	100
		Ungrouped cases	54,5	45,5	100
Cross-validated[b]	Count	A1	91	4	95
		A2	0	57	57
	%	A1	95,8	4,2	100
		A2	0,0	100	100

a. 98,0% of original grouped cases correctly classified.

b. Cross validation is done only for those cases in the analysis. In cross validation, each case is classified by the functions derived from all cases other than that case.

c. 97,4% of cross-validated grouped cases correctly classified.

Summary of the discriminant analysis used to reassign the intermediate morphogroup I into the morphogroups A_1 and A_2.

Specimen	*measured distances (µm)*		
	Marginal Radius (MR)	Thickness (Th)	mediolateral Thickness (MlTh)
96-8-2/2	45	121	105
	133	194	118
	508	575	461
	890	671	547
	1168	672	347
96-8-2/4	45	121	105
	127	175	163
	805	682	582
	1274	835	587
	1555	895	446
96-8-2/5	49	121	105
	197	188	125
	659	503	402
	838	545	370
	1331	592	266
96-8-2-1	45	121	105
	118	194	142
	376	490	376
	1089	605	375
	1177	665	370
96-8-2_11	47	126	109
	90	164	74
	529	634	430
	846	705	586
	1081	790	364
96-8-2_12	55	125	108
	153	164	132
	501	525	371
	716	596	476
	1061	665	314
96-8-2_14	43	129	111
	114	156	127
	489	408	296
	772	446	343
	1034	502	231
96-8-2_15	55	126	109
	90	173	110
	497	493	391
	822	524	418

	1026	586	281
96-8-2_16	43	133	115
	145	196	142
	380	384	267
	662	611	424
	1104	681	253
96-8-2_6	43	118	102
	114	156	111
	490	477	362
	775	509	426
	994	572	282
96-8-2_7	55	141	122
	137	195	140
	739	681	524
	908	712	562
	1315	776	339
96-8-2_9	51	141	122
	168	188	136
	616	595	463
	689	626	458
	908	674	408
96-8-2_10	47	128	111
	129	165	122
	595	642	535
	799	704	536
	1159	759	343

Specimen	*mediolateral Thickness (MlTh)*				*Thickness (Th)*		
	b0	b1	b2	b3	a	b	c
96-8-2/2	2,65E-17	7,3	-0,006	460,3	258,1	0,221	-514,5
96-8-2/4	4,91E-16	6,5	-0,004	682,1	37,5	0,451	-114,0
96-8-2/5	4,98E-16	6,6	-0,005	571,9	61,5	0,352	-145,5
96-8-2-1	1,23E-10	4,8	-0,004	377,1	1.373,1	0,080	-1.761,2
96-8-2_11	6,35E-18	7,5	-0,006	452,3	329,7	0,211	-644,8
96-8-2_12	3,10E-18	7,6	-0,006	511,2	69,9	0,368	-211,8
96-8-2_14	8,50E-17	7,0	-0,006	602,7	57,1	0,340	-94,5
96-8-2_15	3,43E-17	7,3	-0,006	492,3	2.635,0	0,047	-3.063,7
96-8-2_16	7,12E-18	7,5	-0,007	507,3	23,0	0,497	-38,6
96-8-2_6	4,43E-18	7,5	-0,006	560,2	101,8	0,298	-217,3
96-8-2_7	3,02E-17	7,1	-0,005	558,9	162,1	0,278	-385,0
96-8-2_9	3,60E-16	6,9	-0,006	480,9	8,4	0,647	8,0

96-8-2_10	2,19E-16	7,0	-0,006	445,6	3.772,2	0,042	-4.303,7

The five measurements of Marginal Radius (MR), Thickness (Th) and mediolateral Thickness (MlTh) for every specimen investigated from 5 meters water depth, as well as the estimated functional parameters for both growth functions per specimen are given.

Specimen	*measured distances (µm)*		
	Marginal Radius (MR)	Thickness (Th)	mediolateral Thickness (MlTh)
96-7-2_9	47	133	115
	137	196	147
	435	430	369
	814	611	499
	1120	689	329
96-7-2_10	51	133	115
	121	176	121
	599	588	460
	822	689	477
	1178	767	334
96-7-1/5	42	121	105
	124	151	143
	472	405	358
	690	484	419
	1095	545	236
96-7-1/1	39	110	95
	142	145	134
	662	640	504
	966	665	465
	1099	720	347
96-7-1/2	45	139	121
	166	191	177
	581	472	379
	787	557	414
	1252	605	296
96-7-2-1	51	134	116
	115	188	110
	647	568	490
	1119	635	442
	1428	684	229
96-7-2_10	51	141	122
	129	180	121
	603	595	459
	603	697	509
	1175	767	335

96-7-2_6	55	141	122
	149	202	160
	599	555	453
	786	637	426
	1171	697	278
93-3-3-7_4	51	125	108
	137	181	148
	630	470	410
	940	548	388
	1315	611	255
96-7-2_8	63	141	122
	145	196	153
	560	564	389
	1050	689	497
	1168	744	398
96-7-2/4	48	127	110
	148	169	134
	908	653	497
	1609	690	398
	1609	690	323
96-7-2-2	42	121	105
	124	182	137
	634	643	536
	1204	738	458
	1361	799	414
93-3-3-7_1	43	126	109
	157	188	137
	540	494	359
	611	518	389
	799	588	316
96-7-2_7	43	129	111
	154	169	132
	647	544	422
	986	592	447
	1664	641	224
96-7-2_5	57	134	116
	154	196	134
	708	635	480
	829	677	540
	1337	726	343

Specimen	*mediolateral Thickness (MlTh)*				*Thickness (Th)*		
	b0	b1	b2	b3	a	b	c
96-7-2_9	3,01E-17	7,2	-0,006	529,6	21,9	0,500	-30,3
96-7-2_10	2,05E-18	7,6	-0,006	577,9	282,4	0,216	-526,6
96-7-1/5	5,41E-18	7,5	-0,006	540,3	46,2	0,380	-92,8
96-7-1/1	7,77E-17	7,1	-0,006	468,5	230,9	0,230	-427,0
96-7-1/2	2,05E-15	6,4	-0,004	652,5	42,3	0,396	-75,7
96-7-2-1	2,18E-18	7,6	-0,006	561,6	535,3	0,145	-835,5
96-7-2_10	1,21E-15	6,7	-0,006	483,7	242,4	0,241	-522,3
96-7-2_6	2,75E-15	6,5	-0,006	496,6	1.262,4	0,089	-1.660,2
93-3-3-7_4	2,86E-15	6,4	-0,005	567,3	55,8	0,361	-120,4
96-7-2_8	3,83E-16	6,6	-0,004	677,4	60,0	0,391	-183,9
96-7-2/4	6,73E-16	6,4	-0,004	707,7	5.574,5	0,025	-6.017,3
96-7-2-2	4,75E-16	6,6	-0,004	608,9	34,1	0,452	-84,2
93-3-3-7_1	1,70E-16	7,1	-0,007	467,5	4,3	0,728	44,9
96-7-2_7	4,86E-17	6,9	-0,005	664,8	223,5	0,213	-403,5
96-7-2_5	4,55E-17	7,0	-0,005	573,7	269,8	0,222	-560,6

The five measurements of Marginal Radius (MR), Thickness (Th) and mediolateral Thickness (MlTh) for every specimen investigated from 10 meters water depth, as well as the estimated functional parameters for both growth functions per specimen are given.

Specimen	*measured distances (µm)*		
	Marginal Radius (MR)	Thickness (Th)	mediolateral Thickness (MlTh)
96-13-1/1	45	97	84
	117	164	111
	318	327	225
	672	496	387
	1010	545	244
96-13-1/3	39	128	111
	124	157	134
	653	677	572
	935	750	430
	1655	799	201
96-13-1/4	42	127	110
	124	163	134
	785	605	545
	1071	677	420
	1283	732	399
96-13-1/5	39	122	105

	106	169	130
	675	548	461
	1137	623	369
	1307	647	278
96-13-2/3	42	133	115
	142	182	137
	726	645	558
	1132	683	502
	1650	738	288
96-13-2/5	54	139	121
	160	187	155
	628	661	458
	1162	732	496
	1930	762	278
96-15-1/1	54	143	124
	152	176	166
	819	555	463
	1110	637	477
	1327	677	379
96-15-1/7	58	135	117
	159	203	157
	542	454	360
	839	663	495
	1239	710	262
96-15-1-8	47	107	93
	14	150	111
	626	501	407
	982	637	456
	1225	684	332
96-15-1-13	62	121	105
	117	164	125
	480	441	361
	619	534	434
	862	577	317
96-15-1-14	46	135	117
	139	170	138
	513	477	394
	819	548	348
	975	583	313
96-15-1-15	46	142	123
	117	178	129
	555	469	367
	745	548	420
	1077	591	295
96-15-1_20	46	142	123
	125	192	133
	527	534	447

	680	662	467
	1011	713	342
96-15-1_12	46	128	111
	103	164	130
	541	519	422
	783	579	381
	1004	619	304
96-15-1_18	39	113	98
	103	135	111
	399	406	313
	577	541	435
	826	605	281

Specimen	*mediolateral Thickness (MlTh)*				*Thickness (Th)*		
	b0	b1	b2	b3	a	b	c
96-13-1/1	2,56E-10	4,8	-0,005	293,6	80,5	0,323	-190,5
96-13-1/3	1,93E-08	4,1	-0,004	293,5	431,1	0,178	-750,6
96-13-1/4	6,25E-11	4,9	-0,004	406,5	127,1	0,284	-241,4
96-13-1/5	3,46E-16	6,8	-0,005	564,7	2.230,6	0,051	-2.567,3
96-13-2/3	1,08E-13	5,8	-0,004	512,9	6.344,0	0,023	-6.782,7
96-13-2/5	1,17E-10	4,6	-0,003	529,3	3.174,8	0,048	-3.754,5
96-15-1/1	1,09E-15	6,4	-0,004	705,4	9,9	0,587	19,6
96-15-1/7	1,92E-18	7,6	-0,006	588,2	23,0	0,498	-55,5
96-15-1-8	6,17E-17	6,9	-0,005	668,5	6,6	0,642	77,7
96-15-1-13	3,05E-16	7,0	-0,007	435,4	68,4	0,363	-198,8
96-15-1-14	2,37E-15	6,6	-0,006	490,4	25,7	0,468	-41,1
96-15-1-15	1,62E-16	6,9	-0,005	583,9	50,5	0,378	-92,7
96-15-1_20	8,19E-17	7,1	-0,006	498,2	40,5	0,439	-100,7
96-15-1_12	4,20E-12	5,5	-0,005	390,4	110,5	0,301	-242,9
96-15-1_18	1,93E-17	7,6	-0,008	420,6	12,3	0,590	-16,5

The five measurements of Marginal Radius (MR), Thickness (Th) and mediolateral Thickness (MlTh) for every specimen investigated from 20 meters water depth, as well as the estimated functional parameters for both growth functions per specimen are given.

Specimen	*measured distances (µm)*		
	Marginal Radius (MR)	Thickness (Th)	mediolateral Thickness (MlTh)
96-11-1-2/1	47	129	111

	150	196	135
	474	413	268
	1131	725	442
	2051	806	152
96-11-1-2/2	44	122	105
	138	170	152
	812	837	596
	1036	961	748
	1632	1000	393
96-11-1-2/4	51	135	117
	166	196	167
	603	487	383
	789	535	324
	1097	562	266
96-11-1-2/5	41	116	100
	105	142	113
	660	575	449
	952	623	485
	1404	649	264
96-11-1-2/8	51	135	117
	139	216	146
	684	724	594
	755	806	580
	1516	839	247
96-12-1/1	48	103	89
	112	139	116
	554	526	375
	745	702	552
	1053	726	325
96-12-1/4	51	145	126
	142	188	167
	411	430	309
	596	491	369
	847	502	222
96-12-6/1	61	116	100
	157	199	150
	570	564	475
	750	649	460
	1090	660	347
96-12-6/2	51	128	111
	147	218	165
	596	635	518
	785	720	577
	1077	770	376
96-16-11-4	53	126	109
	117	178	146
	587	448	329

	752	485	313
	1089	576	226
96-16-11-8	46	128	111
	139	185	150
	466	385	278
	538	413	310
	840	456	205
96-16-11-2	53	129	111
	132	164	142
	595	477	330
	797	555	376
	1100	583	233
96-12-6_3	35	103	89
	99	143	120
	487	449	332
	734	500	308
	881	519	274
96-16-11_3	61	156	135
	117	214	153
	459	420	336
	644	498	341
	1139	534	192
96-16-11-10	46	146	127
	132	185	153
	331	356	278
	602	384	280
	793	420	139

Specimen	*mediolateral Thickness (MlTh)*				*Thickness (Th)*		
	b0	b1	b2	b3	a	b	c
96-11-1-2/1	1,20E-19	7,6	-0,004	830,8	69,2	0,351	-166,4
96-11-1-2/2	4,34E-18	7,3	-0,005	638,6	177,9	0,296	-473,8
96-11-1-2/4	1,59E-11	5,1	-0,005	453,9	52,6	0,370	-108,1
96-11-1-2/5	9,19E-18	7,3	-0,005	592,3	366,2	0,176	-623,0
96-11-1-2/8	8,58E-16	6,7	-0,005	492,1	2.922,9	0,059	-3.587,8
96-12-1/1	1,54E-18	7,7	-0,006	492,1	45,5	0,435	-170,6
96-12-1/4	6,01E-18	7,7	-0,008	500,4	119,1	0,275	-227,8
96-12-6/1	3,29E-12	5,5	-0,005	362,8	354,0	0,198	-707,8
96-12-6/2	1,33E-17	7,5	-0,006	483,1	82,3	0,364	-240,5
96-16-11-4	3,44E-11	5,0	-0,005	456,2	39,3	0,403	-76,7
96-16-11-8	1,70E-16	7,1	-0,007	504,6	58,7	0,338	-98,4

96-16-11-2	8,12E-18	7,4	-0,006	614,9	55,2	0,372	-135,7
96-12-6_3	5,74E-12	5,4	-0,006	397,3	63,0	0,350	-135,2
96-16-11_3	6,66E-15	6,4	-0,006	548,0	4.357,0	0,027	-4.726,8
96-16-11-10	1,25E-18	8,1	-0,009	450,1	157,3	0,212	-221,0

The five measurements of Marginal Radius (MR), Thickness (Th) and mediolateral Thickness (MlTh) for every specimen investigated from 30 meters water depth, as well as the estimated functional parameters for both growth functions per specimen are given.

Specimen	*measured distances (µm)*		
	Marginal Radius (MR)	Thickness (Th)	mediolateral Thickness (MlTh)
96-11-1/2	61	122	106
	159	196	132
	779	647	522
	941	745	575
	1239	820	420
96-11-1/4	74	164	142
	176	203	189
	792	732	557
	1479	772	370
	1710	812	260
96-11-1/5	58	115	100
	118	176	133
	657	481	374
	955	535	355
	1503	562	181
96-11-1_10	57	135	117
	117	167	111
	441	442	314
	716	513	352
	1310	555	139
96-11-1_7	53	135	117
	166	185	160
	434	377	263
	666	457	331
	1146	492	133
96-18-1/2	54	127	110
	148	181	127
	832	738	522
	1246	797	456
	2051	805	151
96-18-1/4	54	169	146
	157	206	155

	687	582	414
	959	684	351
	1918	702	127
96-18-1-2/4	51	109	94
	133	157	137
	584	569	454
	1025	641	483
	1240	635	282
96-18-2/1	51	108	94
	156	149	141
	586	528	451
	944	609	422
	1300	629	244
96-18-2/3	64	156	135
	190	230	182
	1041	643	508
	1366	732	511
	1767	772	369
96-11-1/3	51	126	109
	122	183	137
	606	555	466
	900	751	520
	1259	772	221
96-18-1/3	54	152	131
	118	200	140
	817	811	612
	1455	950	658
	2136	975	198
96-18-2/2	44	102	88
	132	149	111
	548	467	334
	863	650	468
	1471	678	205
96-18-1-5	52	145	126
	127	193	124
	467	678	369
	1067	788	476
	1503	798	173
96-11-1-6	51	102	88
	112	142	114
	599	548	396
	982	596	345
	1330	630	203

Specimen	*mediolateral Thickness (MlTh)*				*Thickness (Th)*		
	b0	b1	b2	b3	a	b	c
96-11-1/2	2,49E-18	7,3	-0,005	632,3	74,3	0,371	-220,1
96-11-1/4	2,68E-16	6,7	-0,004	646,3	1.188,8	0,104	-1.739,6
96-11-1/5	1,06E-14	6,2	-0,005	571,7	3.261,7	0,037	-3.687,9
96-11-1_10	3,76E-17	7,2	-0,006	537,4	4.063,6	0,031	-4.494,2
96-11-1_7	1,00E-18	7,8	-0,007	591,0	151,0	0,233	-264,6
96-18-1/2	3,45E-16	6,6	-0,004	612,0	3.718,8	0,045	-4.377,2
96-18-1/4	7,03E-11	4,8	-0,004	539,5	1.196,9	0,088	-1.570,1
96-18-1-2/4	1,55E-18	7,7	-0,006	538,1	494,5	0,157	-842,0
96-18-2/1	1,44E-16	7,0	-0,006	481,9	132,4	0,281	-324,3
96-18-2/3	2,37E-16	6,4	-0,003	859,1	37,2	0,423	-78,7
96-11-1/3	6,84E-19	7,9	-0,007	516,7	62,9	0,387	-184,5
96-18-1/3	2,50E-20	7,9	-0,004	769,6	3.014,3	0,059	-3.710,5
96-18-2/2	3,37E-18	7,4	-0,005	561,9	133,5	0,281	-317,4
96-18-1-5	5,37E-20	8,1	-0,006	590,8	7.339,3	0,026	-8.028,0
96-11-1-6	3,35E-14	6,1	-0,005	456,5	1.388,6	0,082	-1.842,2

The five measurements of Marginal Radius (MR), Thickness (Th) and mediolateral Thickness (MlTh) for every specimen investigated from 40 meters water depth, as well as the estimated functional parameters for both growth functions per specimen are given.

Specimen	*measured distances (µm)*		
	Marginal Radius (MR)	Thickness (Th)	mediolateral Thickness (MlTh)
93-3-3-3_2	82	199	173
	203	271	252
	580	477	347
	745	534	401
	1566	584	144
96-19/1	51	133	115
	154	200	157
	889	666	557
	1317	750	413
	1869	780	297
96-19/2	45	121	105
	136	170	148
	908	768	558
	1525	853	444
	1803	877	355

96-19/3	51	115	100
	139	169	140
	1189	968	736
	1225	1028	759
	2726	1053	214
96-19/4	48	170	147
	138	212	161
	1125	805	610
	2057	980	519
	3485	999	188
96-19/5	139	152	131
	139	157	121
	617	513	345
	802	617	434
	1301	635	260
96-19/6	36	90	78
	109	113	112
	548	411	307
	905	512	341
	1543	523	160
96-2-1	74	150	130
	162	210	197
	802	732	535
	1489	839	585
	2451	873	291
96-2-2	61	122	106
	169	203	152
	650	481	355
	1058	536	262
	1489	555	176
96-2-3	58	139	121
	149	196	159
	515	427	289
	969	549	369
	1259	555	251
96-2-5	58	162	141
	183	231	206
	410	386	298
	590	435	261
	894	454	228
96-2-6	44	127	110
	152	170	162
	440	379	248
	623	443	269
	1049	467	127
96-2-7	51	162	141
	162	230	179

	623	596	426
	1038	830	637
	2024	843	219
96-2-9	61	152	131
	183	217	179
	501	535	389
	817	630	452
	1090	643	250
96-8-24-2_3	57	136	99
	139	171	128
	406	335	267
	572	427	287
	1025	463	158

Specimen	*mediolateral Thickness (MlTh)*				*Thickness (Th)*		
	b0	b1	b2	b3	a	b	c
93-3-3-3_2	2,26E-16	6,7	-0,005	773,9	3.417,2	0,034	-3.788,1
96-19/1	2,91E-09	4,2	-0,003	439,1	215,7	0,235	-442,7
96-19/2	1,22E-11	5,0	-0,003	548,0	172,9	0,272	-408,1
96-19/3	4,78E-16	6,4	-0,003	721,7	8.649,9	0,027	-9.591,8
96-19/4	2,41E-09	4,0	-0,002	688,9	955,9	0,115	-1.375,3
96-19/5	2,08E-16	6,8	-0,005	558,4	4.103,0	0,044	-4.924,5
96-19/6	7,59E-17	6,9	-0,005	637,4	202,7	0,207	-364,6
96-2-1	6,36E-13	5,2	-0,003	760,4	318,7	0,206	-636,8
96-2-2	4,53E-10	4,5	-0,004	428,4	172,5	0,228	-323,2
96-2-3	6,70E-18	7,1	-0,004	796,9	94,7	0,292	-182,8
96-2-5	4,05E-10	4,6	-0,005	496,0	101,9	0,266	-144,5
96-2-6	7,68E-17	7,1	-0,007	578,4	94,7	0,270	-136,3
96-2-7	6,26E-20	7,8	-0,004	812,5	207,6	0,242	-406,0
96-2-9	7,46E-18	7,5	-0,006	520,4	108,9	0,308	-259,8
96-8-24-2_3	2,11E-15	6,7	-0,007	468,9	97,2	0,276	-176,0

The five measurements of Marginal Radius (MR), Thickness (Th) and mediolateral Thickness (MlTh) for every specimen investigated from 50 meters water depth, as well as the estimated functional parameters for both growth functions per specimen are given.

Specimen	*measured distances (µm)*		
	Marginal Radius (MR)	Thickness (Th)	mediolateral Thickness (MlTh)
96-20-1	61	168	145

	169	212	162
	753	551	422
	1285	677	425
	2075	732	206
96-20-2	73	187	162
	194	254	234
	1071	720	514
	2196	859	445
	2949	889	218
96-20-4	64	145	126
	169	206	179
	599	592	363
	1077	718	479
	2099	720	148
96-20-5	51	146	126
	157	187	148
	895	617	473
	1715	750	469
	3031	780	244
96-29_1	59	149	129
	176	196	164
	541	642	347
	865	752	474
	1480	767	151
96-29-3	78	173	150
	211	258	207
	565	611	382
	1061	712	415
	1636	728	157
96-29-4	63	141	122
	129	196	124
	619	399	315
	1002	525	285
	1472	543	173
96-4-2	81	162	141
	217	231	206
	724	460	327
	1188	555	309
	1781	575	156
96-4-3	85	177	153
	196	237	173
	596	406	343
	903	476	284
	1638	494	138
96-4-4	46	142	123
	150	210	181
	545	413	293

	1049	564	327
	1801	582	139
96-4-5	71	162	141
	196	230	181
	711	664	442
	938	806	500
	1378	820	322
96-4-6	74	176	152
	240	278	227
	650	474	315
	1337	548	214
	1835	562	134
96-4-8	62	142	123
	179	230	195
	606	596	443
	1242	723	309
	1730	732	142
96-4-9	68	122	105
	183	194	148
	731	433	366
	1281	507	280
	2187	514	140
96-20-3	54	145	126
	178	206	176
	602	665	388
	1389	811	301
	1697	847	197

Specimen	*mediolateral Thickness (MlTh)*				*Thickness (Th)*		
	b0	b1	b2	b3	a	b	c
96-20-1	4,66E-15	6,0	-0,003	816,6	175,1	0,240	-330,6
96-20-2	3,79E-18	6,7	-0,002	1329,8	615,2	0,141	-970,5
96-20-4	8,78E-17	6,7	-0,004	777,4	837,9	0,115	-1.221,9
96-20-5	8,81E-08	3,4	-0,002	612,8	771,8	0,115	-1.107,0
96-29_1	2,91E-19	7,9	-0,006	612,4	538,8	0,163	-945,6
96-29-3	4,69E-18	7,3	-0,005	709,9	4.164,8	0,039	-4.800,1
96-29-4	9,95E-15	6,1	-0,004	662,5	155,8	0,229	-268,8
96-4-2	5,27E-16	6,4	-0,004	885,4	336,4	0,164	-544,1
96-4-3	8,26E-11	4,7	-0,004	558,8	3.720,8	0,027	-4.029,0
96-4-4	1,27E-15	6,3	-0,004	847,4	219,8	0,196	-340,5
96-4-5	2,00E-17	7,0	-0,005	689,5	96,6	0,346	-295,1

96-4-6	4,56E-08	3,7	-0,003	569,2	2.715,1	0,038	-3.032,7
96-4-8	1,27E-11	5,1	-0,004	459,0	718,9	0,138	-1.149,0
96-4-9	5,87E-09	4,0	-0,003	496,3	4.447,7	0,025	-4.823,2
96-20-3	8,57E-16	6,4	-0,004	709,6	112,8	0,320	-295,5

The five measurements of Marginal Radius (MR), Thickness (Th) and mediolateral Thickness (MlTh) for every specimen investigated from 60 meters water depth, as well as the estimated functional parameters for both growth functions per specimen are given.

Specimen	*measured distances (µm)*		
	Marginal Radius (MR)	Thickness (Th)	mediolateral Thickness (MlTh)
93-8-11-13-2	51	126	109
	121	164	117
	337	251	193
	530	300	192
	877	329	159
96-21-22_1	67	169	147
	154	236	190
	1059	908	623
	1354	980	522
	1990	998	287
96-21-22_2	51	145	126
	124	206	168
	826	569	337
	1333	678	361
	2015	684	172
96-21-22_3	54	121	105
	136	169	140
	808	460	383
	1604	556	363
	2495	581	226
96-21-22_5	70	176	152
	212	254	203
	1047	720	508
	1968	915	455
	3346	944	200
96-21-22-4	48	133	115
	127	181	141
	687	532	401
	1121	692	503
	1299	726	365
96-21-22-6	64	133	115
	175	206	174

	796	726	548
	1893	892	516
	2952	901	223
96-31-10	78	164	142
	211	227	176
	525	486	332
	787	601	370
	1402	619	156
96-31-2	68	135	117
	156	189	152
	298	319	191
	498	381	242
	853	386	129
96-31-3	47	108	94
	129	176	137
	548	513	319
	884	662	441
	1604	663	144
96-31-4	71	176	152
	210	231	186
	345	300	234
	590	361	164
	1151	372	89
96-31-5	68	163	141
	179	230	199
	454	447	281
	691	554	413
	1246	582	190
96-31-6	64	122	105
	112	172	115
	467	386	298
	627	441	270
	921	467	230
96-31-7	34	84	73
	71	108	86
	504	298	203
	878	365	195
	1347	396	117
96-31-9	74	163	149
	190	258	224
	685	603	401
	984	746	573
	2582	776	179

Specimen	*mediolateral Thickness (MlTh)*				*Thickness (Th)*		
	b0	b1	b2	b3	a	b	c
93-8-11-13-2	2,08E-11	5,0	-0,005	567,9	25,1	0,404	0,0
96-21-22_1	1,40E-11	5,0	-0,003	556,5	939,2	0,133	-1.519,9
96-21-22_2	1,37E-18	7,1	-0,003	1097,9	986,9	0,095	-1.312,2
96-21-22_3	7,46E-10	4,1	-0,002	708,6	1.052,2	0,078	-1.339,3
96-21-22_5	1,03E-10	4,3	-0,002	890,6	675,4	0,139	-1.081,4
96-21-22-4	2,11E-16	6,6	-0,004	739,5	675,0	0,139	-1.081,4
96-21-22-6	4,45E-10	4,3	-0,002	594,4	191,1	0,247	-400,5
96-31-10	1,81E-18	7,5	-0,006	666,0	918,7	0,106	-1.320,2
96-31-2	1,27E-16	7,2	-0,007	519,3	983,9	0,075	-1.215,0
96-31-3	2,51E-19	7,8	-0,005	658,0	1.807,1	0,068	-2.271,4
96-31-4	1,54E-10	4,7	-0,005	616,6	2.628,7	0,026	-2.759,9
96-31-5	1,22E-17	7,3	-0,006	654,3	893,0	0,101	-1.227,4
96-31-6	3,02E-10	4,7	-0,005	377,1	1.661,3	0,060	-2.016,1
96-31-7	2,86E-11	4,9	-0,004	536,4	175,1	0,186	-262,9
96-31-9	1,31E-18	7,1	-0,003	1034,9	423,1	0,171	-669,0

The five measurements of Marginal Radius (MR), Thickness (Th) and mediolateral Thickness (MlTh) for every specimen investigated from 70 meters water depth, as well as the estimated functional parameters for both growth functions per specimen are given.

Specimen	*measured distances (µm)*		
	Marginal Radius (MR)	Thickness (Th)	mediolateral Thickness (MlTh)
96_26_6	74	183	158
	227	251	215
	470	454	361
	890	532	376
	1511	564	154
96_32/1.1	58	162	141
	176	244	179
	758	562	350
	1453	660	428
	2376	684	244
96_32/3.1	91	224	194
	267	325	264
	961	589	408
	2234	711	381
	3551	820	253

96-26/2	82	188	162
	206	248	203
	411	363	239
	714	448	232
	1258	447	98
96-26-1	57	163	141
	182	236	202
	895	599	382
	1729	723	241
	2027	733	160
96-27/1	65	161	140
	172	260	189
	309	278	224
	507	326	188
	859	333	118
96-32/1	74	169	147
	196	250	216
	555	420	304
	925	522	333
	1960	542	158
96-32/2	47	149	129
	176	217	175
	816	487	363
	1052	533	352
	1611	562	237
96-32/5	61	143	124
	159	201	168
	399	298	188
	581	351	200
	833	372	138

Specimen	*mediolateral Thickness (MlTh)*				*Thickness (Th)*		
	b0	b1	b2	b3	a	b	c
96_26_6	9,70E-17	6,9	-0,005	667,2	326,3	0,164	-490,6
96_32/1.1	3,62E-17	6,4	-0,003	1220,5	573,0	0,138	-923,9
96_32/3.1	4,32E-11	4,2	-0,001	1551,7	503,5	0,131	-682,8
96-26/2	1,07E-13	5,8	-0,005	697,3	380,8	0,131	-491,5
96-26-1	8,81E-13	5,2	-0,003	794,3	128,2	0,269	-239,8
96-27/1	1,96E-07	3,7	-0,005	364,5	8.543,8	0,008	-8.641,0
96-32/1	4,21E-09	4,0	-0,003	685,2	9.292,6	0,013	-9.647,9
96-32/2	9,21E-13	5,3	-0,003	742,6	94,2	0,278	-142,3

96-32/5	4,41E-12	5,3	-0,005	590,8	95,7	0,248	-126,2

The five measurements of Marginal Radius (MR), Thickness (Th) and mediolateral Thickness (MlTh) for every specimen investigated from 80-90 meters water depth, as well as the estimated functional parameters for both growth functions per specimen are given.